# GROWTH AND STRESS RESPONSE MECHANISMS UNDERLYING POST-FEEDING ORGAN REGENERATIVE GROWTH IN SNAKES

by

AUDRA LEANN ANDREW

Presented to the Faculty of the Graduate School of Biology

The University of Texas at Arlington in Partial Fullfillment

of the Requirements

for the Degree of

DOCTOR OF PHILOSOPHY

THE UNIVERSITY OF TEXAS AT ARLINGTON

August 2017

Acknowledgements

I would like to thank many faculty, staff, and collegues who have contributed greatly to my success as a graduate student at UT Arlington. I would like to thank my advisor Todd Castoe for encouraging me during my four years here through countless hours of teaching and mentorship. I would also like to thank my doctoral committee members, Matt Fujita, Matt Walsh, Jeff Demuth, and Esther Betran, for their valuable contributions to my dissertation research. I would like to thank Linda Taylor and Gloria Burlingham for fielding countless questions during my time here, as well as Shawn Christensen for his advisment during the course of earning my degree. I would also like to thank my labmates and friends for their support and encouragement throughout my time here, namely Giulia Pasquesi, Daren Card, Drew Shield, Richard Adams, Blair Perry, Nicky Hales, Diwash Jangam, Jill Castoe, and Rachel Wostl.

I would also like to thank many outside collaborators who have contributed substantially to this work, including Stephen Secor at the University of Alabama who is an expert on the physiological responses of snakes during feeding and conducted all feeding experiements in this study, Amit Choudhary at the Broad Institute for his work with python blood plasma and mammalian systems, and Suzanne McGaugh at the University of Minnesota for her advice and contributions on pathway analysis programs and techniques.

I would also like to thank my family for their support and encouragement over these four years. My husband has been here since day one with words of encouragement, and my son has provided much needed relief from the hard work.

August 3, 2017

Abstract

GROWTH AND STRESS RESPONSE MECHANISMS UNDERLYING POST-FEEDING ORGAN REGENERATIVE GROWTH IN SNAKES

Audra Andrew, PhD

The University of Texas at Arlington, 2017

Supervising professor: Todd Castoe

Snakes represent an emerging model in biological research and provide a valuable system for studying multiple extreme phenotypes unparallel to those seen in mammals. Recently, snakes have become increasingly used in studies of extreme organ regenerative growth due to the ability of some species to rapidly and reversibly upregulate organ form and function upon feeding. The predominant model used to study this feeding response has been the Burmese python (*Python molurus bivittatus*) because of the particulalry extreme nature of this post-feeding response in this species. Specifically, the wet masses of major organs increase by 50-100% within just 48 hours post-feeding with rapid spikes in metabolism greater than those seen in any other vertebrate. Once digestion is complete, organs rapidly atrophy back to fasted levels. My transcriptome analyses have implicated the differential expression of thousands of genes during this feeding response, and many of these genes are involved in key cellular pathways, including cell cycling, apoptosis, and WNT signaling. Post-feeding organ regenerative growth has also been demonstrated in other species of snakes, including the vipers. By leveraging comparative transcriptomic data from species that do and do not regenerate their organs upon feeding, my dissertation work has uncovered several

key growth and stress response pathway that appear to regulate regenerative growth in the Burmese python and rattlesnake. Specifically, it seems that mTOR interacts with several growth pathways, including PI3K-AKT, MAPK, and lipid signaling pathways to coordinate this growth response across time. Additionally, consistent activation of the NRF2-mediated oxidative stress response during growth likely leads to protection of the cells against apoptosis during extreme functional and metabolic fluctuations.

# TABLE OF CONTENTS

List of Illustrations

List of Tables

Chapter 1

# Rapid changes in gene expression direct rapid shifts in intestinal form and function in the Burmese python after feeding

Andrew et al. 2015, *Physiological Genomics*

## Introduction

Snakes represent an emerging model system for studying extreme vertebrate phenotypes, including extreme examples of modulation of physiological form and function (1, 13, 19, 23, 31, 37, 69, 70). Studying such extreme examples of vertebrate phenotypes and physiology may provide novel insight into vertebrate biology and how snakes have evolutionarily manipulated vertebrate pathways to achieve such phenotypes. Furthermore, such studies have the potential to demonstrate how conserved vertebrate pathways may be modulated to achieve desired therapeutic phenotypes in other vertebrates, such as humans. A particularly interesting feature to study is the ability of certain snake species to rapidly and reversibly remodel major organ systems, including growth of new organ tissue, in response to feeding. Multiple species of snakes appear to have evolved the ability to massively downregulate metabolic and physiological functions during periods of fasting, including the atrophy of organs, such as the heart, liver, kidney, and intestine (44, 51, 58, 59). Upon feeding, their metabolism, along with the size and function of these major organ systems, is massively and rapidly upregulated to accommodate the digestion of prey. While some snake species represent the most extreme exemplars of such remodeling, complex cyclic physiological remodeling has been documented in other ectotherms including frogs and fishes, and is proposed to

have evolved as a mechanism to reduce daily energy needs while enduring long periods (months or years) of fasting (10, 51, 52, 58, 59).

Among snake species that experience such large fluctuations in physiology with each meal, the Burmese python (*Python molurus bivittatus*) is the most well studied (2, 10, 15, 45, 51, 55, 56, 60). Within 48 hours of feeding, Burmese pythons experience major shifts in systemic physiology, including as much as 44-fold increases in metabolic rate and 160-fold increases in plasma triglyceride content (56, 58). Major organ-specific changes also occur within 72 hours of feeding, including 40-100% increases in the mass of the heart, liver, pancreas, kidneys, and small intestine (15, 34, 51, 55, 64).

Evolutionary processes have driven improvement of anatomical and physiological traits of the digestive system to ensure that organisms can effectively digest and assimilate large meals. The extreme phenotypic plasticity of the Burmese python small intestine has been well documented, with results indicating major fluctuations in form and function of this organ between fasted and post-fed animals. Within just 24 hours after feeding, the wet mass of the small intestine doubles, including a doubling of the mucosal enterocyte volume and a six-fold increase in microvillus length (34). Within 48 hours, intestinal nutrient transport capacity increases 20-fold compared to fasted levels (15, 44). The pH of the stomach also drops by as much as 4.6 (from 7.5 to 2.9) within 12 hours of feeding, indicating that every 3 hours there is a 10-fold increase in intragastric hydrogen ions [H+] (53). Digestion is completed within 6-10 days, and this completion coincides with the downregulation of intestinal form and function to fasted levels (15, 55). These extreme cycles of physiological fluctuations with feeding suggest tightly regulated gene expression patterns that coordinate massive reconstructions of the anatomy and physiology of the python digestive system.

Recent studies on the Burmese python have demonstrated that rapid, massive changes in gene expression do indeed broadly coincide with physiological remodeling phenotypes, and that these differentially expressed genes involved in remodeling include those known to be involved in human development, metabolism, and disease (10). Previous studies have, however only surveyed two post-feeding timepoints during this post-feeding response –1 day post feeding (1DPF; when phenotypes are continuing to increase), and 4DPF (when phenotypes have just begun to regress), and lacked any substantial analyses linking changes in gene expression with corresponding changes in phenotypes and physiological function (10). Therefore, major gaps in our understanding remain, including how patterns of gene expression precisely underlie shifts in intestinal phenotype and function throughout the intestinal remodeling process, how rapidly gene expression responses occur post-feeding, and how different temporal phases of gene expression direct temporal phases of intestinal phenotypic and functional change.

In this study we address gaps in our understanding of how the python intestine undergoes such transformations of form and function by substantially increasing sampling of gene expression data to include more biological replicates and post-feeding timepoints. Though of a distinct body form, the Burmese python shares with humans and other vertebrates the same structure and function of organs at the tissue and cellular levels, including the intestine, making them a useful system for investigating the regulation of vertebrate organ structure and function (55, 58, 60).This expanded sampling allows us to link shifts in gene expression through time with the phenotypic and functional shifts that co-occur in the intestine by linking particular gene expression programs to cellular and functional physiological processes that they underlie. Our integrated analyses of gene expression and intestinal physiology provide new perspectives on the surprising scales associated with this response, and new insight into

the molecular mechanisms and foundations driving these extensive shifts in phenotype and physiology.

## Materials and Methods

*Feeding experiements*

Burmese pythons were obtained as hatchlings from commercial breeders and maintained on a weekly to biweekly diet of pre-killed rodents. All animal care and experiments were conducted under approved protocols of the University of Alabama Institutional Animal Care and Use Committee. Two to three year old Burmese pythons (mean mass = 910g, range = 415-5776g) were maintained at 30°C, and studied fasted (30 days since last meal), as well as at 6 hours post-feeding (6HPF), 12HPF, 1 day post-feeding (1DPF), 4DPF, and 10DPF following the consumption of meals (pre-killed rats) equaling at least 25% of their body mass (Table 1). The sampling times were chosen to represent episodes of clear shifts in tissue physiology and gene expression (10, 11, 15, 51). Each timepoint was sampled with multiple biological replicates (multiple animals). Snakes were humanely euthanized by severing the spinal cord immediately behind the head and, following a mid-ventral incision, organs were immediately extracted and weighed (44). For fed snakes, elements of the digestive tract were emptied of their contents and reweighed. Segments of the anterior third of the small intestine were placed in ice-cold reptilian Ringer's solution (for nutrient uptake), fixed in reptilian Ringer's-buffered 10% formalin solution (for light microscopy), fixed in reptilian Ringer's-buffered 2.5% gluteraldehyde solution (for electron microscopy), and snap frozen in liquid $N_2$ and stored at -80°C (for enzyme assays and gene expression analyses).

*Analysis of tissue and cellular structure*

We used light microscopy to examine postprandial changes in intestinal tissue thickness and enterocyte size. Formalin-fixed intestinal samples were embedded in paraffin, cross-sectioned (6 μm), and stained with hematoxylin and eosin on glass slides. Samples were viewed with a light microscope linked to a computer loaded with image-analysis software (Motic Image Plus, Richmond, British Columbia, Canada). From each cross section, we measured mucosal/submucosal thickness at 10 locations along with muscularis/serosa thickness, and enterocyte height and width. We calculated enterocyte volume using the formula for a cylinder. We assessed ultrastructural changes to the intestinal brushborder membrane using transmission electron microscopy. Small pieces of intestinal mucosa were fixed in 2.5% gluteraldehyde, postfixed in 1% osmium tetroxide, dehydrated in a graded series of ethanol, and embedded in Spurr's epoxy resin. Ultra thin sections (~80 nm) were cut and placed on copper mesh grids and examined with a Hitachi (H-7650) transmission electron microscope. Sections of microvillus membrane were viewed with the scope's high definition camera (Orca) and image analysis software (Advance Microscopy Techniques Corp.). For each sample, we measured the height and width of 100 individual microvilli and calculated microvillus surface area using the equation width x π x height.

*Measuring intestinal function*

We quantified intestinal nutrient uptake and hydrolase activities to determine the magnitude that intestinal function is modulated with feeding and fasting. We used the everted-sleeve technique to measure the brush-border uptake of the amino acids L-leucine and L-proline and of the sugar D-glucose (28, 63). Sleeves (1 cm) of everted intestine were pre-incubated in reptile Ringer's solution for 5 minutes at 30$^{o}$C and

incubated for 2 minutes at 30$^{o}$C in reptile Ringer's solution containing both an unlabeled and radiolabeled nutrient ($^{3}$H-L-leucine, $^{3}$H- L-proline, or $^{14}$C-D-glucose), and a radiolabeled adherent fluid marker ($^{14}$C-polyethylene glycol for the amino acids or $^{3}$H-L-glucose for D-glucose). We quantified total uptake (carrier-mediated and passive) of each amino acid, and carrier-mediated uptake of D-glucose, as nmoles of nutrient per minute per mg of tissue (29, 63). We used colorimetric methods to quantify (μmole min$^{-1}$ mg$^{-1}$ protein) the activities of the membrane-bound intestinal aminopeptidase N (APN) (15).

*Transcriptome library generation*

Total RNA was extracted from snap-frozen intestinal cross-sections (SI) and intestinal mucosa (Muc) using Trizol Reagent (Invitrogen). The details of the sampling design and the numbers of replicates per timepoint are outlined in Table 1. Illumina mRNAseq barcoded libraries were constructed using either the Illumina TruSeq RNAseq kit or the NEB Next RNAseq kit, both of which included poly-A selection, RNA fragmentation, cDNA synthesis, and indexed Illumina adapter ligation. Completed RNAseq libraries were quantified on a BioAnalyzer (Agilent), pooled in various multiplex arrangements, and sequenced on either an Illumina GAIIx or Illumina HiSeq2000.

*Analysis of gene expression*

Raw Illumina RNAseq reads were quality filtered, trimmed, and mapped to the complete annotated transcript set of the Burmese python genome (10). The numbers of mapped reads per sample are provided in Table 1. Based on preliminary analyses, we found intestinal mucosa and intestinal cross section samples to be extremely similar in terms of gene expression (Fig. 1). Mucosal and intestinal sections were therefore analyzed together, and where both samples existed for a single specimen (same animal),

these reads were combined for final analysis. In instances where replicates of a sample were available (e.g., same

library sequenced in multiple different runs), replicated samples were combined and mapped for each individual. Mapping of reads to the reference transcriptome of the Burmese python (10) was conducted in CLC Genomics Workbench using the following parameters: maximum number of mismatches = 2, minimum length fraction = 0.8, minimum similarity fraction = 0.8, and maximum number of hits for a read = 10. Expression was determined by counting the number of unique gene reads that mapped to a particular annotated transcript, while excluding reads that mapped to multiple positions. Combined with data previously published (10), new data is accessioned in the NCBI Short Read Archive (SRP051827).

The raw expression counts were normalized using TMM normalization in edgeR (50) and all statistical analyses of gene expression used these normalized data. We identified genes that were significantly differentially expressed between timepoints using two different approaches. First, we estimated significant changes in gene expression between pairs of timepoints using pairwise exact tests for the binomial distribution calculated in edgeR (50), which integrates both common and tagwise dispersion. Second, to accommodate the time-series nature of the experimental design of this study we also conducted step-wise regression analysis of gene expression in maSigPro (14).

To facilitate analyses of candidate genes, we annotated Burmese python genes by using reciprocal best blast and one-way tblastx (7) estimates of homology to gene sets from *Anolis carolinensis*, *Homo sapiens*, and *Gallus gallus*. Results of these analyses allowed a large proportion of python genes to be assigned to a homologous human gene, and therefore assigned a human Ensembl ID.

We identified statistically overrepresented gene expression profile clusters using STEM (21). For STEM analyses, we input our TMM normalized gene expression data (averaged across replicates per time-point) using default settings, further log normalized these data as recommended in the STEM manual, and conducted STEM analyses over our entire time series dataset (fasted – 10DPF). We set the maximum number of model profiles to 50, and limited the maximum unit change (between consecutive timepoints) within model profiles to 3; together these settings allow for a large number of sampled model profiles while maintaining a conservative estimate of expression fluctuations within a profile.

## Results

*Rapid shifts in gene expression upon feeding*

To quantify which temporal periods following feeding have the most extreme shifts in gene expression, we conducted pairwise analyses between timepoints (Table 2). Our comparisons show the general trend that bursts of up- or downregulated genes early after feeding are effectively reversed around 1-4DPF, and return to near baseline by 10DPF or earlier (Table 2). These comparisons also show that much of the observed differential expression occurs within the first 6 hours after feeding (6HPF), with 2,489 genes undergoing differential expression at this time compared to the fasted state. Nearly equal numbers of genes were up- and downregulated in the first 6 hours (1,367 genes upregulated vs. 1,122 genes downregulated; Table 2).

Only a few more genes were upregulated in the remaining time of the first 24 hours, as seen in the 6 versus 12 hour and 12 versus 24 hour as well as the 0 versus 24 hour comparisons (Table 2). The return to near-fasting gene expression levels was not as

rapid as the early post-feeding response, with only 864 significantly differentially expressed between 24 and 96 hours, and 538 significantly differentially expressed genes between 96 hours and 10 days post-feeding. By 10 days, expression levels are nearly back to starting conditions, with only 31 genes significantly differentially expressed between 0 hours versus 10 days (Table 2).

Our analysis of significantly over-represented patterns of gene expression in STEM yielded 11 significant gene profile clusters, and many of the genes identified in these clusters were significantly downregulated upon feeding while others were significantly upregulated within the first 6 to 12 hours post-feeding (Fig. 2). Overall, we observed a wide variety of expression patterns for differentially expressed genes in the small intestine after feeding, with genes experiencing peak low or high expression values at various times, and many clusters either broadly corresponded with patterns of morphological and physiological changes, or directly opposed them. As expected based on the comparisons in Table 1, the profiles all return to near baseline (fasted) levels of expression levels by 10 days post-feeding or earlier (Fig. 2).

Analyses of shifts in gene expression across all timepoints via pairwise comparisons and by regression analyses both identified a large number of significantly differentially expressed genes across the entire time series before and after feeding (4,432 identified via pairwise analysis and 1,772 identified via regression analysis). Regression analysis was, however, substantially more conservative than pairwise analysis in its estimation of the number of genes significantly differentially expressed, and a large majority of genes (1,711) identified by regression analyses overlapped with those identified by pairwise comparisons. Given the large numbers of genes estimated by both methods, we focus primarily on the more conservative estimates of significance derived from regression analyses hereafter to dissect the biologically relevant features of this

transcriptional response. Regression analyses identified a total of 1,772 genes that were significantly differentially expressed across the entire time course from fasted to 10 days post-feeding (DPF; Fig. 3A). As discussed in greater detail below, it is notable that rapid shifts in gene expression correspond well to physiological and morphological changes in the intestine, returning to near baseline (fasted) levels as early as 4DPF (Fig. 3A).

To illustrate this correlation of the timing of meal breakdown and passage with shifts in intestinal gene expression, we have plotted stomach and small intestinal contents (relative to meal mass) as a function of time post-feeding (Fig. 3B). Meals (adult rats) were consumed intact. After six hours they had not experienced any discernable loss in material within the snakes' stomachs. By 12 hours, a small amount of material from the rat's head had passed into the small intestine. At 24 hours, on average, 17% of the rat meal had exited the stomach and was moving through the small intestine. Over the next three days, the majority (~70%) of the rat meal was converted to chyme, had exited the stomach, and filled the small intestine. After four days, the stomach and the small intestine gradually emptied. Only remnants of the meal were found within the distal small intestine at day 10. This physiological response correlates well with the patterns of differential gene expression described above, as the most pronounced shifts in gene expression between 6HPF and 1DPF (as the meal is exiting the stomach and moving through the small intestine), and begin to revert to fasted expression levels by 4DPF (when both the intestine and stomach are emptying their contents).

*Intestinal structure and function*

To further dissect cellular processes regulating intestinal physiological remodeling, we identified genes known to play important roles in both cell cycle progression and apoptosis that were significantly differentially expressed across

timepoints. Mitogen activating kinases, as well as various cyclins and kinesin family members important to cell cycle progression experience significant differential expression during digestion of a meal, which highlights the role of both cell growth and cell division in the process of intestinal remodeling (Fig. 4A). Genes regulating apoptosis (i.e., tumor necrosis factors and caspases, among others) also experience significant differential expression across timepoints, consistent with apoptosis playing a role in the atrophy of the small intestine following the completion of digestion (Fig. 4A).

At a phenotypic level, feeding generated significant trophic responses of the small intestine at multiple levels of organization. Small intestinal wet mass increased by 50% within 12 hours after feeding and peaked at day 4 following an 87% increase in mass (Fig. 4B). Six days later, the small intestine had decreased in mass by 30%. Both mucosa/submucosa and muscularis/serosa thickness varied significantly ($P$'s $< 0.034$) across sampling timepoints. Mucosa/submucosa thickness increased post-feeding (by 53%), whereas the thickness of the muscularis/serosa layer decreased by 32% (Figs. 4C & 4D).

The WNT signaling pathway likely plays a role in growth and maintenance of the small intestine upon feeding, with multiple genes within this cascade experiencing significant differential expression throughout the digestion process. Genes such as *frizzled class 4 receptor* (*FZD4*) and *wingless-type MMTV integration site 5A* (*WNT5A*) show significant differential expression across timepoints post-fed, along with *axis inhibition protein 2* (*AXIN2*) and *transcription factor 7-like 2* (*TCF7L2*; Fig. 4E & 4F).

Trafficking and cytoskeletal genes, as well as genes important to microvilli structure were significantly differentially expressed upon feeding, indicative of tightly regulated patterns of expression underlying the phenotypic changes of intestinal structures across time (Fig. 5A). Significantly differentially expressed genes included

those central to intestinal function, consistent with the changes in intestinal form and digestive function. Metabolism increases substantially following a large meal, and our gene expression data shows corresponding significant upregulation of genes involved in oxidative phosphorylation as well as glucose up-take. Nutrient transporters and hydrolases essential to digestion and nutrient absorption also experience sharp increases in expression upon feeding (Fig. 5A).

These changes in expression of genes underlying intestinal form and function correlate well with the upregulation of intestinal physiology. Feeding triggers the significant upregulation of the python's intestinal function, including increased enterocyte height and width (and thus volume) during meal digestion (P's < 0.00001; Fig. 5B). Within 24 hours of feeding, enterocyte volume had peaked, representing a 2.6-fold increase compared to the fasted state. Enterocyte volume remained elevated through day 4, before declining toward fasted values by day 10 (Fig. 5B). At the ultrastructural level, feeding generated a 4-fold increase in the length of the intestinal microvilli (Fig. 5C), which regressed to pre-feeding levels by between 4DPF and 10DPF (Fig. 5C).

Mass-specific rates of D-glucose, L-proline, and L-leucine uptake varied significantly among sampling times (P values < 0.0009), as each nutrient significantly increased uptake within 12-24 hours of feeding (Fig. 5D-F, respectively). For all three, uptake rates peaked at 1DPF, increasing from fasting levels 5.3, 2.8, and 2.1 fold respectively. Nutrient uptake rates remained elevated through day 4, before becoming significantly down regulated by day 10 (Fig. 5D-F). Intestinal APN exhibited a similar up-regulatory response, peaking at 1-4 DPF following a 3.6-fold increase. By day 10, APN activity had returned to fasted levels (Fig. 5G).

## Discussion

The Burmese python is an exceptional model for the study of extreme physiological remodeling, as few organisms exhibit this large and discretely staged response to feeding. This study, as well as previous studies (10, 15, 55, 59), have shown the process of organ remodeling in the python to be highly regulated, exhibiting controlled waves of gene expression that coincide with large changes in intestinal form and function. Despite substantial efforts, however, the cellular mechanisms that facilitate rapid organ growth and tissue remodeling in snakes remain poorly understood.

Our analysis demonstrates that extensive and rapid shifts in gene expression accompany rapid and massive changes in intestinal form and function upon feeding in the Burmese python. Perhaps the most surprising finding of the current study is that approximately 2,500 genes are significantly differentially expressed within the first six hours after feeding (Table 2). This extremely rapid response has been previously overlooked due to a lack of fine-scale sampling of post-feeding timepoints following feeding (10). We find that patterns of differential expression largely mirror (and often precede) physiological changes in the intestine, with peaks of differential gene expression occurring around 1DPF when the organ is experiencing the greatest increases in mass and functional performance (15, 51, 55). Equally remarkable, patterns of gene expression as well as physiological form and function rapidly return to baseline fasted levels within 10DPF, indicating a tight association between differential gene expression and the rapid and cyclic physiological remodeling of the intestine. From STEM analysis, we see a number of distinct co-expressed clusters of genes that shift in expression with shifts in this remodeling process, indicating that various waves of expression are responsible for the tight regulation of intestinal remodeling (Fig. 2). A

complete understanding of the roles of these discrete waves of co-expressed loci may elucidate novel and discrete mechanisms controlling organ growth and functional change. We have taken the first steps towards dissecting these roles by linking genes involved in cellular processes and intestinal function with shifts in intestinal phenotype and function.

We found that genes involved in modulating the cell cycle and cellular development are differentially expressed during the feeding response, and thus direct substantial increases in organ mass and form. Previous studies of the Burmese python have shown that intestinal remodeling is accomplished by both hypertrophy (increase in cell size) and hyperplasia (cell division) (2, 25, 34, 49, 61, 66). Our gene expression results indicated tight regulation of the cell cycle through time. From observed expression patterns, it appears that the intestinal cells experience pro-mitotic pressure 6 hours after feeding and are actively cycling by 4DPF, which, interestingly, is when the organ form and gene expression patterns begin to revert to fasted levels (Fig. 4A). Results of previous studies have also implicated cellular replication in intestinal remodeling in the python (25); based on these previous data, the number of replicating cells/mm increases over time and levels out at around 3 days post-feedings (25). These clear signals of cell cycle progression indicate that hyperplastic organ growth begins relatively early in the process of intestinal remodeling.

Potent cell cycle promoters, *mitogen activated protein kinase 6* (*MAPK6*) and *cyclin H* (*CCNH*), are upregulated 6-12 hours after feeding. *MAPK6* is a serine/threonine protein kinase that activates *cyclin D3* (*CCND3*), which promotes cell growth and S-phase entry, and is implicated in several cancers (26, 67). *Cyclin H* acts with *cyclin-dependent kinase 7* (*CDK7*) as a broad activator of cyclin activity and is essential for cell cycle progression (30, 36). Upregulation of the cell cycle antagonist *cyclin-dependent kinase inhibitor 1A* (*CDKN1A*) during this same period suggests that intestinal cells may

be preparing for, but not freely entering the cell cycle (22). Later, at 4DPF, we see evidence of several stages of cell division. *Cyclin-dependent kinase 2* (*CDK2*), which drives cells into S-phase and G2 (4), is upregulated, as are *cyclin B3* (*CCNB3*) and *cyclin-dependent kinase 1* (*CDK1*) genes, which together are responsible for progression through mitosis (40, 42, 43) (Fig. 4A). Clearly, with increased activity of cell cycle regulators at various early and late timepoints post-feeding, we can identify cell division as a key aspect to the remodeling of the intestine upon feeding.

At 4DPF, we also see increased activity of genes responsible for the regulation of the cytoskeleton related to mitotic processes. *Kinesin 4B* (*KIF4B*) and *kinesin 20B* (*KIF20B*) are responsible intracellular trafficking during metaphase to anaphase, and anaphase to telophase/cytokinesis transitions respectively (16). Several indicators of cells undergoing cytokinesis are also observed at 4DPF, notably components of the contractile ring apparatus *Ras homolog gene family, member A* (*RhoA*), *myosin light chain kinase* (*MYLK*), and *Septin 2* (*SEPT2*), which are essential for cell shape reconfigurations (27, 47). For the Burmese python, as for other infrequently feeding snakes, the surface area of the intestine is massively expanded primarily due to an increase in microvillus length of up to six-fold following feeding (34, 51, 52, 62), entailing a substantial increase in the ability of the small intestine to absorb nutrients (15, 55). In contrast, snakes that feed more frequently in nature (along with fishes, amphibians, other reptiles, birds, and mammals) maintain consistent microvillus length with feeding and fasting and hence experience only modest regulatory changes in intestinal function (9, 18, 20, 39, 52, 54, 62). It is also notable that the pulse of contractile machinery at 4DPF likely additionally plays a role in initiating the shortening of microvilli that begins at this time (Fig. 4A).

A particularly intriguing result from our analysis of gene expression underlying intestinal remodeling is evidence that WNT signaling may play a central role in coordinating rapid shifts in cellular processes in response to feeding. The WNT signaling pathway is a key signal transduction pathway crucial to appropriate embryonic development and includes signaling that leads to correct axis formation as well as proliferation, cell fate specification, cell migration, and planar cell polarity (12, 46). Dysregulation of WNT signaling also contributes to several cancer pathologies, including breast and colorectal cancer (48). We found that increased expression of both *WNT* and its extracellular receptor, *Frizzled*, occurs 6-12 hours after feeding. During this same period, *Axis inhibition protein 2* (*AXIN2*), an intracellular inhibitor of WNT signaling, is substantially downregulated within 6 hours. We also find that *transcription factor 7-like 2* (*TCF7L2*) is downregulated within the first 6 hours and remains low through 10DPF. *TCF7L2* acts in concert with beta catenin in response to WNT signaling, but in the absence of WNT pathway activity inhibits expression of WNT target genes (6). Interestingly, the *TCF7L2* gene is known to be necessary for the maintenance of stem cell compartments in the epithelium of the small intestine (41). These and earlier observations implicate WNT signaling in the proliferative and physiological response to feeding (Fig. 4E & 4F). Collectively, these results indicate that the python intestinal remodeling response may provide a unique and novel system for investigating the role of WNT signaling in trophic physiological contexts such as feeding.

Once digestion is complete, we see a complete reversal in intestinal remodeling as the organ atrophies and metabolism and nutrient uptake are downregulated. This and previous studies have shown that in the Burmese python, the post-feeding increase in enterocyte proliferation and sharp increase in intestinal activity are followed by an increase in apoptosis upon completion of digestion and a sharp decline in absorption and

digestion (25, 55). Our results here indicate that this apoptotic response appears to occur as a two-stage process, primed first by the expression of apoptosis regulators and completed by the expression of potent downstream factors that execute apoptosis.

We observed the differential expression of genes regulating apoptosis by 6HPF, indicating that regulation of apoptosis begins early in digestion. At 6HPF there is increased expression of *TNF-related apoptosis-inducing ligand* (*TRAIL*), which activates extracellular death receptors and promotes of apoptosis (71). *Apoptosis inducing factor 3* (*AIFM3*) is also expressed at this point. AIF proteins are mitochondrial flavoproteins that normally act as NADH oxidases but can trigger caspase-independent cell death in cells under pro-apoptotic pressure (8, 17). In contrast, two negative regulators of apoptosis, *MDM2 proto-oncogene*, known for its role in inhibiting p53, and *Baculoviral IAP repeat containing 3* (*BIRC3*), a caspase inhibitor, showed increased expression at six hour post feeding. Together these observations indicate that by 6HPF some intestinal cells are exposed to extracellular and intracellular signaling promoting cell death but many cells exhibit intracellular resistance to this process by expressing inhibitors of apoptosis. Competing factors that promote or antagonize apoptosis are also expressed later. Around 96 hours post-feeding there is a significant increase in expression of both *tumor necrosis factor receptor 10* (*TNFSF10*), an apoptosis inducing death receptor (35, 71), and *ring finger and FYVE-like domain E3 ubiquitin protein* (*RFFL*), a negative regulator of apoptosis (38) (Fig. 4A).

While expression of upstream activators and inhibitors of apoptosis are highly variable, we see a clear pattern of caspase gene expression: both *caspase 6* and *caspase 3* are activated at 4DPF which, as clarified above, is the time when the organ begins to atrophy and revert to fasted levels of gene expression and nutrient absorption. Many types of caspases are known to play key roles in the execution of apoptosis upon

activation by various intra- and extra-cellular signals. The caspases identified here are known as executioner caspases, activated by initiator caspases, which are capable of irreversibly triggering cell death (32). This controlled activation and execution of apoptosis has not been documented by previous studies on the Burmese python small intestine (Fig. 4A).

*Genes involved in intestinal function that are significantly differentially expressed*

In addition to gene expression programs related to regulation of cellular processes (e.g., cell division and apoptosis), we observed major shifts in expression in diverse classes of genes associated with the upregulation of digestive and absorptive functionality of the intestine upon feeding (15, 55). This included genes related to metabolism, transport, and hydrolase activity, which allow for increased absorption and processing of large meals. Physiological data also indicates rapid increases in absorption of D-glucose, L-proline, and L-leucine within the same time frame that genes for transporters and hydrolases for these types of nutrients are being rapidly upregulated (Figs. 5A & 5D-F). Genes related to trafficking and microvillus regulation are also upregulated rapidly upon feeding and act to expand (and later reduce) the surface area of the small intestine following feeding by facilitating the six-fold increase in microvillus length (6A & 5C). A likely method for this lengthening of intestinal microvilli upon feeding is the triggering of existing pools of cytoskeletal and linking proteins to migrate to the microvilli and insert at the tips; this is likely followed by *de novo* construction of new cytoskeletal proteins, membranes, regulatory, and trafficking molecules (51). The expansion of enterocyte volume and increase in microvillus length observed in physiological experiments (Figs. 5B-C) coincides well with this pattern of significant differential expression of candidate genes related to microvillus regulation and transport.

Here, and in previous studies, it has been demonstrated that extreme increases in nutrient absorption occur within the first 24-48 hours of feeding, along with large increases in metabolic rates and the mass of the organ (55, 57). In this study we have identified a number of associated candidate genes related to these shifts in phenotype and show coincident shifts in gene expression such that their expression levels mirror the physiology of the organ throughout digestion (Fig. 5A).

The discrete temporal regulation and the large number of coordinated, significant changes in gene expression observed in the python intestine post-feeding make it an excellent potential model for understanding the regulation of a number of important pathways, including cell cycle regulation, apoptosis, and WNT signaling in a physiological context in differentiated tissues of an adult vertebrate organ, as opposed to a developmental context in an undifferentiated embryonic tissue, for example. In most systems, the continuous nature of metabolism and growth obscures discrete gene expression regimes underlying such shifts in form and function because of the need for persistent and moderate activity. In contrast, examining the extreme physiological responses observed in the python may provide the opportunity to clarify fundamental relationships between gene expression and basic changes in vertebrate physiology. Our exploration of gene expression and analysis of candidate genes demonstrates that intestinal remodeling in pythons involves the regulation of gene expression programs associated with cell division, cytoskeletal remodeling, and apoptosis during growth and regression of the small intestine to modulate intestinal form, in addition to other gene expression programs regulating intestinal function (e.g., hydrolases and transporters).

Studies such as this one, that investigate extreme physiology and dramatic shifts in structural, functional and transcriptional dynamics, provide a new avenue for gaining novel insights into basic mechanisms controlling key aspects of vertebrate biology. This

may offer new information about the links between genotypes, phenotypes and adaptation in nature, and may also provide new information relevant to understanding and treating human disease. Damage of the intestinal tract can occur for various reasons in humans, including damage from cancer treatments using radiation or chemotherapeutics (33, 65), which can have chronic or even lethal effects, or complications due to inflammatory bowel disease, such as Crohn's Disease or ulcerative colitis (3). Using the Burmese python as a model system for understanding how the vertebrate intestine may be regulated to induce shifts in form and function is therefore potentially relevant for understanding diseases and conditions that affect the intestine, and for understanding how intestinal regulation may be modulated to treat various diseases. Additionally, colorectal and intestinal cancers (5, 24, 48), and many other types of cancers (48, 68), involve dysregulation of WNT signaling. Evidence that python intestinal remodeling involves cell division and apoptosis, modulated at least in part by WNT signaling, suggests the python intestine may represent a valuable model for studying the interactions of metabolism with the regulation of cell division/death and WNT signaling relevant to cancer.

## References


1. **Adade CM, Cons BL, Melo PA, and Souto-Padron T**. Effect of Crotalus viridis viridis snake venom on the ultrastructure and intracellular survival of Trypanosoma cruzi. *Parasitology* 1-13, 2010.

2. **Andersen JB, Rourke BC, Caiozzo VJ, Bennett AF, and Hicks JW**. Physiology: postprandial cardiac hypertrophy in pythons. *Nature* 434: 37-38, 2005.

3. **Baumgart DC, and Sandborn WJ**. Inflammatory bowel disease: clinical aspects and established and evolving therapies. *Lancet* 369: 1641-1657, 2007.

4. **Bertoli C, Skotheim JM, and de Bruin RA**. Control of cell cycle transcription during G1 and S phases. *Nature reviews Molecular cell biology* 14: 518-528, 2013.

5. **Bienz M, and Clevers H**. Linking colorectal cancer to Wnt signaling. *Cell* 103: 311-320, 2000.

6. **Brantjes H, Barker N, van Es J, and Clevers H**. TCF: Lady Justice casting the final verdict on the outcome of Wnt signalling. *Biological chemistry* 383: 255-261, 2002.

7. **Camacho C, Coulouris G, Avagyan V, Ma N, Papadopoulos J, Bealer K, and Madden TL**. BLAST+: architecture and applications. *BMC Bioinformatics* 10: 421, 2009.

8. **Cande C, Cecconi F, Dessen P, and Kroemer G**. Apoptosis-inducing factor (AIF): key to the conserved caspase-independent pathways of cell death? *J Cell Sci* 115: 4727-4734, 2002.

9. **Carey HV, and Sills NS**. Hibernation enhances D-glucose uptake by intestinal brush border membrane vesicles in ground squirrels. *J Comp Physiol B* 166: 254-261, 1996.

10. **Castoe TA, de Koning AP, Hall KT, Card DC, Schield DR, Fujita MK, Ruggiero RP, Degner JF, Daza JM, Gu W, Reyes-Velasco J, Shaney KJ, Castoe JM, Fox SE, Poole AW, Polanco D, Dobry J, Vandewege MW, Li Q, Schott RK, Kapusta A, Minx P, Feschotte C, Uetz P, Ray DA, Hoffmann FG, Bogden R, Smith EN, Chang BS, Vonk FJ, Casewell NR, Henkel CV, Richardson MK, Mackessy SP, Bronikowski AM, Yandell M, Warren WC, Secor SM, and Pollock DD**. The Burmese python genome reveals the molecular basis for extreme adaptation in snakes. *Proc Natl Acad Sci U S A* 110: 20645-20650, 2013.

11. **Castoe TA, Fox SE, Jason de Koning A, Poole AW, Daza JM, Smith EN, Mockler TC, Secor SM, and Pollock DD**. A multi-organ transcriptome resource for the Burmese Python (Python molurus bivittatus). *BMC research notes* 4: 310, 2011.

12. **Clevers H**. Wnt/beta-catenin signaling in development and disease. *Cell* 127: 469-480, 2006.

13. **Cohn MJ, and Tickle C**. Developmental basis of limblessness and axial patterning in snakes. *Nature* 399: 474-479, 1999.

14. **Conesa A, Nueda MJ, Ferrer A, and Talon M**. maSigPro: a method to identify significantly differential expression profiles in time-course microarray experiments. *Bioinformatics* 22: 1096-1102, 2006.

15. **Cox CL, and Secor SM**. Matched regulation of gastrointestinal performance in the Burmese python, Python molurus. *The Journal of experimental biology* 211: 1131-1140, 2008.

16. **Cross RA, and McAinsh A**. Prime movers: the mechanochemistry of mitotic kinesins. *Nature reviews Molecular cell biology* 15: 257-271, 2014.

17. **Daugas E, Nochy D, Ravagnan L, Loeffler M, Susin SA, Zamzami N, and Kroemer G**. Apoptosis-inducing factor (AIF): a ubiquitous mitochondrial oxidoreductase involved in apoptosis. *FEBS Lett* 476: 118-123, 2000.

18. **Day R, Tibbetts IR, and Secor SM**. Physiological responses to short-term fasting among herbivorous, omnivorous, and carnivorous fishes. *J Comp Physiol B* 184: 497-512, 2013.

19. **Di-Poi N, Montoya-Burgos JI, Miller H, Pourquie O, Milinkovitch MC, and Duboule D**. Changes in Hox genes' structure and function during the evolution of the squamate body plan. *Nature* 464: 99-103, 2010.

20. **Dunel-Erb S, Chevalier C, Laurent P, Bach A, Decrock F, and Le Maho Y**. Restoration of the jejunal mucosa in rats refed after prolonged fasting. *Comp Biochem Physiol A Mol Integr Physiol* 129: 933-947, 2001.

21. **Ernst J, and Bar-Joseph Z**. STEM: a tool for the analysis of short time series gene expression data. *BMC Bioinformatics* 7: 191, 2006.

22. **Gartel AL, and Radhakrishnan SK**. Lost in transcription: p21 repression, mechanisms, and consequences. *Cancer Res* 65: 3980-3985, 2005.

23. **Gomez C, Ozbudak EM, Wunderlich J, Baumann D, Lewis J, and Pourquie O**. Control of segment number in vertebrate embryos. *Nature* 454: 335-339, 2008.

24. **Gregorieff A, and Clevers H**. Wnt signaling in the intestinal epithelium: from endoderm to cancer. *Genes & development* 19: 877-890, 2005.

25. **Helmstetter C, Reix N, T'Flachebba M, Pope RK, Secor SM, Le Maho Y, and Lignot JH**. Functional changes with feeding in the gastro-intestinal epithelia of the Burmese python (Python molurus). *Zoolog Sci* 26: 632-638, 2009.

26. **Hoeflich KP, Eby MT, Forrest WF, Gray DC, Tien JY, Stern HM, Murray LJ, Davis DP, Modrusan Z, and Seshagiri S**. Regulation of ERK3/MAPK6 expression by BRAF. *Int J Oncol* 29: 839-849, 2006.

27. **Joo E, Surka MC, and Trimble WS**. Mammalian SEPT2 is required for scaffolding nonmuscle myosin II and its kinases. *Developmental cell* 13: 677-690, 2007.

28. **Karasov WH, and Diamond JM**. A Simple Method for Measuring Intestinal Solute Uptake Invitro. *Journal of Comparative Physiology* 152: 105-116, 1983.

29. **Karasov WH, Pond RS, 3rd, Solberg DH, and Diamond JM**. Regulation of proline and glucose transport in mouse intestine by dietary substrate levels. *Proc Natl Acad Sci U S A* 80: 7674-7677, 1983.

30. **Kim KK, Chamberlin HM, Morgan DO, and Kim SH**. Three-dimensional structure of human cyclin H, a positive regulator of the CDK-activating kinase. *Nat Struct Biol* 3: 849-855, 1996.

31. **Kohlsdorf T, Cummings MP, Lynch VJ, Stopper GF, Takahashi K, and Wagner GP**. A molecular footprint of limb loss: sequence variation of the autopodial identity gene Hoxa-13. *J Mol Evol* 67: 581-593, 2008.

32. **Lamkanfi M, Festjens N, Declercq W, Vanden Berghe T, and Vandenabeele P**. Caspases in cell survival, proliferation and differentiation. *Cell death and differentiation* 14: 44-55, 2007.

33. **Lee CS, Ryan EJ, and Doherty GA**. Gastro-intestinal toxicity of chemotherapeutics in colorectal cancer: the role of inflammation. *World journal of gastroenterology : WJG* 20: 3751-3761, 2014.

34. **Lignot JH, Helmstetter C, and Secor SM**. Postprandial morphological response of the intestinal epithelium of the Burmese python (Python molurus). *Comp Biochem Physiol A Mol Integr Physiol* 141: 280-291, 2005.

35. **Locksley RM, Killeen N, and Lenardo MJ**. The TNF and TNF receptor superfamilies: integrating mammalian biology. *Cell* 104: 487-501, 2001.

36. **Lolli G, and Johnson LN**. CAK-Cyclin-dependent Activating Kinase: a key kinase in cell cycle control and a target for drugs? *Cell Cycle* 4: 572-577, 2005.

37. **Matsubara K, Tarui H, Toriba M, Yamada K, Nishida-Umehara C, Agata K, and Matsuda Y**. Evidence for different origin of sex chromosomes in snakes, birds, and mammals and step-wise differentiation of snake sex chromosomes. *Proc Natl Acad Sci U S A* 103: 18190-18195, 2006.

38. **McDonald ER, 3rd, and El-Deiry WS**. Suppression of caspase-8- and -10-associated RING proteins results in sensitization to death ligands and inhibition of tumor cell growth. *Proc Natl Acad Sci U S A* 101: 6170-6175, 2004.

39. **Misch DW, Giebel PE, and Faust RG**. Intestinal microvilli: responses to feeding and fasting. *European journal of cell biology* 21: 269-279, 1980.

40. **Morgan DO**. Principles of CDK regulation. *Nature* 374: 131-134, 1995.

41. **Muncan V, Faro A, Haramis AP, Hurlstone AF, Wienholds E, van Es J, Korving J, Begthel H, Zivkovic D, and Clevers H**. T-cell factor 4 (Tcf7l2) maintains proliferative compartments in zebrafish intestine. *EMBO reports* 8: 966-973, 2007.

42. **Nguyen TB, Manova K, Capodieci P, Lindon C, Bottega S, Wang XY, Refik-Rogers J, Pines J, Wolgemuth DJ, and Koff A**. Characterization and expression of mammalian cyclin b3, a prepachytene meiotic cyclin. *The Journal of biological chemistry* 277: 41960-41969, 2002.

43. **Norbury C, and Nurse P**. Animal cell cycles and their control. *Annual review of biochemistry* 61: 441-470, 1992.

44. **Ott BD, and Secor SM**. Adaptive regulation of digestive performance in the genus Python. *The Journal of experimental biology* 210: 340-356, 2007.

45. **Overgaard J, Busk M, Hicks JW, Jensen FB, and Wang T**. Respiratory consequences of feeding in the snake Python molorus. *Comp Biochem Physiol A Mol Integr Physiol* 124: 359-365, 1999.

46. **Petersen CP, and Reddien PW**. Wnt signaling and the polarity of the primary body axis. *Cell* 139: 1056-1068, 2009.

47. **Piekny A, Werner M, and Glotzer M**. Cytokinesis: welcome to the Rho zone. *Trends in cell biology* 15: 651-658, 2005.

48. **Polakis P**. Wnt signaling and cancer. *Genes & development* 14: 1837-1851, 2000.

49. **Riquelme CA, Magida JA, Harrison BC, Wall CE, Marr TG, Secor SM, and Leinwand LA**. Fatty acids identified in the Burmese python promote beneficial cardiac growth. *Science* 334: 528-531, 2011.

50. **Robinson MD, McCarthy DJ, and Smyth GK**. edgeR: a Bioconductor package for differential expression analysis of digital gene expression data. *Bioinformatics* 26: 139-140, 2010.

51. **Secor SM**. Digestive physiology of the Burmese python: broad regulation of integrated performance. *The Journal of experimental biology* 211: 3767-3774, 2008.

52. **Secor SM**. Evolutionary and cellular mechanisms regulating intestinal performance of amphibians and reptiles. *Integr Comp Biol* 45: 282-294, 2005.

53. **Secor SM**. Gastric function and its contribution to the postprandial metabolic response of the Burmese python Python molurus. *The Journal of experimental biology* 206: 1621-1630, 2003.

54. **Secor SM**. Physiological responses to feeding, fasting and estivation for anurans. *The Journal of experimental biology* 208: 2595-2608, 2005.

55. **Secor SM, and Diamond J**. Adaptive responses to feeding in Burmese pythons: pay before pumping. *The Journal of experimental biology* 198: 1313-1325, 1995.

56. **Secor SM, and Diamond J**. Determinants of the postfeeding metabolic response of Burmese pythons, Python molurus. *Physiological zoology* 70: 202-212, 1997.

57. **Secor SM, and Diamond J**. Effects of meal size on postprandial responses in juvenile Burmese pythons (Python molurus). *The American journal of physiology* 272: R902-912, 1997.

58. **Secor SM, and Diamond J**. A vertebrate model of extreme physiological regulation. *Nature* 395: 659-662, 1998.

59. **Secor SM, and Diamond JM**. Evolution of regulatory responses to feeding in snakes. *Physiol Biochem Zool* 73: 123-141, 2000.

60. **Secor SM, Fehsenfeld D, Diamond J, and Adrian TE**. Responses of python gastrointestinal regulatory peptides to feeding. *P Natl Acad Sci USA* 98: 13637-13642, 2001.

61. **Secor SM, Lane JS, Whang EE, Ashley SW, and Diamond J**. Luminal nutrient signals for intestinal adaptation in pythons. *American journal of physiology Gastrointestinal and liver physiology* 283: G1298-1309, 2002.

62. **Secor SM, and Ott BD**. Adaptive correlation between feeding habits and digestive physiology for boas and python. In: *Biology of the boas and pythons*. Eagle Mountain, Utah: Eagle Mountain Publishing, 2007.

63. **Secor SM, Stein ED, and Diamond J**. Rapid upregulation of snake intestine in response to feeding: a new model of intestinal adaptation. *The American journal of physiology* 266: G695-705, 1994.

64. **Secor SM, and White SE**. Prioritizing blood flow: cardiovascular performance in response to the competing demands of locomotion and digestion for the Burmese python, Python molurus. *Journal of Experimental Biology* 213: 78-88, 2010.

65. **Shadad AK, Sullivan FJ, Martin JD, and Egan LJ**. Gastrointestinal radiation injury: symptoms, risk factors and mechanisms. *World journal of gastroenterology : WJG* 19: 185-198, 2013.

66. **Starck JM, and Beese K**. Structural flexibility of the intestine of Burmese python in response to feeding. *The Journal of experimental biology* 204: 325-335, 2001.

67. **Sun MY, Wei YY, Yao LY, Xie JH, Chen XN, Wang HZ, Jiang JH, and Gu JX**. Identification of extracellular signal-regulated kinase 3 as a new interaction partner of cyclin D3. *Biochem Bioph Res Co* 340: 209-214, 2006.

68. **Taipale J, and Beachy PA**. The Hedgehog and Wnt signalling pathways in cancer. *Nature* 411: 349-354, 2001.

69. **Tempone AG, Sartorelli P, Mady C, and Fernandes F**. Natural products to anti-trypanosomal drugs: an overview of new drug prototypes for American Trypanosomiasis. *Cardiovasc Hematol Agents Med Chem* 5: 222-235, 2007.

70. **Wall CE, Cozza S, Riquelme CA, McCombie WR, Heimiller JK, Marr TG, and Leinwand LA**. Whole transcriptome analysis of the fasting and fed Burmese python heart: insights into extreme physiological cardiac adaptation. *Physiol Genomics* 43: 69-76, 2011.

71. **Wiley SR, Schooley K, Smolak PJ, Din WS, Huang CP, Nicholl JK, Sutherland GR, Smith TD, Rauch C, Smith CA, and et al.** Identification and characterization of a new member of the TNF family that induces apoptosis. *Immunity* 3: 673-682, 1995.

Tables

Table 1.1. **Sampling design and number of mapped reads per sample.** The number of reads mapped to at least one transcript from the Burmese python transcriptome. Each row represents a single replicate (individual animal), which are grouped by timepoint. Mapped reads are composed of RNAseq reads generated using cross-sectional (SI) or mucosal (Muc) samples of intestinal tissue or from both types of sampling.

| Sample | Mass (g) | Tissue | Timepoint | Mapped Reads |
|---|---|---|---|---|
| AI6 | 462.5 | SI | 0h | 1,511,751 |
| AJ6 | 445.8 | SI | 0h | 3,965,717 |
| Ai8 | 414.5 | SI | 0h | 800,799 |
| U25 | 5,800 | SI | 0h | 372,003 |
| AF2 | 581 | SI | 0h | 950,773 |
| S19 | 868.4 | Muc | 0h | 203,389 |
| AJ7 | 610 | SI | 6h | 881,249 |
| AJ7 | 610 | Muc | 6h | 1,492,138 |
| Ak25 | 725 | SI | 6h | 1,626,270 |
| Ak25 | 725 | Muc | 6h | 403,645 |
| R27 | 815.7 | Muc | 6h | 590,892 |
| W11 | 788.7 | Muc | 6h | 532,607 |
| Ak4 | 635 | SI | 12h | 936,987 |
| Ak4 | 635 | Muc | 12h | 928,321 |
| Ak10 | 747 | Muc | 12h | 936,420 |
| U7 | 796.3 | Muc | 12h | 797,731 |
| U13 | 774.8 | Muc | 12h | 654,142 |
| Z14 | 467 | SI | 24h | 3,420,055 |
| V43 | 782 | SI | 24h | 678,000 |
| Z18 | 525 | SI | 24h | 596,198 |
| W20 | 797.8 | SI | 24h | 1,280,360 |
| S6 | 809 | SI | 24h | 1,281,658 |
| S6 | 809 | Muc | 24h | 974,889 |
| Y5 | 839 | SI | 96h | 1,911,844 |
| Y18 | 971 | SI | 96h | 2,099,417 |
| Y23 | 802 | SI | 96h | 1,016,261 |
| Y24 | 957 | SI | 96h | 871,196 |
| V40 | 867.5 | SI | 96h | 503,975 |
| W2 | 807.7 | Muc | 96h | 235,595 |
| W22 | 764 | SI | 10d | 481,585 |
| W22 | 764 | Muc | 10d | 923,344 |
| U1 | 767.9 | Muc | 10d | 532,607 |
| V29 | 825 | Muc | 10d | 2,688,732 |
| W12 | 981.6 | Muc | 10d | 799,404 |

Table 1.2. **Numbers of significantly differentially expressed genes between pre- and post-feeding timepoints.** For each pairwise timepoint comparison, the number of up and downregulated genes, as inferred using pairwise analysis (Benjamini-Hochberg corrected p-value < 0.05), is indicated.

| | Timepoint comparisons | | | | | | | |
|---|---|---|---|---|---|---|---|---|
| | 0h-6h | 6h-12h | 12h-24h | 24h-96h | 96h-10d | 0h-24h | 0h-96h | 0h-10d |
| UP | 1,367 | 2 | 11 | 498 | 202 | 1,468 | 730 | 25 |
| DOWN | 1,122 | 22 | 5 | 366 | 336 | 1,225 | 469 | 6 |

Figures

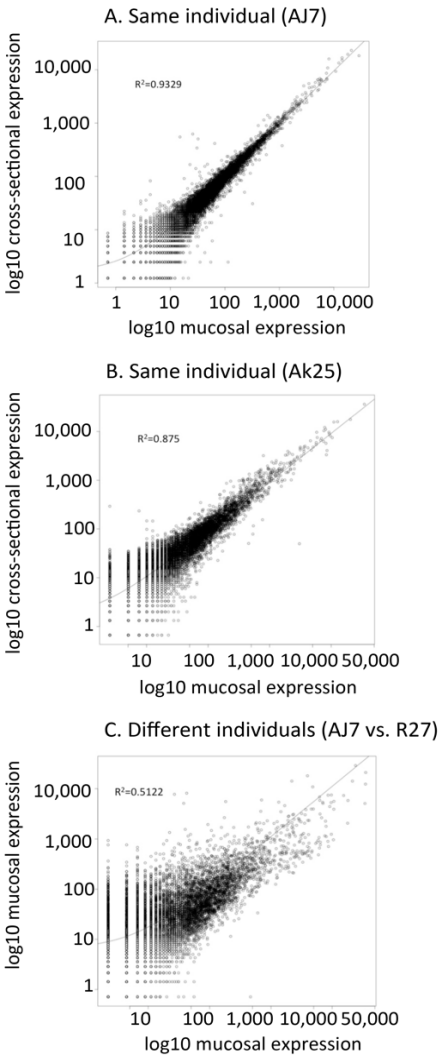


Figure 1.1. **Scatterplots comparing gene expression in intestinal mucosal and intestinal cross-section samples.** (A) Mucosal and cross-sectional samples from individual AJ7. (B) Mucosal and cross-sectional samples from individual Ak25. (C) Mucosal samples from two different individuals (AJ7 and R27). It is clear that the two different types of samples (cross-sectional and mucosal) from the same individual (A & B) are more similar than the same type of sample from different individuals (C).

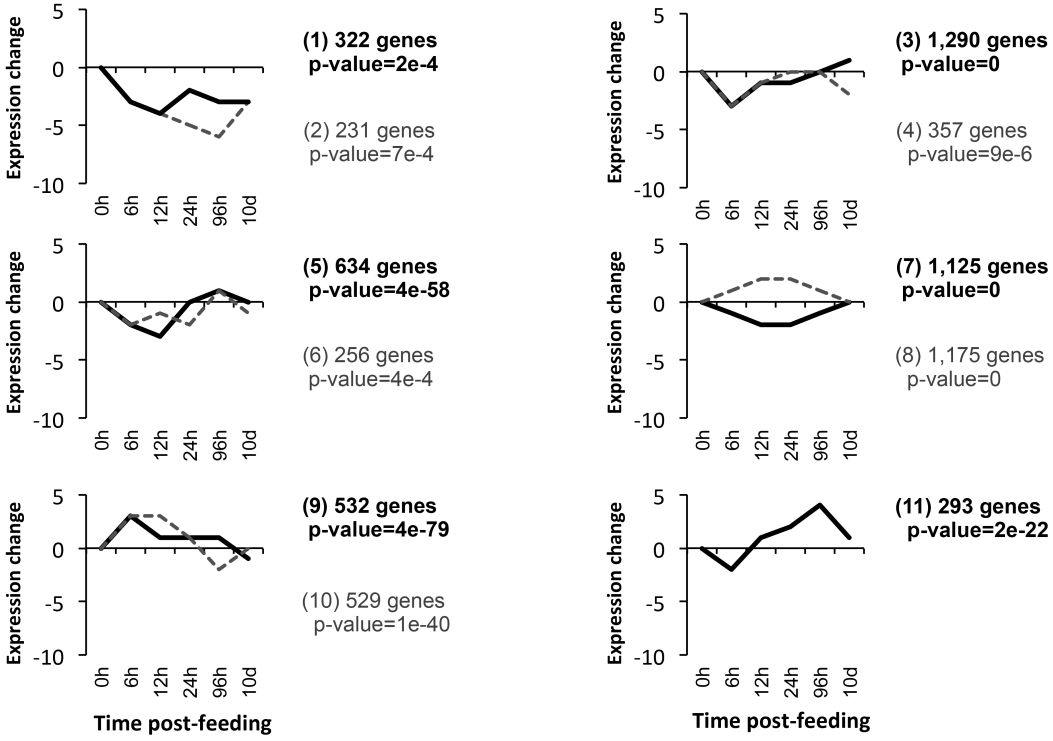


Figure 1.2. **General trends in gene expression across post-fed timepoints in the Burmese python intestine analyzed using STEM time-series analyses.** Generalized trends in gene expression that are significantly overrepresented in the python small intestine based upon cluster analysis of gene expression profiles and identification of statistically over-populated profiles. The numbers of genes clustered and p-value of these clusters is shown along with linear trends in expression.

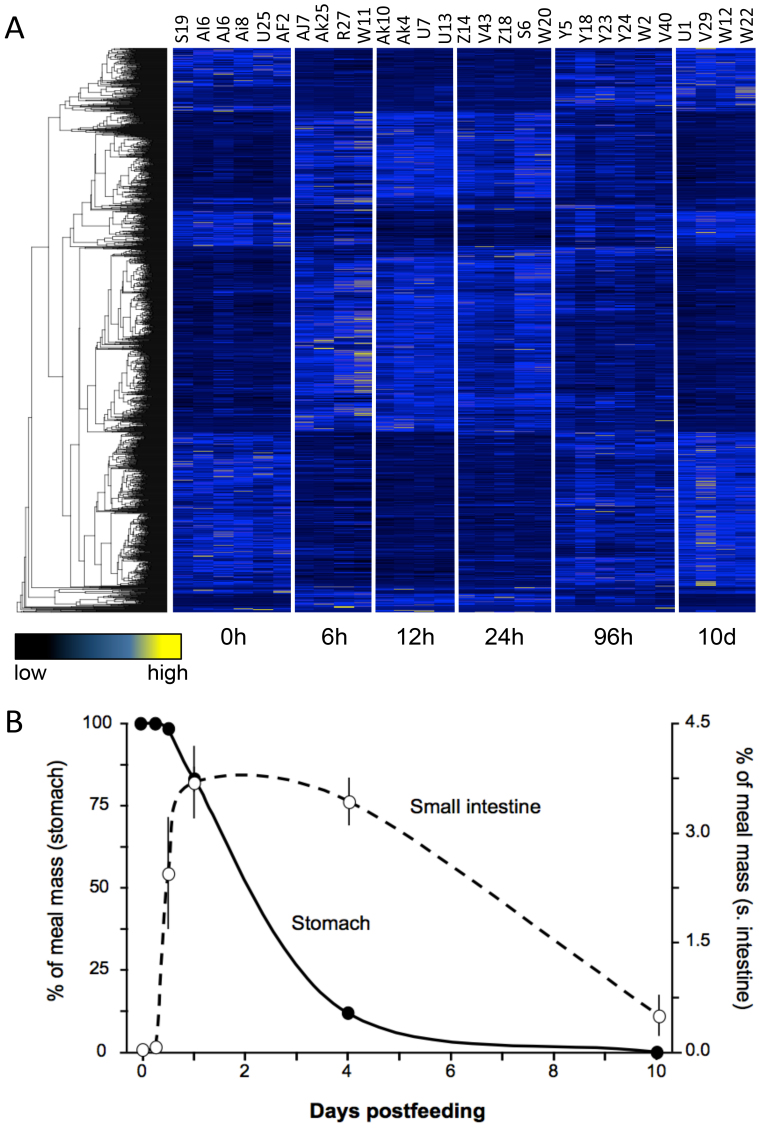


Figure 1.3. **General trends of gene expression and digestion across post-fed timepoints.** (A) Heatmap of gene expression for 1,772 genes found to be significantly differentially expressed across tiempoints based on regression analysis. Each column respresents a replicate, with timepoints clearly delimited, and each row represents a gene, which are clustered by similiarity using average linkage hierarchical clustering. (B) Percent mass of meal in stomach (filled circles and solid line) and small intestine (open circles and dashed line) across post-feeding timepoints.

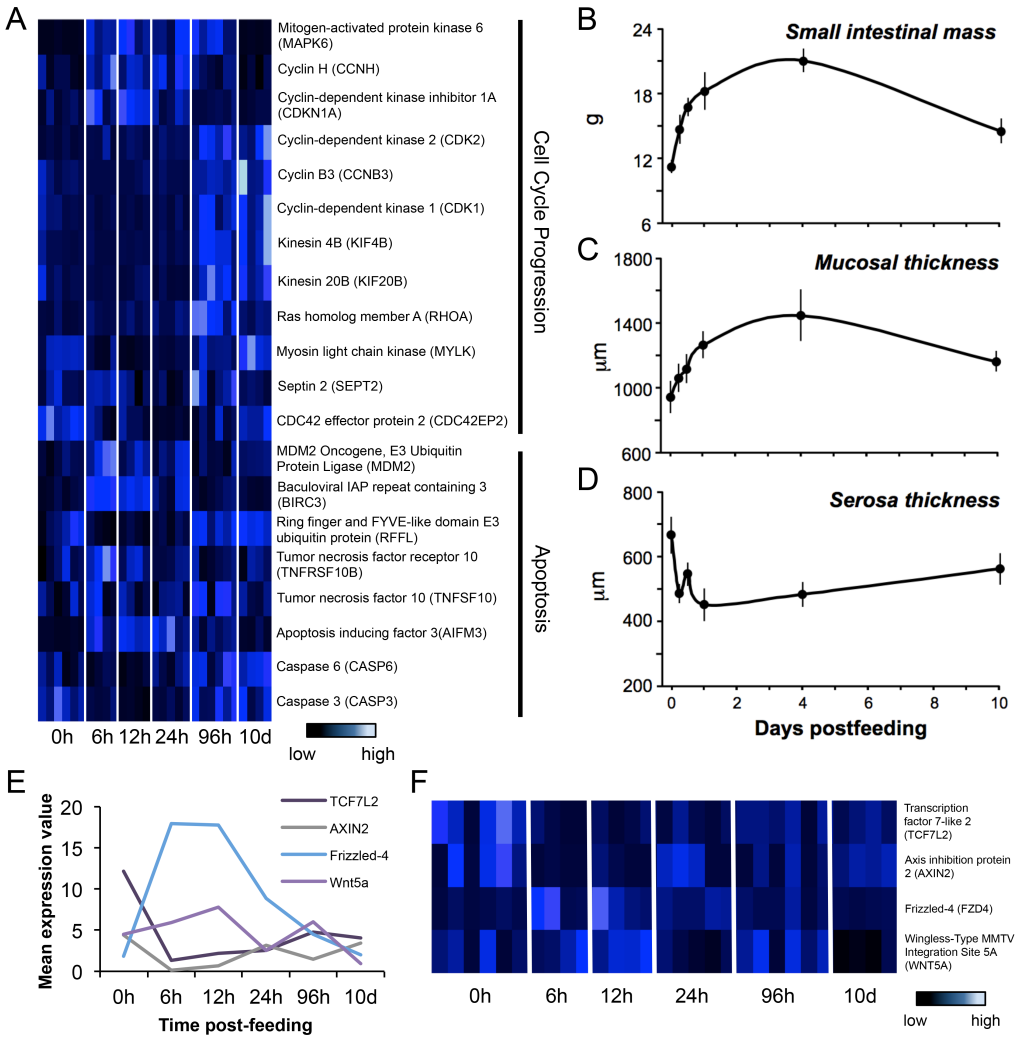


Figure 1.4. **Patterns of expression for genes involved in cell cycling, apoptosis, and WNT signaling along with corresponding physiological changes in the small intestine.** (A) Heatmap of genes involved in cell cycle progression and apoptosis that were shown to be significantly differentially expressed across timepoints, identified from pairwise and regression analysis. (B) Change in small intestinal mass across time. (C) Change in mucosal thickness across time. (D) Change in serosa thickness across time. (E) Average expression values for Wnt signaling genes plotted across post-fed timepoints. (F) Heatmap of expression values for all replicates across post-fed timepoints, with each row representing a gene and each column representing an individual, which are manually clustered by timepoints. This pathway is known to be important in development and processes such as asymmetric cell division.

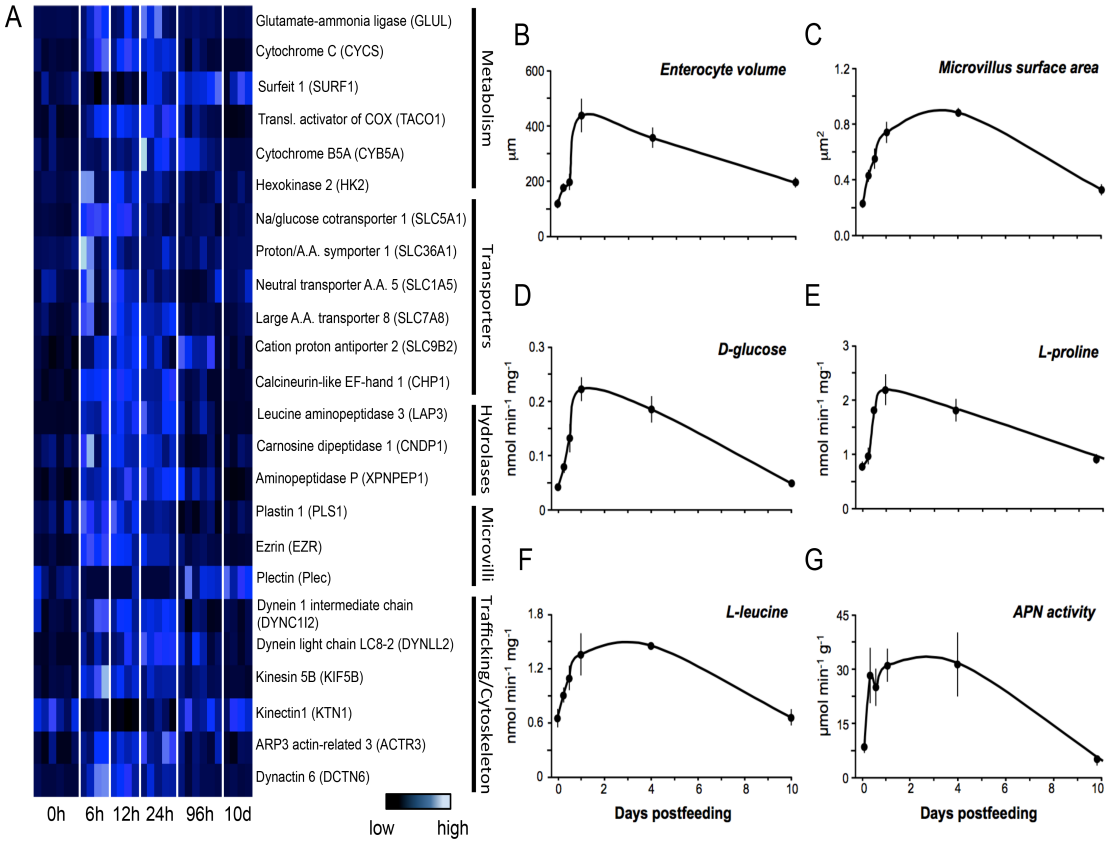


Figure 1.5. **Patterns of expression for genes involved with intestinal form and function alongside corresponding morphological or physiological changes in the small intestine.** (A) Heatmap of genes involved in various intestinal functional processes that were shown to be significantly differentially expressed across timepoints via pairwise or regression analysis. (B) Change in enterocyte volume through time. (C) Change in microvillus surface area across time post-feeding. (D) Change in absorption of D-glucose across post-fed timepoints. (E) Change in absorption of L-proline across post-fed timepoints. (F) Change in absorption of L-leucine across post-fed timepoints. (G) Change in activity of aminopeptidase N (APN) across post-fed timepoints.

Chapter 2

# Growth and stress response mechanisms underlying post-feeding regenerative organ growth in the Burmese python

Andrew et al. 2017, *BMC Genomics*

## Introduction

The ability to massively downregulate metabolic and physiological functions during extended periods of fasting has evolved in multiple species of snakes. This downregulation of physiological form includes the atrophy of organs such as the heart, kidney, liver, and small intestine. Upon feeding, the size and function of these organs, along with oxidative metabolism, is massively upregulated to accommodate digestion [1-4]. Of the snake species that experience these large fluctuations in physiology, the Burmese python (*Python molurus bivittatus*) is the most well-studied [5]. Within 48 hours of feeding, Burmese pythons can undergo up to a 44-fold increase in metabolic rate and >100-fold increases in plasma triglyceride content [3, 6]. Major organs also experience dramatic shifts in physiological form, including 40-100% increases in the mass of the heart, liver, pancreas, kidneys, and small intestine [2, 7-10]. This extreme organ regenerative growth and atrophy is unparalleled across vertebrates, and studies indicate that this organ growth is driven by multiple cellular processes, including cellular hypertrophy in the heart and mixtures of hypertrophy and hyperplasia in the kidney, liver, and small intestine [3, 5, 11, 12]. Organ growth peaks around 1-2 days post-feeding (DPF), and by 10-14DPF, organ form and function, as well as gene expression patterns, have completely reversed back to fasted levels [1, 2, 5, 7-9, 13].

Previous studies have examined aspects of this post-feeding response using morphological and physiological assays [2, 3, 7, 14-16], analyses of gene expression [5, 13], and combinations of the two [5, 14]. Together, these studies have demonstrated that transcriptional responses following feeding are extremely rapid and massive, both in the magnitude of expression changes and in the number of genes with significant differential expression. Genes important in a number of developmental, metabolic, proliferative, apoptotic, and growth processes have been shown to be involved in these major shifts in organ form and function [5, 11, 13]. Previous studies have shown that mammalian cells respond to the growth signals in post-fed python serum, which likely indicates a conserved response to core signaling molecules [11, 17]. We therefore hypothesize that a relatively small number of core molecular regulatory molecules and signaling pathways may underlie these responses. However, the identification of a core set of upstream regulatory molecules and mechanisms has been hindered by the large number of genes that are significantly differentially expressed during this response, making manual interpretation of this gene expression data difficult. Additionally, the lack of comparable replicated sampling across multiple organs has further prevented meaningful across-organ comparisons of changes in gene expression in previous studies [13]. Accordingly, major gaps remain in our understanding of the specific mechanisms and growth pathways that are responsible for driving these extreme shifts in Burmese python organ size and function, as well as how these mechanisms may vary across different organ systems.

Our previous study of the Burmese python feeding response addressed some gaps through the use of increased replicates and more frequent time point sampling for one organ, the small intestine [5]. We identified over 1,700 genes that were significantly differentially expressed during post-feeding regeneration in the small intestine with many

of these genes being functionally linked to cellular processes such as WNT signaling, cell cycling, and apoptosis. This study also linked changes in gene expression with functional and phenotypic shifts by comparing RNAseq data with physiological and histological data. This detailed analysis was only conducted on the small intestine, however, and failed to address any upper-level signaling mechanisms and pathways.

Here, we leverage fully replicated organ-specific time courses detailing gene-level responses to infer canonical pathways and regulatory molecules driving post-feeding organ growth in the Burmese python. We examined gene expression across four major organ systems – the heart, liver, kidney, and small intestine. We combined increased replicated sampling with statistical inferences of pathway activation and regulatory molecule prediction to identify the mechanistic drivers of cross-tissue, post-feeding organ regeneration. Despite highly organ-specific gene expression responses associated with organ regenerative growth, we found evidence for high degrees of overlap in predicted pathways and regulatory molecules underlying these growth processes between organs. Pathways predicted to be involved in regulating this physiological response include LXR/RXR activation, PI3K/AKT, and mTOR signaling. Interestingly, we also found strong and consistent evidence for the involvement of NRF2-mediated oxidative stress response and other stress-response pathways in this extreme example of rapid organ growth. Our results suggest that post-feeding, regenerative organ growth in the Burmese python may stem from small numbers of key effector molecules mediating a core set of growth and stress-response pathways, which in turn activate diverse, tissue-specific signaling cascades.

## Materials and Methods

### *Feeding experiments*

Burmese pythons were obtained from commercial breeders. All animal care and tissue sampling was conducted using protocols approved by the University of Alabama Institutional Animal Care and Use Committee (14-06-0075). Burmese pythons were sampled at three physiological states: fasted (30 days since last meal), 1 day post-feeding (1DPF) and 4DPF, with the meal consumed equaling at least 25% of their body mass. Previous studies have shown that organ masses and functional phenotypes climax between 1 and 3 DPF [1, 2, 5, 9] and that phenotypes begin to decline by 4DPF [2, 3, 7, 9]. We therefore chose sampling time points here to capture gene expression patters during the period before phenotypes climax (1DPF) and early in their regression (4DPF). Snakes were humanely euthanized by severing the spinal cord immediately behind the head, and organs were immediately extracted, snap frozen in liquid nitrogen, and stored at -80°C. Between three and six biological replicates (i.e., animals) were sampled for each time point. See Additional file 1, Supplementary Methods for additional details.

### *Transcriptome library generation*

Total RNA was extracted from ~50mg of snap-frozen tissue using Trizol Reagent (Invitrogen), followed by mechanical cell disruption using a TissueLyzer for 10 minutes at 20 strokes/minute, and precipitation of RNA using isopropanol. Individual Illumina mRNAseq libraries were constructed using either the Illumina TruSeq RNAseq kit or the NEB Next RNAseq kit, both of which included poly-A selection, RNA fragmentation,

cDNA synthesis, and indexed Illumina adapter ligation. Completed RNAseq libraries were quantified on a BioAnalyzer (Agilent), pooled in equal molar ratios in various multiplex arrangements, and sequenced on either an Illumina GAIIx or Illumina HiSeq2000 (see Additional File 1, Table S1).

*Quantifying and visualizing gene expression*

Raw demultiplexed Illumina RNAseq reads were quality filtered and trimmed with Trimmomatic v. 0.32 [18]. In instances where the same library was sequenced in multiple different runs, reads were combined and mapped for each individual and time point. Mapping of reads to the reference transcriptome of the Burmese python [13] was conducted using BWA v. 0.6.1 [19] with the following parameters: mismatch penalty=2, gap open penalty=3, and alignment score minimum=20. Expression was determined using SAMtools v. 0.1.19 [20] by counting the number of unique gene reads that mapped to an annotated transcript, while excluding reads that mapped to multiple positions. New RNAseq data for various time points and replicates was analyzed together with previously published data from other individuals and replicates [5, 13]. Newly-generated sequencing data were archived on the NCBI Short Read Archive (NCBI: SRP051827).

Raw expression counts were normalized using TMM normalization in edgeR [21] and all statistical analyses of gene expression were conducted using normalized data. We identified genes that were significantly differentially expressed between time points using two approaches. First, we estimated significant changes in gene expression between pairs of time points using pairwise exact tests for the binomial distribution calculated in edgeR, integrating both common and tagwise dispersion [21]. Second, to accommodate the time-series nature of the experimental design, we also conducted step-wise regression analysis of gene expression in maSigPro [22]. Regression analysis

enabled the detection of genes with significant patterns of differential expression across all three time points. Gene expression heatmaps were generated in R and clustered with the package vegan [23], with gene clustering calculated using average linkage hierarchical clustering based on a Bray-Curtis dissimilarity matrix. We used the program STEM [24] to identify and visualize significant expression profiles for all genes in our RNAseq data.

*Assigning homology for functional analysis*

To facilitate the use of various pathway activation and regulatory molecule predictions, we annotated the full Burmese python transcript set [13] with orthologous human gene Ensembl [25] identifiers. Reciprocal tblastx was first conducted between *Anolis carolinensis* and Burmese python, and *Anolis* gene IDs identified as orthologous to python genes were converted to human Ensembl identifiers using homology tables from Ensembl's Biomart [26]. The same process of reciprocal best blast using tblastx was performed between Burmese python and *Gallus gallus*, followed by conversion of chicken Ensembl identifiers to human Ensembl identifiers using homology tables from Ensembl's Biomart [26]. We also performed reciprocal best blast of the python with *Homo sapiens*. Finally, we used one-way tblastx with anolis, chicken, and human to annotate python genes that were not assigned an ortholog from reciprocal best blast. Using this annotation approach, we were able to assign human Ensembl IDs to 22,393 of 25,385 total python reference transcripts.

*Pathway and upstream regulatory molecule analysis*

To infer the involvement of upstream regulatory molecules and pathways, we performed Core Analysis in Ingenuity Pathway Analysis (IPA; Qiagen), using default parameters. IPA uses gene identifiers and the fold-change value for each differentially

expressed gene to identify enrichment patterns for Canonical Pathway Analysis (CPA) and Upstream Regulatory Molecule Analysis (URMA), and to infer the activation direction (activated versus inhibited) between particular time points. These two analyses both use observed gene expression data to infer unobserved features (e.g., activation state of key signaling molecules), but differ fundamentally in how they use expression data to make inferences. CPA predicts the involvement and activation/inhibition of canonical pathways based on observed evidence from gene expression data, specifically for genes that participate as higher-level regulatory molecules within a given pathway; analysis of observed gene expression data incorporates information from the Ingenuity Knowledge Base (including genes known to be involved within a given pathway) to provide both a statistical value of enrichment and a prediction of the biological involvement for the pathway as a whole (i.e. activated or inhibited; IPA documentation, Qiagen). In contrast, URMA uses observed changes in gene expression specifically for genes at lower levels within pathways (e.g., low level effectors) to predict activation or inhibition of regulatory molecules upstream of these genes [27]. Due to differences in these approaches, together these two methods provide a well-rounded set of comparable inferences for dissecting molecular mechanisms (Fig. 1).

For IPA analyses, we used only genes identified as significant in pairwise differential expression analyses between time intervals (per organ), and we input fold changes per gene averaged across biological replicates, along with our estimate of the orthologous human Ensembl ID for each gene. Pathways important to cross-tissue physiological responses were isolated using the IPA CPA (included with Core Analysis), with a right-tailed Fisher's exact test p-value of less than 0.01. We examined only those pathways that were significant, based on a predicted activation z-score, in at least one of the four organs for at least one of the post-feeding time points. For IPA analyses, the z-

score is used to determine the statistical significance of the number of activated and inhibited predictions, and the sign of the value indicates the overall activation state (i.e., positive versus negative activation). We used a p-value cutoff of 0.01 for the CPA in IPA to reduce potentially spurious inferences. Upstream regulators and hypotheses for global signaling molecules were identified using URMA in IPA, with a Fisher's exact test overlap p-value threshold of 0.05. Pathway network figures were modified manually from predicted network figures generated in IPA. For analysis of specific pathways (mTOR signaling and NRF2-mediated oxidative stress response), we also determined the number of genes involved in each pathway that were assigned python orthologs by our orthology analyses, and how many of these genes were expressed at some level in our dataset (see Additional file 1, Table S2).

## Results

### *Trends in gene expression across organs*

We used our expression data from all python samples (see Additional file 1, Table S1) to examine the degree to which different organ systems 'turn on' upon feeding and then experience 'regression' towards pre-feeding patterns of expression at 4DPF. We found that for each organ, the majority of differentially expressed genes showed immediate up- or downregulation from fasting to 1DPF. Interestingly, each of the four organs examined appeared to experience regression towards fasting levels of expression by 4DPF to widely different extents, indicating that each organ may have its own unique temporal program of growth followed by atrophy. Across organs, the heart appeared to shift towards regression the fastest. Other organs experienced reversals of fasted to 1DPF expression shifts to varying degrees by 4DPF, ranging from the moderately paced

small intestine and kidney, to the slow-paced liver (Table 1). STEM analysis further supported these temporal patterns of up-regulation and regression across organs (see Additional file 1, Fig. S1).

Regression analysis across time points, which tends to be conservative, identified hundreds of genes that were significantly differentially expressed across all three time points with 722 genes in the heart, 750 genes in the kidney, 711 genes in the liver, and 1,284 genes in the small intestine. Of the 2,922 total genes differentially expressed across all four organs, 21% are unique to the heart, 16% are unique to the kidney, 15% are unique to the liver, and 32% are unique to the small intestine (Fig. 2). Only a single gene was identified as significant in all four organs across all time points: *coagulation factor X* (*F10*).

To further dissect patterns of expression change following feeding, we conducted pairwise analyses of gene expression between time points for each organ. In the heart, pairwise analyses identified 436 significantly differentially expressed genes between fasted and 1DPF (208 upregulated and 228 downregulated; Table 1), and 76 genes were significantly differentially expressed between 1DPF and 4DPF (36 upregulated and 40 downregulated). In the kidney, 344 genes were significantly differentially expressed between the fasted state and 1DPF (244 upregulated and 100 downregulated), while only 8 genes were significantly differentially expressed from 1DPF to 4DPF (5 upregulated and 3 downregulated). In contrast to the heart, we found many genes (147) significantly differentially expressed between fasted and 4DPF in the kidney. In the liver, 461 genes were differentially expressed within 1DPF (335 upregulated and 126 downregulated), while only 41 genes were significantly differentially expressed from 1DPF to 4DPF (29 upregulated and 12 downregulated). With 371 genes significantly differentially expressed between fasted and 4DPF, among all four organs, the liver was the least ‘reset’ to the

fasting condition by 4DPF. Finally, the small intestine showed higher levels of differential expression than the other three organs. Within 1DPF, 2,313 genes were significantly differentially expressed (1,271 upregulated and 1,042 downregulated). From 1DPF to 4DPF, 268 genes were upregulated and 146 genes were downregulated, and 892 genes were differentially expressed between fasted and 4DPF (Table 1).

*Genes and pathways implicated in differential expression in individual tissues*

To move beyond gene-specific responses and towards deciphering the mechanisms that may underlie growth responses across different organs, we identified pathways that were significantly activated/repressed between fasting and 1DPF (Fig. 3). We found consistent evidence that the NRF2 stress-response pathway is activated in all tissues, except in the heart, where there was insufficient data to determine the direction of activation. We also found relatively consistent evidence for activation of the related growth pathways mTOR and PI3K/AKT across organs, although this inference was most significant in the heart and small intestine. We also inferred the involvement of the related pathways: LXR/RXR, LPS/IL-1-mediated inhibition of RXR function, PPAR/RXR, and PPAR signaling in multiple organs; the direction of stimulation of these pathways was both variable across organs and inconclusive in some organs. Substantial involvement of cytoskeletal pathways, including Actin cytoskeleton signaling and Actin nucleation by ARP-WASP complex, was also inferred across organs and positive in the kidney and small intestine, yet negative or inconclusive for the heart and liver, respectively.

In addition to pathway activation/repression patterns shared across organs, a number of pathways showed substantial organ-specific directionality of response. Examples of this pattern include the growth-related AMPK signaling pathway (which was activated in the heart, repressed in the kidney and small intestine, and ambiguous in the

liver), ERK5 signaling (activated in the heart and repressed in the small intestine), and Integrin signaling (stimulated in the heart and repressed in the small intestine). Lastly, a number of pathways appeared to be organ-specific, including p38 MAPK and ERK5 signaling in the heart and 14-3-3-mediated signaling in the small intestine (Fig. 3).

*Upstream regulatory molecule analysis of 1 DPF responses*

Our inferences of upstream regulatory molecules (URMs) between the fasted and 1 DPF time points supported many of the same molecular mechanisms underlying organ growth identified via CPA, such as stress response, growth, and lipid signaling pathways. We explored URM predictions for all classes of URMs except biological drugs, chemicals, and microRNAs. We found that many predicted URMs were shared among organs, with 51 shared among all four organs. Predicted URMs also showed substantial organ-specific patterns, with a large number of URMs uniquely predicted for each organ. The heart showed the largest number of unique URM predictions (269), while only 123, 167, and 137 unique URMs were predicted in the kidney, liver, and small intestine, respectively (Fig. 4A).

To identify regulators with broadly relevant patterns across multiple organs, we focused on URMs predicted significantly in at least three organs and with moderate to high activation z-score ($z > |1.5|$) in at least one organ. A subset of the URMs meeting these criteria is shown in Fig. 4B, and the full set is shown in Additional file 1, Fig. S2. Many of these URM predictions coincided directly with predicted canonical pathways. NFE2L2 and ATF4, key regulators within the NRF2-mediated oxidative stress response pathway, were predicted to be strongly activated in the small intestine, liver, and kidney, consistent with the canonical pathway analysis predictions of activation of the overall NRF2 pathway in these three organs. We also predicted involvement of NFkB and NFkBIA, two key regulators within the NFkB signaling response pathway – this

inflammatory response pathway is thought to be inhibited by activation of the NRF2-mediated oxidative stress response pathway [28, 29]. NFkB was predicted to be inhibited in the liver and heart, weakly activated in the kidney, and absent in the small intestine, while NFkBIA was predicted to be inhibited in the liver, weakly activated in the heart and kidney, and again absent in the small intestine. Activation of the growth pathways mTOR and PI3K/AKT were additionally supported by activation of predicted regulators such as mTORC1 and RAF1, respectively, and the inhibition of PTEN. Lipid signaling pathways such as LXR/RXR signaling, LPS/IL-1-mediated inhibition of RXR function, PPAR/RXR, and PPAR signaling were supported by several predicted URMs such as PXR ligand, NR1H3, NR1I2, NR1I3, SREBF1, SREBF2, PPARA, PPARG, RXRA, PPARGC1A, and PPARGC1B (Fig. 4). These URMs were consistently predicted as activated in the small intestine, liver, and kidney and either absent or predicted as inhibited in the heart.

It is notable that while the inferences of activation directions of lipid signaling pathways across organs were largely ambiguous and sometimes inconsistent in our CPA (Fig. 3), the associated URMs display a consistent trend of predicted activation in the small intestine, liver, and kidney, and either predicted inhibition or absence in the heart (Fig. 4). Additionally, several URMs, particularly for the mTOR pathway, were predicted as inconsistent or even contradictory to the results of CPA or our experimental data. For example, while mTORC1 is predicted as significantly activated in the small intestine by URMA, this molecule is downregulated in our experimental data (see Discussion for details). Additionally, the mTOR protein that is involved in forming both of the main complexes of the mTOR signaling pathway (mTORC1 and mTORC2) is predicted to be strongly inhibited in the small intestine and weakly inhibited in the kidney and heart. Both of these URM predictions appear to contradict the positive activation of the mTOR signaling pathway inferred for the small intestine and heart as inferred from the CPA.

In addition to URMs involved in key predicted canonical pathways, upstream regulatory analysis predicted several other notable URMs with strong activation or informative trends across organs. Insulin and INSR were both predicted as strongly activated regulators in the kidney, liver, and small intestine, suggesting a possible role of insulin receptor signaling in facilitating this regenerative response, which is also consistent with activation of the mTOR pathway. Myc, a regulator within the ERK5 and p38 MAPK signaling pathways, was predicted as activated in all four organs, although strongest in the liver. Several regulators within the MAPK signaling pathway were also predicted in URMA, with ATF4 and ATF6 predicted as activated in the kidney, liver, and small intestine, and ERK predicted as activated in the kidney and inhibited in the heart and liver. These URMs suggest the involvement of the ERK and MAPK signaling pathways in this response, even though CPA predictions for these two pathways were not substantially strong (Figs. 3 & 4).

*Detailed dissection of NRF2 and mTOR pathway responses to feeding*

We were particularly interested in our findings that the NRF2 stress response and the mTOR growth pathways appear to be involved in post-feeding growth in multiple organs. To investigate these inferences further, we fully dissected evidence from our gene expression data for activation of these pathways by visualizing observed and inferred evidence for activation of these pathways in the context of IPA-generated pathway maps (Figs. 5-6; Additional file 1, Figs. S3-S6). Specifically, we generated pathway predictions that integrate both observed shifts in gene expression from our data (from fasting - 1DPF), and estimates of activation/inhibition of molecules downstream of these observed genes that are inferred based on canonical signaling patterns in these pathways. Relevant to our power to detect pathway-wide signals of activity, we were able

to associate over 70% of human genes within the mTOR and NRF2 pathways with python orthologs that were expressed at some level in our dataset (see Additional file 1, Table S2); thus, we expect that our power and degree of resolution of pathway activation for these particular pathways is quite good.

Pathways maps for mTOR responsiveness between fasted and 1DPF show both common and divergent patterns of pathway activation among organs (Figs. 5 & Additional file 1, Fig. S3). The heart (Fig. 5A) and kidney (see Additional file 1. Fig. S3) both show similar patterns of mTOR activation, including the activation of both the mTORC1 and mTORC2 complexes. Major differences in mTOR activation between these two organs includes strong evidence for downregulation of AMPK and the eIF4 complex in the heart, yet, no direct and/or clear evidence for up- or downregulation of these complexes in the kidney. In the small intestine, the mTOR pathway was inferred to be strongly downregulated, as is AKT; AMPK and the eIF4 complex showed mixed signs of activation (both positive and negative) (Fig. 5B). It is also notable that different organs showed different levels of internal consistency in the integration of results with the known functionality within the mTOR pathway. For example, the heart and kidney have either zero or one pathway connection in which gene expression results contradict the direction of activation of the pathway (pink arrows in Figs. 5A & Additional file 1, Fig. S3) – for the kidney this disagreement occurs in the relationship between RSK and inhibition of TSC1 (see Additional file 1, Fig. S3). In the small intestine, eight such disagreements occur (Fig. 5B), and most of these occur at the steps immediately above or below activation of mTORC1 and mTORC2 complexes. The liver was the only organ that contained no signal for the activation or repression of mTOR pathway (i.e., no differentially expressed genes in this pathway were observed). It should be noted that inferences for mTOR activation from CPA are at times contradictory to those identified via URMA (Figs. 3-5;

Additional file 1, Fig. S3). While predictions based on the pathway maps indicate downregulation of mTOR in the small intestine, the z-score suggests slight upregulation of this pathway during regenerative growth in this tissue. URMA predicts inhibition of the mTOR molecule in the heart, kidney, and small intestine, while mTORC1 activation is predicted in both the kidney and small intestine, and undefined in the heart. Thus, while mTOR involvement in organ regenerative growth is clear across organs, the relationships between pathway scores, molecule-level inferences, and URMs are complex.

Pathway maps for the NRF2-mediated oxidative stress response between fasted and 1DPF indicate consistent activation of this pathway in the kidney, liver, and small intestine (Fig. 6; Additional file 1, Figs. S4-S6). In addition to predicted responses inferred from CPA (Figs. 2 & 5; Additional file 1, Figs. S4-S6), multiple observed genes in our dataset downstream of NRF2 are upregulated in these three organs, including *thioredoxin* (TXN), *glutathione s-transferase mu 1* (GST), and *peroxiredoxin 1* (PRDX1), providing confirmatory evidence of NRF2 activation. The response of this pathway in the heart is, however, less clear (see Additional file 1, Fig. S4). In the heart, NRF2 responses were predicted based on the observed fold-change values of only four genes, and predictions suggest inhibition of this pathway in the heart (see Additional file 1, Fig. S4) although the direction (activation versus inhibition) was not statistically significant (Fig. 3). It is also notable that we observed differences in the inferred consistency of integrated gene expression results and activation/inhibition inferences across organs (Fig. 6; Additional file 1, Figs. S4-S6): in the heart, only two inconsistencies are observed while the kidney, liver, and intestine have one, two, or four inconsistencies, respectively. Inferences from URMA for the activation of NRF2 are highly consistent with activation inferences from CPA, including significant URM activation predicted for NFE2L1 in the liver and intestine and significant activation of NFE2L2 in kidney, liver, and small intestine

(Fig. 4). In contrast, upstream regulators of this pathway were not predicted to be significantly activated or inhibited in the heart, inconsistent with the predictions given in the pathway figure (Figs. 4 & Additional file 1, Fig. S4).

*Expression response between 1 and 4 DPF*

In comparison to expression between fasting and 1DPF, the IPA analyses conducted on genes differentially expressed between 1DPF and 4DPF across organs predicted a substantially smaller number of pathways as significantly enriched, the majority of which were predicted with ambiguous directions of activation. This is likely due to the substantially smaller number of significantly differentially expressed genes identified in all organs between 1DPF and 4DPF, which is expected because 4DPF represents a sampling time intermediate between the peaking of organ growth and the regression of these phenotypes. This time interval (1DPF-4DPF) aimed to capture the early stages of organs shifting expression towards organ atrophy and towards a reversion to the fasted state, and we expected to observe partial reversals in pathways predicted to be active between fasted and 1DPF, and perhaps additional new pathways involved in apoptosis and atrophy. However, we found few consistent or clear patterns of interpretable pathway involvement between the 1DPF and 4DPF time points (see Additional file 1, Fig. S7). Pathways predicted for this time interval include various pathways related to biosynthesis and stress response, such as unfolded protein response. We also inferred inconsistent involvement of these pathways across organs, and none were predicted with a direction of activation (see Additional file 1, Fig. S7). Only one pathway, mitotic roles of polo-like kinase, was predicted as significant and with a direction of activation between 1DPF and 4DPF, and was predicted only in the small intestine. While we did infer a single lipid signaling pathway that also was indicated by

CPA predictions from the fasted to 1DPF interval (LPS/IL-1 mediated inhibition of RXR function), the lack of predicted directions of activation and unclear involvement across organs prevents informative interpretation of the activity of this pathway between 1DPF and 4DPF. Collectively, these results suggest that the 4DPF time point may not be sufficient to capture shifts in gene expression that elucidate the mechanisms involved in the early stages of regression of organ phenotypes.

## Discussion

A detailed understanding of the molecular mechanisms capable of driving regenerative growth in vertebrates may provide important insights into the treatment of diverse human diseases. Because traditional vertebrate model systems offer limited insight into natural organ regenerative processes, non-traditional model systems, including snakes in general and Burmese pythons in particular, hold great potential for providing unique insights into vertebrate regenerative organ growth processes. In this study we have found that multiple integrated growth pathways, in addition to multiple stress-response pathways, appear to underlie the coordinated organ regenerative process in Burmese pythons upon feeding. Despite distinct patterns of gene expression associated with growth for each organ, pathway and upstream regulatory molecule analyses reveal substantial similarities in pathways associated with post-feeding, extreme-growth responses across multiple organs. Specifically, we found evidence for a consistent interactive role of three major types of pathways underlying growth responses in python organs following feeding, including the related growth pathways mTOR and PI3K/AKT, lipid-signaling pathways such as PPAR and LXR/RXR, and stress-response/cell-protective pathways including NRF2.

*mTOR and other growth pathways underlying organ growth*

Across the four organs examined, we found evidence for the involvement of the mTOR signaling pathway as a key integrator of growth signals underlying post-feeding regenerative organ growth. This pathway integrates processes for the use of energy and nutrients to regulate growth and homeostasis [30]. mTOR interacts with multiple other pathways, including PI3K/AKT, several lipid metabolism and signaling pathways [30, 31], and the NRF2-mediated oxidative stress response [32, 33] – all of which are also active in multiple organs during growth (Figs. 3-5). mTOR complex 1 (mTORC1) is the most well-characterized of the two mTOR complexes and integrates signaling from growth factors, energy status, oxygen, and amino acids to promote cell growth when activated [31]. The TSC1/2 complex transmits upstream signals from growth factor and insulin signaling to modulate the activity of mTORC1 and its interaction with other pathways including PI3K/AKT [30, 31, 34]. The effector kinases of these external pathways inactivate the TSC complex through phosphorylation, thus, indirectly activating mTORC1 [30, 31]. AKT can also directly activate mTORC1 through phosphorylation of an mTORC1 inhibitor. In a low energy state, AMPK inhibits mTORC1 by phosphorylating regulatory associated protein of mTORC1 (RAPTOR) [30, 31]. mTORC2 signaling is less well-understood, but is known to respond to growth factors through PI3K signaling [30].

CPA of gene expression in the first 24 hours after feeding indicate that involvement of the mTOR signaling pathway is significant in the small intestine (predicted activation), but insignificant in both the heart (predicted activation) and kidney (activation state undetermined). The liver lacked evidence of involvement of the mTOR signaling pathway from CPA (Figs. 3-4). In URM analysis, the mTOR molecule itself was predicted to be downregulated in the heart, liver, and intestine with no presence in the kidney,

which contrasts our CPA results (Figs. 3-4). However, URMA-predicted activation of the mTORC1 complex is supported in both the kidney and small intestine with undefined involvement in the heart, and the liver shows no signal for mTORC1 (Fig. 4). Interestingly, CPA indicate mTORC1 is downregulated in the small intestine at 0-1DPF (Fig. 6), yet this downregulated state of mTORC1 is based only on the downregulation of a single gene, G protein subunit beta 1 like (GNB1L), which IPA identifies as a subunit of the mTORC1 complex. In contrast, AMPK signaling is predicted to be downregulated in the kidney and small intestine, indicative of elevated ATP levels and active mTORC1 [30, 31] (Fig.3). It is notable that nearly all genes in the mTOR pathway were associated with python orthologs that were observed as expressed across our dataset (see Additional file 1, Table S2), which suggests that our inferences of non-responsive genes within the mTOR pathway are biologically meaningful (e.g., true negatives), rather than representative of a lack of data. Thus, mTOR signaling in python tissues during regenerative organ growth may include non-canonical features compared to typical models of mTOR signaling that account for the partial responsiveness of genes and targets inferred from our CPA.

Our results identify mTOR as a central regulator and integrator of a number of diverse growth signals that drive post-feeding regenerative organ growth in Burmese pythons. Insulin signaling represents a key-regulating factor of the mTOR pathway [31], and we found multiple lines of evidence indicating roles of insulin signaling in post-feeding growth responses. Specifically, 0-1DPF URMA inferred the activation of INSR and insulin, and the inhibition of INSIG1 and INSIG2, in the kidney, small intestine, and liver, and the inverse of these activation patterns in the heart. INSIG1 and INSIG2 are negative regulators of SCAP [35, 36], which in turn regulates SREBP activity. Consistent with inferences of inhibition of INSIG1-2, URMA predicted the upregulation of SREBF1

and SREBF2, which provide evidence of an increase in sterol-regulatory element activity coincident with organ growth [36, 37] (Fig. 4). In addition to the interaction of insulin signaling and mTOR activity, we also found multiple lines of evidence for PI3K/AKT signaling that would interact with mTOR. Our URMA indicates significant downregulation of PTEN, an upstream regulator of the PI3K/AKT pathway, across all four organs, and CPA predicts activation of the PI3K/AKT signaling pathway in the small intestine and liver.

Evidence from previous studies also support the role of mTOR, PI3K/AKT, and AMPK signaling mechanisms in python post-feeding growth, at least in the heart. Western blots of python cardiac tissue post-feeding support the inference of early activation of mTOR and PI3K/AKT pathways by demonstrating that phosphorylated AKT and MTOR proteins increase significantly in abundance between 12 and 24 hours post-feeding [11]. These western blots also demonstrated phosphorylated AMPK protein was upregulated within 24 hours post-feeding, but lagging temporally behind the peak in phosphorylated MTOR and AKT [11], consistent with the antagonistic relationship between AMPK and MTOR/AKT [30]. These independent lines of evidence for the roles of mTOR, PI3K/AKT, and AMPK signaling in python post-feeding organ growth confirm our inferences of the central roles of these pathways, and support the power of pathway and URM inferences for inferring signaling mechanisms.

MAPK and related pathways also appear to be prominently involved in organ growth responses post-feeding, which is sensible given their known interactions with multiple growth pathways, including PI3K/AKT signaling and mTOR [38-40]. Our data reveal the involvement of MAPK signaling most clearly in the heart, with significant enrichment and predicted inhibition of p38 MAPK signaling and significant activation of ERK5 signaling (Fig. 3). ERK5 is a member of the Mitogen-activated protein kinases

(MAPKs) that is crucial to cell proliferation and activated in response to growth factors and oxidative stress [41, 42]. MYC is a downstream transcription factor regulated by the MAPK pathway and ERK5 specifically [43, 44], and an essential regulator of development and cell proliferation [45-47]. Our URMA predict significant activation of MYC in all four organs, indicating a broad role of active MAPK signaling in post-feeding organ growth in the python.

*NRF2 – protective function and interaction with growth pathways*

One of the strongest and most consistent signals in the canonical pathway and upstream regulatory molecule analyses was the involvement of the NRF2-mediated oxidative stress response pathway. Commonly associated with anti-aging and longevity [48-50], injury repair, and mitigation of inflammation [51], evidence for the central involvement of the NRF2-mediated oxidative stress response pathway in the small intestine, liver, and kidney begs the question of whether there is an important yet largely unappreciated role for stress-response signaling pathways in growth responses, and regenerative organ growth in particular.

The NRF2 pathway was significantly upregulated in small intestine, kidney, and liver within the first day following feeding (Fig. 3), and the NRF2 transcription factor (NFE2L2) was one of the most significant and highest in magnitude URMs predicted in these three organs (p-values < $1.55e^{-10}$, z-scores > 3.0) (Fig. 4). The 24 hour period following feeding in Burmese pythons involves unparalleled rates and magnitudes of organ growth, and also includes massive upregulation of metabolism – up to 44-fold increases in aerobic metabolism, which is among the highest fluctuation known for any vertebrate [3]. It is, therefore, sensible that activation of NRF2 is related to these major shifts in oxidative metabolism, and associated generation of reactive oxygen species [1,

2, 6, 9]. An open question, however, is what broader role the activation of NRF2 may play in facilitating the extraordinary growth responses associated with feeding in pythons. For example, post-fed Burmese python blood plasma has been shown to convey resistance to apoptosis to mammalian cells, even with exposure to high fatty acid concentrations that would otherwise cause cell death [11, 17]; such cell-protective qualities may be related to signals that activate NRF2 and/or other stress-response pathways. Interestingly, in addition to cell-protective roles of NRF2, this pathway also contains multiple points of integration with various growth pathways, including those activated in python organ regenerative growth.

The NRF2-mediated oxidative stress response pathway interacts with multiple pathways predicted in our canonical pathway analysis [52-57] (Figs. 3-4). The PI3K/AKT signaling pathway, predicted to be upregulated upon feeding in both the liver and small intestine, is essential for regulating the antioxidant functions of NRF2, and studies have shown that inhibition of this signaling pathway leads to attenuation of NRF2 activities [58, 59]. This interaction is evident when examining the role of NRF2 in the proliferation of cancer cells. Studies have shown that NRF2 is able to redirect glucose and glutamine into anabolic pathways through activation of PI3K/AKT signaling [60]. The activated PI3K/AKT pathway leads to greater accumulation of NRF2 in the nucleus, which allows NRF2 to enhance metabolic activities as well as promote cell proliferation and cytoprotection [60]. The PI3K/AKT signaling pathway activates mTOR activity in response to growth factors, and this and previous studies [11] have shown that PI3K/AKT and mTOR signaling are key growth pathways underlying organ regenerative growth in the Burmese python. Therefore, there appears to be strong and coordinated links between growth signaling (via PI3k/AKT and mTOR) and stress response signaling via NRF2 underlying organ growth in pythons following feeding. Like mTOR, a large majority of

genes in the NRF2 pathway were associated with python orthologs and were observed as expressed across our dataset (see Additional file 1, Table S2), which indicates that our inferences of non-responsive genes within the NRF2 pathway are likely true negatives, rather than artifacts due to a lack of ortholog identification in the python. Accordingly, predicted but unobserved expression responses in the NRF2 pathway in pythons suggest that the absence of expected responses may represent novel or non-canonical aspects of python biology or of the organ regeneration response in pythons.

In addition to NRF2-mediated oxidative stress response, evidence for the involvement of other stress response signaling mechanisms in python post-feeding organ growth was also observed. EIF2 signaling, important in translational control and responsiveness to conditions of environmental stress [61, 62], is strongly downregulated in the intestine, yet, absent in the other three organs (Fig. 3). Acute phase response signaling, which is involved in restoring homeostasis following inflammation or injury [63], is predicted to be strongly downregulated in the liver and moderately upregulated (but non-significant in the heart; Fig. 3). The precise roles of these additional stress response mechanisms in regenerative organ growth in the python remains an open question, although there is strong and consistent signal for the involvement of multiple stress response pathways overall in python post-feeding organ growth.

*Role of lipid signaling in driving growth*

Previous studies have shown evidence that molecules responsible for triggering python post-feeding organ growth circulate in the blood of the Burmese python [11, 64]. Riquelme et al. demonstrated that post-feeding python plasma was capable of inducing cardiomyocyte growth in pythons and mice, and that fasted python plasma supplemented with three particular fatty acids successfully stimulated cardiomyocyte growth in mice

[11]. Because these fatty acids only facilitated a growth response in the presence of fasted Burmese python serum, it is likely that python plasma contains additional factors required for successful post-feeding regenerative growth and that fatty acids are only partially responsible for stimulating growth responses. In the heart, we found significant enrichment and predicted activation for the LXR/RXR activation pathway as well as predicted activation of this pathway (although insignificant enrichment with $P>0.01$) in the small intestine (Fig. 3). LXR is a potent activator of the SREBP-1c gene [65], and our data predict clear and significant activation of both SREBF1 and SREBF2 upon feeding in the kidney, liver, and small intestine with significant downregulation and undefined direction for SREBF1 and SREBF2 in the heart, respectively (Fig. 4). When activated, these proteins directly enhance genes important for the uptake and synthesis of various lipids. SCAP, important for the activation of these SREB molecules, is also predicted to be strongly activated in the kidney, liver, and small intestine (Fig. 4) [35, 36, 66].

We also examined PPAR signaling as a potential pathway for lipid signaling during this regenerative growth, given the central role of PPAR in mediating fatty acid signaling as well as its effects on gene expression [67]. PPAR has also been identified as an important regulator of cell survival during wound repair and regeneration [68]. Although CPA did not detect significant PPAR signaling activation, URMA significantly predicted PPARA, PPARG, PPARGC1A, and PPARGC1b involvement across organs, typically inhibited in the heart and activated in the other three organs in 0-1DPF comparisons (Fig. 4). Given the variations in pathway and URM inferences between the heart and the other three organs, the question of whether fatty acids also play a similar stimulatory role in regenerative growth in the small intestine, liver, and kidney as they do in the heart remains. Our results do, however, argue for a poorly understood yet central role of lipid-signaling in these growth responses, and suggest that the unusually strong

bioactivity of fatty acids may elicit growth through conserved canonical pathway signaling mechanisms.

*Early phases of organ regression following digestion*

Physiological studies have shown that python post-feeding organ growth peaks between 1DPF and 3DPF [1, 2, 5, 9] and that phenotypes begin to decline by 4DPF [2, 3, 7, 9]. Thus, as post-feeding growth phenotypes reverse from 1DPF to 4DPF, we expected to observe shifts towards the fasted state, such as the reversal or inhibition of growth-associated pathways. Relative to comparisons between fasting and 1DPF, comparisons between 1DPF and 4DPF yielded nearly an order of magnitude fewer significantly differentially expressed genes (Table 1). Accordingly, expression heatmaps (Fig. 2) and expression profile summaries (see Additional file 1, Fig. S1) show that expression profiles of many genes at 4DPF tend to remain elevated (i.e., similar to levels at 1DPF), or exist at intermediate levels (between fasted and 1DPF levels of expression). We did not observe any particularly informative trends in canonical pathways and upstream regulator molecule predictions (see Additional file 1, Fig. S7) associated with shifts in gene expression from 1DPF to 4DPF, and this result is not surprising given the relatively small number of genes that significantly change between these time points. Among the predicted pathways were several that are related to stress response and biosynthesis (see Additional file 1, Fig. S7), although a lack of predicted direction of activation prevents detailed interpretation of the involvement of nearly all pathways predicted between 1DPF and 4DPF. The only pathway predicted as significant and with a direction of activation between 1DPF and 4DPF was the mitotic roles of polo-like kinase pathway, which was activated in the small intestine (see Additional file 1, Fig. S7). It therefore remains an open question whether atrophy and other processes involved in

reverting to the fasting state are controlled actively (via a new signal that stimulates the apoptotic and atrophy processes), passively (the signal(s) that stimulates the initial cascade of responses fades or stops), or some combination of the two mechanisms. Collectively, our results suggest that comparisons between the 1DPF to 4DPF time points may not be sufficient to predict the physiological mechanisms involved in phenotypic regression with adequate power. Further experiments, possibly with multiple later-stage time point sampling, may be required to address outstanding questions about how these growth phenotypes are reversed.

*Comparison of python organ regeneration to other regenerative model systems*

Organ regeneration in snakes represents an extreme and unique phenotype among vertebrates. However, other examples of regenerative growth do exist among vertebrates, such as limb regeneration in salamanders [69], fin regeneration in fish [70], and regenerative heart growth in zebrafish [71, 72] and prenatal mammals [73]. This begs the question of whether or not these regenerative responses share common mechanisms, and as we continue to better understand the mechanisms driving regenerative growth in snakes, such key comparisons can begin to be made. While none of these other vertebrate regenerative growth systems directly parallel regenerative organ growth in snakes, regeneration of heart tissue in zebrafish is the most analogous comparison, as it occurs in adult organisms and represents regenerative growth of organ tissue specifically. Following injury or amputation of cardiac tissue, zebrafish hearts grow primarily by dedifferentiation and subsequent proliferation of cardiomyocytes [72]. Conversely, python hearts grow only by hypertrophy [3, 11, 74], and therefore may be driven by largely different regenerative mechanisms. The python small intestine, liver, and kidney, however, do grow via by hypertrophy and hyperplasia [3, 5, 11, 12]; while

they represent different organ systems than the zebrafish heart, they may be driven by similar pathways that regulate cell proliferation in general. Indeed, there are parallels between zebrafish and python responses in the shared involvement of p38 MAPK signaling, a negative regulator of cardiomyocyte proliferation in zebrafish [71] that we infer to be inhibited in the Burmese python heart between fasting and 1DPF (Fig. 3). Additionally the mitotic roles of polo-like kinase pathway, which was the only pathway we predicted as significant and with a direction of activation between 1DPF and 4DPF (activated in the small intestine; see Additional file 1, Fig. S7) is also involved in zebrafish regenerative heart growth. Cell-cycle regulation by polo-like kinase 1 is an important component of cardiomyocyte proliferation in zebrafish [72], and therefore may be playing a similar role in the python small intestine, although it is notable that it was not predicted as significant between fasting and 1DPF, when growth is presumably greatest in this organ [3, 5]. Other pathways involved in zebrafish regenerative growth, such as IGF signaling, FGF signaling, HIPPO signaling, and TGF-Beta signaling [71], were not inferred as significant based on canonical pathway analyses of either post-feeding time interval in our study of the Burmese python. TGFB1 and IGF1 growth factors were, however, inferred in our URMA analysis of the fasting to 1DPF interval (see Additional file 1, Fig. S2), suggesting that there may still be some involvement of these growth factors in the regulation of regenerative growth in the Burmese python. A key conclusion based on our study is that, to our knowledge, mTOR signaling and NRF2-mediated oxidative stress response pathways have not been implicated in zebrafish regenerative growth. Thus, regenerative organ growth in the Burmese python appears to remain quite unique among vertebrates, both in the nature of the phenotype, and now in the molecular mechanisms underlying growth.

*Conclusions*

Multiple coordinated growth pathways appear to play an important role in facilitating regenerative organ growth in multiple tissues of the Burmese python, and the overlap of pathways across organs suggests common signaling molecules may drive this response – consistent with evidence that common factors circulating in the plasma of pythons are capable of eliciting growth [11, 64]. Our analyses provide strong evidence for the involvement of particular growth and stress response pathways in post-feeding organ growth responses in multiple organs, although it is notable that our inferences of the activation versus inhibition of mechanisms was not always consistent across analyses (e.g., CPA versus URMA). As discussed above, such conflicting inferences could be due to the fundamental differences in CPA and URMA (e.g., Fig. 1), in that they are integrating very different sources of evidence, coupled with the possibility that the continuous nature of this response may survey various mechanisms during an inflection point of activity that can confound inferences of directionality. However, contradictory inferences of mechanistic activation may also suggest that some of these core signaling pathways function differentially in snakes, or that some molecules or pathways are signaling via non-canonical mechanisms. Experiments have demonstrated that exposure to Burmese python 2DPF blood serum elicits significant growth of rat cardiomyocytes [11], as well as increases in size and insulin production of human pancreatic beta cells [17]. These findings suggest that even if regenerative organ growth in snakes is achieved in part by non-canonical pathway or regulator activity, core aspects of signaling underlying organ growth in pythons is conserved across vertebrates. Among the most intriguing results of this study is the consistent predicted activation of the NRF2-mediated oxidative stress response pathway, and NRF2-related signaling molecules, during

regenerative organ growth. The integration of NRF2 signaling with other growth pathways, including mTOR, provide an exciting and novel mechanistic hypothesis for how NRF2 and other stress-response pathways may play an important yet largely unappreciated role in regenerative growth responses in vertebrates.

## References


1. 1.Ott BD, Secor SM: **Adaptive regulation of digestive performance in the genus Python**. *J Exp Biol* 2007, **210**(Pt 2):340-356.

2. Secor SM: **Digestive physiology of the Burmese python: broad regulation of integrated performance**. *J Exp Biol* 2008, **211**(Pt 24):3767-3774.

3. Secor SM, Diamond J: **A vertebrate model of extreme physiological regulation**. *Nature* 1998, **395**(6703):659-662.

4. Secor SM, Diamond JM: **Evolution of regulatory responses to feeding in snakes**. *Physiol Biochem Zool* 2000, **73**(2):123-141.

5. Andrew AL, Card DC, Ruggiero RP, Schield DR, Adams RH, Pollock DD, Secor SM, Castoe TA: **Rapid changes in gene expression direct rapid shifts in intestinal form and function in the Burmese python after feeding**. *Physiol Genomics* 2015, **47**(5):147-157.

6. Secor SM, Diamond J: **Determinants of the postfeeding metabolic response of Burmese pythons, Python molurus**. *Physiol Zool* 1997, **70**(2):202-212.

7. Cox CL, Secor SM: **Matched regulation of gastrointestinal performance in the Burmese python, Python molurus**. *J Exp Biol* 2008, **211**(Pt 7):1131-1140.

8. Lignot JH, Helmstetter C, Secor SM: **Postprandial morphological response of the intestinal epithelium of the Burmese python (Python molurus)**. *Comp Biochem Physiol A Mol Integr Physiol* 2005, **141**(3):280-291.

9. Secor SM, Diamond J: **Adaptive responses to feeding in Burmese pythons: pay before pumping**. *J Exp Biol* 1995, **198**(Pt 6):1313-1325.

10. Secor SM, White SE: **Prioritizing blood flow: cardiovascular performance in response to the competing demands of locomotion and digestion for the Burmese python, Python molurus**. *J Exp Biol* 2010, **213**(1):78-88.

11. Riquelme CA, Magida JA, Harrison BC, Wall CE, Marr TG, Secor SM, Leinwand LA: **Fatty acids identified in the Burmese python promote beneficial cardiac growth**. *Science* 2011, **334**(6055):528-531.

12. Helmstetter C, Reix N, T'Flachebba M, Pope RK, Secor SM, Le Maho Y, Lignot JH: **Functional changes with feeding in the gastro-intestinal epithelia of the Burmese python (Python molurus)**. *Zoolog Sci* 2009, **26**(9):632-638.

13. Castoe TA, de Koning AP, Hall KT, Card DC, Schield DR, Fujita MK, Ruggiero RP, Degner JF, Daza JM, Gu W *et al*: **The Burmese python genome reveals the molecular basis for extreme adaptation in snakes**. *Proc Natl Acad Sci U S A* 2013, **110**(51):20645-20650.

14. Wall CE, Cozza S, Riquelme CA, McCombie WR, Heimiller JK, Marr TG, Leinwand LA: **Whole transcriptome analysis of the fasting and fed Burmese python heart: insights into extreme physiological cardiac adaptation**. *Physiol Genomics* 2011, **43**(2):69-76.

15. Secor SM, Lane JS, Whang EE, Ashley SW, Diamond J: **Luminal nutrient signals for intestinal adaptation in pythons**. *Am J Physiol Gastrointest Liver Physiol* 2002, **283**(6):G1298-1309.

16. Secor SM: **Gastric function and its contribution to the postprandial metabolic response of the Burmese python Python molurus**. *J Exp Biol* 2003, **206**(Pt 10):1621-1630.

17. Secor S, Choudhary A, Lundh M, Wagner B: **Is extreme physiology of Burmese pythons relevant to diabetes?(1108.8)**. *The FASEB Journal* 2014, **28**(1 Supplement):1108.1108.

18. Bolger AM, Lohse M, Usadel B: **Trimmomatic: a flexible trimmer for Illumina sequence data**. *Bioinformatics* 2014, **30**(15):2114-2120.

19. Li H, Durbin R: **Fast and accurate short read alignment with Burrows-Wheeler transform**. *Bioinformatics* 2009, **25**(14):1754-1760.

20. Li H, Handsaker B, Wysoker A, Fennell T, Ruan J, Homer N, Marth G, Abecasis G, Durbin R, Genome Project Data Processing S: **The Sequence Alignment/Map format and SAMtools**. *Bioinformatics* 2009, **25**(16):2078-2079.

21. Robinson MD, McCarthy DJ, Smyth GK: **edgeR: a Bioconductor package for differential expression analysis of digital gene expression data**. *Bioinformatics* 2010, **26**(1):139-140.

22. Conesa A, Nueda MJ, Ferrer A, Talon M: **maSigPro: a method to identify significantly differential expression profiles in time-course microarray experiments**. *Bioinformatics* 2006, **22**(9):1096-1102.

23. Dixon P: **VEGAN, a package of R functions for community ecology**. *J Veg Sci* 2003, **14**(6):927-930.

24. Ernst J, Bar-Joseph Z: **STEM: a tool for the analysis of short time series gene expression data**. *BMC Bioinformatics* 2006, **7**:191.

25. Aken BL, Ayling S, Barrell D, Clarke L, Curwen V, Fairley S, Banet JF, Billis K, Girón CG, Hourlier T: **The Ensembl gene annotation system**. *Database* 2016, **2016**:baw093.

26. Cunningham F, Amode MR, Barrell D, Beal K, Billis K, Brent S, Carvalho-Silva D, Clapham P, Coates G, Fitzgerald S *et al*: **Ensembl 2015**. *Nucleic Acids Res* 2015, **43**(Database issue):D662-669.

27. Krämer A, Green J, Pollard J, Tugendreich S: **Causal analysis approaches in ingenuity pathway analysis (ipa)**. *Bioinformatics* 2013:btt703.

28. Cuadrado A, Martín-Moldes Z, Ye J, Lastres-Becker I: **Transcription factors NRF2 and NF-κB are coordinated effectors of the Rho family, GTP-binding protein RAC1 during inflammation**. *J Biol Chem* 2014, **289**(22):15244-15258.

29. Wardyn JD, Ponsford AH, Sanderson CM: **Dissecting molecular cross-talk between Nrf2 and NF-κB response pathways**. *Biochem Soc T* 2015, **43**(4):621-626.

30. Laplante M, Sabatini DM: **mTOR Signaling in Growth Control and Disease**. *Cell* 2012, **149**(2):274-293.

31. Laplante M, Sabatini DM: **mTOR signaling at a glance**. *J Cell Sci* 2009, **122**(20):3589-3594.

32. Okouchi M, Okayama N, Alexander JS, Aw TY: **NRF2-dependent glutamate-L-cysteine ligase catalytic subunit expression mediates insulin protection against hyperglycemia-induced brain endothelial cell apoptosis**. *Curr Neurovasc Res* 2006, **3**(4):249-261.

33. Lee J, Giordano S, Zhang JH: **Autophagy, mitochondria and oxidative stress: cross-talk and redox signalling**. *Biochem J* 2012, **441**:523-540.

34. LoPiccolo J, Blumenthal GM, Bernstein WB, Dennis PA: **Targeting the PI3K/Akt/mTOR pathway: effective combinations and clinical considerations**. *Drug Resist Updat* 2008, **11**(1-2):32-50.

35. Yang T, Espenshade PJ, Wright ME, Yabe D, Gong Y, Aebersold R, Goldstein JL, Brown MS: **Crucial step in cholesterol homeostasis: Sterols promote binding of SCAP to INSIG-1, a membrane protein that facilitates retention of SREBPs in ER**. *Cell* 2002, **110**(4):489-500.

36. Espenshade PJ: **SREBPs: sterol-regulated transcription factors**. *J Cell Sci* 2006, **119**(6):973-976.

37. Shao W, Espenshade PJ: **Expanding Roles for SREBP in Metabolism**. *Cell Metab* 2012, **16**(4):414-419.

38. Aksamitiene E, Kiyatkin A, Kholodenko BN: **Cross-talk between mitogenic Ras/MAPK and survival PI3K/Akt pathways: a fine balance**. *Biochem Soc T* 2012, **40**:139-146.

39. Pappalardo F, Russo G, Candido S, Pennisi M, Cavalieri S, Motta S, McCubrey JA, Nicoletti F, Libra M: **Computational Modeling of PI3K/AKT and MAPK Signaling Pathways in Melanoma Cancer**. *Plos One* 2016, **11**(3).

40. Wong MH, Xue A, Baxter RC, Pavlakis N, Smith RC: **Upstream and Downstream Co-inhibition of Mitogen-Activated Protein Kinase and PI3K/Akt/mTOR Pathways in Pancreatic Ductal Adenocarcinoma**. *Neoplasia* 2016, **18**(7):425-435.

41. Kato Y, Chao TH, Hayashi M, Tapping RI, Lee JD: **Role of BMK1 in regulation of growth factor-induced cellular responses**. *Immunol Res* 2000, **21**(2-3):233-237.

42. Gomez N, Erazo T, Lizcano JM: **ERK5 and Cell Proliferation: Nuclear Localization Is What Matters**. *Front Cell Dev Biol* 2016, **4**(105).

43. English JM, Pearson G, Baer R, Cobb MH: **Identification of substrates and regulators of the mitogen-activated protein kinase ERK5 using chimeric protein kinases**. *J Biol Chem* 1998, **273**(7):3854-3860.

44. Wang X, Tournier C: **Regulation of cellular functions by the ERK5 signalling pathway**. *Cell Signal* 2006, **18**(6):753-760.

45. Davis AC, Wims M, Spotts GD, Hann SR, Bradley A: **A null c-myc mutation causes lethality before 10.5 days of gestation in homozygotes and reduced fertility in heterozygous female mice**. *Genes Dev* 1993, **7**(4):671-682.

46. Mateyak MK, Obaya AJ, Adachi S, Sedivy JM: **Phenotypes of c-Myc-deficient rat fibroblasts isolated by targeted homologous recombination**. *Cell Growth Differ* 1997, **8**(10):1039-1048.

47. Shao Y, Qu Y, Dang S, Yao B, Ji M: **MiR-145 inhibits oral squamous cell carcinoma (OSCC) cell growth by targeting c-Myc and Cdk6**. *Cancer Cell Int* 2013, **13**(1):51.

48. Lewis KN, Mele J, Hayes JD, Buffenstein R: **Nrf2, a guardian of healthspan and gatekeeper of species longevity**. *Integr Comp Biol* 2010, **50**(5):829-843.

49. Lewis KN, Wason E, Edrey YH, Kristan DM, Nevo E, Buffenstein R: **Regulation of Nrf2 signaling and longevity in naturally long-lived rodents**. *Proc Natl Acad Sci USA* 2015, **112**(12):3722-3727.

50. Sykiotis GP, Bohmann D: **Keap1/Nrf2 signaling regulates oxidative stress tolerance and lifespan in Drosophila**. *Dev Celll* 2008, **14**(1):76-85.

51. Reddy NM, Kleeberger SR, Kensler TW, Yamamoto M, Hassoun PM, Reddy SP: **Disruption of Nrf2 impairs the resolution of hyperoxia-induced acute lung injury and inflammation in mice**. *J Immunol* 2009, **182**(11):7264-7271.

52. Kensler TW, Wakabayash N, Biswal S: **Cell survival responses to environmental stresses via the Keap1-Nrf2-ARE pathway**. *Annu Rev Pharmacol* 2007, **47**:89-116.

53. Braun S, Keller UAD, Steiling H, Werner S: **Fibroblast growth factors in epithelial repair and cytoprotection**. *Philos T Roy Soc B* 2004, **359**(1445):753-757.

54. Shibata T, Saito S, Kokubu A, Suzuki T, Yamamoto M, Hirohashi S: **Global Downstream Pathway Analysis Reveals a Dependence of Oncogenic NF-E2-Related Factor 2 Mutation on the mTOR Growth Signaling Pathway**. *Cancer Res* 2010, **70**(22):9095-9105.

55. Beyer TA, Werner S: **The cytoprotective Nrf2 transcription factor controls insulin receptor signaling in the regenerating liver**. *Cell Cycle* 2008, **7**(7):874-878.

56. Kannan S, Whitehead KJ, Wang L, Gomes AV, Litwin SE, Kensler TW, Abel ED, Hoidal JR, Soorappan RN: **Nrf2 Deficiency Prevents Reductive Stress Induced Hypertrophic Cardiomyopathy**. *Free Radical Bio Med* 2013, **65**:S83-S83.

57. Hayes JD, Ashford MLJ: **Nrf2 Orchestrates Fuel Partitioning for Cell Proliferation**. *Cell Metab* 2012, **16**(2):139-141.

58. Wang L, Chen Y, Sternberg P, Cai J: **Essential roles of the PI3 kinase/Akt pathway in regulating Nrf2-dependent antioxidant functions in the RPE**. *Invest Ophthalmol Vis Sci* 2008, **49**(4):1671-1678.

59. Papaiahgari S, Zhang Q, Kleeberger SR, Cho HY, Reddy SP: **Hyperoxia stimulates an Nrf2-ARE transcriptional response via ROS-EGFR-PI3K-Akt/ERK MAP kinase signaling in pulmonary epithelial cells**. *Antiox redox signal* 2006, **8**(1-2):43-52.

60. Mitsuishi Y, Taguchi K, Kawatani Y, Shibata T, Nukiwa T, Aburatani H, Yamamoto M, Motohashi H: **Nrf2 redirects glucose and glutamine into anabolic pathways in metabolic reprogramming**. *Cancer Cell* 2012, **22**(1):66-79.

61. Wek RC, Jiang HY, Anthony TG: **Coping with stress: eIF2 kinases and translational control**. *Biochem Soc T* 2006, **34**:7-11.

62. Boyce M, Bryant KF, Jousse C, Long K, Harding HP, Scheuner D, Kaufman RJ, Ma DW, Coen DM, Ron D *et al*: **A selective inhibitor-of eIF2 alpha dephosphorylation protects cells from ER stress**. *Science* 2005, **307**(5711):935-939.

63. Moshage H: **Cytokines and the hepatic acute phase response**. *J Pathol* 1997, **181**(3):257-266.

64. Secor SM, Fehsenfeld D, Diamond J, Adrian TE: **Responses of python gastrointestinal regulatory peptides to feeding**. *P Natl Acad Sci USA* 2001, **98**(24):13637-13642.

65. Raghow R, Yellaturu C, Deng X, Park EA, Elam MB: **SREBPs: the crossroads of physiological and pathological lipid homeostasis**. *Trends Endocrinol Metab* 2008, **19**(2):65-73.

66. Matsuda M, Korn BS, Hammer RE, Moon YA, Komuro R, Horton JD, Goldstein JL, Brown MS, Shimomura I: **SREBP cleavage-activating protein (SCAP) is required for increased lipid synthesis in liver induced by cholesterol deprivation and insulin elevation**. *Genes Dev* 2001, **15**(10):1206-1216.

67. Schoonjans K, Staels B, Auwerx J: **Role of the peroxisome proliferator-activated receptor (PPAR) in mediating the effects of fibrates and fatty acids on gene expression**. *J Lipid Res* 1996, **37**(5):907-925.

68. Gurtner GC, Werner S, Barrandon Y, Longaker MT: **Wound repair and regeneration**. *Nature* 2008, **453**(7193):314-321.

69. Brockes JP, Kumar A: **Plasticity and reprogramming of differentiated cells in amphibian regeneration**. *Nat Rev Mol Cell Biol* 2002, **3**(8):566-574.

70. Poss KD, Keating MT, Nechiporuk A: **Tales of regeneration in zebrafish**. *Dev Dynam* 2003, **226**(2):202-210.

71. Kikuchi K: **Advances in understanding the mechanism of zebrafish heart regeneration**. *Stem cell research* 2014, **13**(3):542-555.

72. Jopling C, Sleep E, Raya M, Martí M, Raya A, Belmonte JCI: **Zebrafish heart regeneration occurs by cardiomyocyte dedifferentiation and proliferation**. *Nature* 2010, **464**(7288):606-609.

73. Porrello ER, Mahmoud AI, Simpson E, Hill JA, Richardson JA, Olson EN, Sadek HA: **Transient regenerative potential of the neonatal mouse heart**. *Science* 2011, **331**(6020):1078-1080.

74. Andersen JB, Rourke BC, Caiozzo VJ, Bennett AF, Hicks JW: **Physiology: postprandial cardiac hypertrophy in pythons**. *Nature* 2005, **434**(7029):37-38.

Tables

Table 2.1. **Numbers of differentially expressed genes between pre- and post-feeding time points for the four organs studied.** For each comparison, the numbers of up and downregulated genes were inferred using pairwise analysis with a Benjamini-Hochberg corrected p-value < 0.05.

| | **Time point Comparisons** | | | | | |
|---|---|---|---|---|---|---|
| | **fasted v 1DPF** | | **1DPF v 4DPF** | | **fasted v 4DPF** | |
| | **Up** | **Down** | **Up** | **Down** | **Up** | **Down** |
| **Heart** | 208 | 228 | 36 | 40 | 5 | 3 |
| **Kidney** | 244 | 100 | 5 | 3 | 125 | 22 |
| **Liver** | 335 | 126 | 29 | 12 | 295 | 76 |
| **Small Intestine** | 1,271 | 1,042 | 268 | 146 | 547 | 345 |

Table 2.S1. **Sequencing information for all included python samples.** PE76 and PE120 stand for the sequence read type (e.g., Paired-end 76bp). The year provided represents the year in which the sample was sequenced.

| Tissue | Timepoint | Animal ID | Instrument | cDNA prep kit | Year | Sequence type | Library Name |
|---|---|---|---|---|---|---|---|
| Heart | fasted | AI6_1 | GAIIx | Illumina Truseq | 2010 | PE76 | TC01 |
| Heart | fasted | AI6_2 | GAIIx | Illumina Truseq | 2011 | PE120 | TC05 |
| Heart | fasted | AI11 | GAIIx | Illumina Truseq | 2010 | PE76 | TC01 |
| Heart | fasted | AI8 | HiSeq | NEB Next | 2013 | SE50 | pRNA-A |
| Heart | fasted | U25 | HiSeq | NEB Next | 2013 | SE50 | pRNA-B |
| Heart | 1DPF | Z12 | GAIIx | Illumina Truseq | 2010 | PE76 | TC01 |
| Heart | 1DPF | Z14_1 | GAIIx | Illumina Truseq | 2010 | PE76 | TC01 |
| Heart | 1DPF | Z14_2 | GAIIx | Illumina Truseq | 2011 | PE120 | TC05 |
| Heart | 1DPF | Z18 | GAIIx | Illumina Truseq | 2010 | PE76 | TC01 |
| Heart | 4DPF | Y5_1 | GAIIx | Illumina Truseq | 2010 | PE76 | TC01 |
| Heart | 4DPF | Y5_2 | GAIIx | Illumina Truseq | 2011 | PE120 | TC05 |
| Heart | 4DPF | Y18 | GAIIx | Illumina Truseq | 2010 | PE76 | TC01 |
| Heart | 4DPF | Y23 | GAIIx | Illumina Truseq | 2010 | PE76 | TC01 |
| Kidney | fasted | AI8 | HiSeq | NEB Next | 2013 | SE50 | pRNA-A |
| Kidney | fasted | U25 | HiSeq | NEB Next | 2013 | SE50 | pRNA-B |
| Kidney | fasted | AI6_1 | HiSeq | Illumina Truseq | 2011 | SE50 | s1 |
| Kidney | fasted | AI6_2 | GAIIx | Illumina Truseq | 2011 | PE120 | SP03 |
| Kidney | fasted | AI11_1 | HiSeq | Illumina Truseq | 2011 | SE50 | s1 |
| Kidney | fasted | AI11_2 | GAIIx | Illumina Truseq | 2011 | PE120 | SP03 |
| Kidney | fasted | AJ6_1 | HiSeq | Illumina Truseq | 2011 | SE50 | s1 |
| Kidney | fasted | AJ6_2 | GAIIx | Illumina Truseq | 2011 | PE120 | SP03 |
| Kidney | fasted | AJ6_3 | GAIIx | Illumina Truseq | 2011 | PE120 | TC05 |
| Kidney | 1DPF | Z12_1 | HiSeq | Illumina Truseq | 2011 | SE50 | s1 |
| Kidney | 1DPF | Z12_2 | GAIIx | Illumina Truseq | 2011 | PE120 | SP03 |
| Kidney | 1DPF | Z14_1 | HiSeq | Illumina Truseq | 2011 | SE50 | s1 |
| Kidney | 1DPF | Z14_2 | GAIIx | Illumina Truseq | 2011 | PE120 | SP03 |
| Kidney | 1DPF | Z18_1 | HiSeq | Illumina Truseq | 2011 | SE50 | s1 |
| Kidney | 1DPF | Z18_2 | GAIIx | Illumina Truseq | 2011 | PE120 | SP03 |
| Kidney | 1DPF | Z18_3 | GAIIx | Illumina Truseq | 2011 | PE120 | TC05 |
| Kidney | 1DPF | V43 | HiSeq | NEB Next | 2013 | SE50 | pRNA-B |
| Kidney | 1DPF | Z14_3 | HiSeq | NEB Next | 2013 | SE50 | pRNA-B |

| | | | | | | | |
|---|---|---|---|---|---|---|---|
| Kidney | 4DPF | Y18_1 | HiSeq | NEB Next | 2013 | SE50 | pRNA-B |
| Kidney | 4DPF | Y24 | HiSeq | NEB Next | 2013 | SE50 | pRNA-A |
| Kidney | 4DPF | Y5_1 | HiSeq | Illumina Truseq | 2011 | SE50 | s1 |
| Kidney | 4DPF | Y5_2 | GAIIx | Illumina Truseq | 2011 | PE120 | SP03 |
| Kidney | 4DPF | Y5_3 | GAIIx | Illumina Truseq | 2011 | PE120 | TC05 |
| Kidney | 4DPF | Y18_2 | HiSeq | Illumina Truseq | 2011 | SE50 | s1 |
| Kidney | 4DPF | Y18_3 | GAIIx | Illumina Truseq | 2011 | PE120 | SP03 |
| Kidney | 4DPF | Y23_1 | HiSeq | Illumina Truseq | 2011 | SE50 | s1 |
| Kidney | 4DPF | Y23_2 | GAIIx | Illumina Truseq | 2011 | PE120 | SP03 |
| Liver | fasted | AI6_1 | GAIIx | Illumina Truseq | 2010 | PE76 | TC01 |
| Liver | fasted | AI6_2 | GAIIx | Illumina Truseq | 2011 | PE120 | TC05 |
| Liver | fasted | AI8 | HiSeq | NEB Next | 2013 | SE50 | pRNA-A |
| Liver | fasted | AI11 | HiSeq | NEB Next | 2013 | SE50 | pRNA-B |
| Liver | fasted | U25 | HiSeq | NEB Next | 2013 | SE50 | pRNA-B |
| Liver | 1DPF | V43 | HiSeq | NEB Next | 2013 | SE50 | pRNA-B |
| Liver | 1DPF | Z14 | HiSeq | NEB Next | 2013 | SE50 | pRNA-A |
| Liver | 1DPF | Z18 | HiSeq | NEB Next | 2013 | SE50 | pRNA-B |
| Liver | 1DPF | Z12_1 | GAIIx | Illumina Truseq | 2010 | PE76 | TC01 |
| Liver | 1DPF | Z12_2 | GAIIx | Illumina Truseq | 2011 | PE120 | TC05 |
| Liver | 4DPF | Y5_1 | GAIIx | Illumina Truseq | 2010 | PE76 | TC01 |
| Liver | 4DPF | Y5_2 | GAIIx | Illumina Truseq | 2011 | PE120 | TC05 |
| Liver | 4DPF | Y18 | HiSeq | NEB Next | 2013 | SE50 | pRNA-B |
| Liver | 4DPF | Y23 | HiSeq | NEB Next | 2013 | SE50 | pRNA-B |
| Liver | 4DPF | Y24 | HiSeq | NEB Next | 2013 | SE50 | pRNA-A |
| Small intestine | fasted | AI8 | HiSeq | NEB Next | 2013 | SE50 | pRNA-A |
| Small intestine | fasted | AI11 | HiSeq | NEB Next | 2013 | SE50 | pRNA-B |
| Small intestine | fasted | U25 | HiSeq | NEB Next | 2013 | SE50 | pRNA-A |
| Small intestine | fasted | AI6_1 | HiSeq | Illumina Truseq | 2011 | SE50 | s1 |
| Small intestine | fasted | AI6_2 | GAIIx | Illumina Truseq | 2011 | PE120 | SP03 |
| Small intestine | fasted | AI11_1 | HiSeq | Illumina Truseq | 2011 | SE50 | s1 |
| Small intestine | fasted | AI11_2 | GAIIx | Illumina Truseq | 2011 | PE120 | SP03 |
| Small intestine | fasted | AJ6_1 | HiSeq | Illumina Truseq | 2011 | SE50 | s1 |
| Small intestine | fasted | AJ6_2 | GAIIx | Illumina Truseq | 2011 | PE120 | TC05 |
| Small intestine | fasted | AJ6_3 | GAIIx | Illumina Truseq | 2011 | PE120 | TC05 |
| Small intestine | 1DPF | Z12_1 | HiSeq | Illumina Truseq | 2011 | SE50 | s1 |
| Small intestine | 1DPF | Z12_2 | GAIIx | Illumina Truseq | 2011 | PE120 | SP03 |
| Small intestine | 1DPF | Z14_1 | HiSeq | Illumina Truseq | 2011 | SE50 | s1 |

| | | | | | | | |
|---|---|---|---|---|---|---|---|
| Small intestine | 1DPF | Z14_2 | GAIIx | Illumina Truseq | 2011 | PE120 | SP03 |
| Small intestine | 1DPF | Z14_3 | GAIIx | Illumina Truseq | 2011 | PE120 | TC05 |
| Small intestine | 1DPF | Z18_1 | HiSeq | Illumina Truseq | 2011 | SE50 | s1 |
| Small intestine | 1DPF | Z18_2 | GAIIx | Illumina Truseq | 2011 | PE120 | SP03 |
| Small intestine | 1DPF | V43 | HiSeq | NEB Next | 2013 | SE50 | pRNA-B |
| Small intestine | 1DPF | Z18_3 | HiSeq | NEB Next | 2013 | SE50 | pRNA-B |
| Small intestine | 4DPF | Y24 | HiSeq | NEB Next | 2013 | SE50 | pRNA-B |
| Small intestine | 4DPF | Y5_1 | HiSeq | Illumina Truseq | 2011 | SE50 | s1 |
| Small intestine | 4DPF | Y5_2 | GAIIx | Illumina Truseq | 2011 | PE120 | SP03 |
| Small intestine | 4DPF | Y18_1 | HiSeq | Illumina Truseq | 2011 | SE50 | s1 |
| Small intestine | 4DPF | Y18_2 | GAIIx | Illumina Truseq | 2011 | PE120 | SP03 |
| Small intestine | 4DPF | Y18_3 | GAIIx | Illumina Truseq | 2011 | PE120 | TC05 |
| Small intestine | 4DPF | Y23_1 | HiSeq | Illumina Truseq | 2011 | SE50 | s1 |
| Small intestine | 4DPF | Y23_2 | GAIIx | Illumina Truseq | 2011 | PE120 | SP03 |

Table 2.S2. **The number of genes involved in each pathway as defined by IPA, the number of genes in the pathway that were assigned python orthologs via tblastx, and the number of those python orthologs observed with a non-zero level of expression in our dataset.**

| Pathway | Organ | Number of Genes | Number of genes assigned an orthologous python gene | Number of genes assigned an orthologous python gene and observed as expressed in dataset |
|---|---|---|---|---|
| mTOR | Heart | 199 | 172 | 169 |
| | Kidney | | | 170 |
| | Liver | | | 167 |
| | Small Int. | | | 171 |
| NRF2 | Heart | 292 | 223 | 220 |
| | Kidney | | | 222 |
| | Liver | | | 218 |
| | Small Int. | | | 220 |

Figures

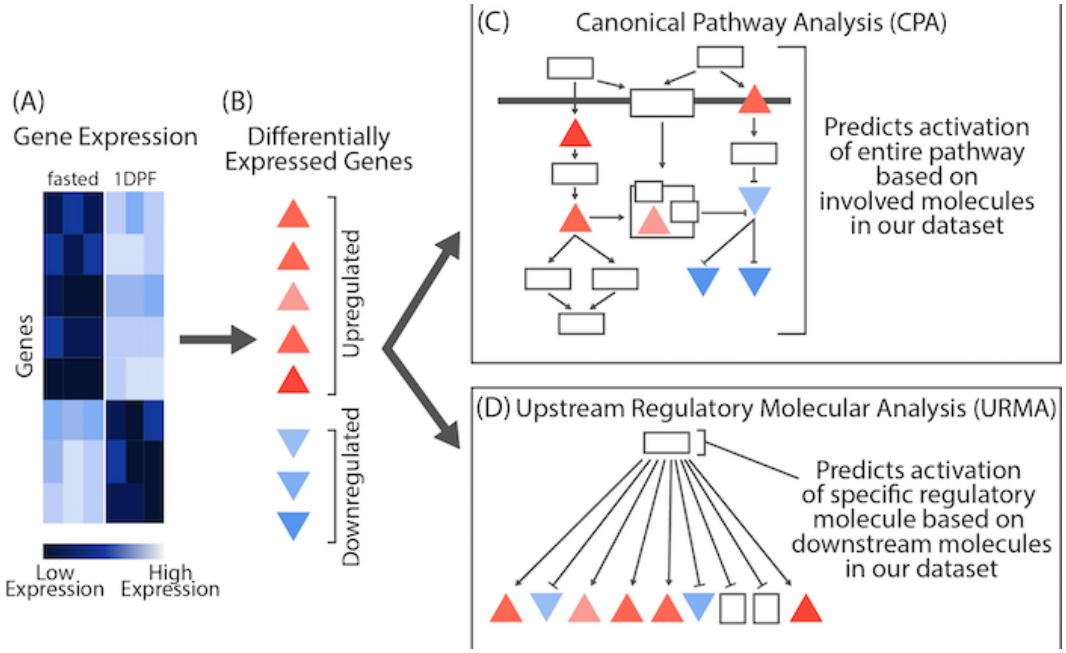


Figure 2.1. **Conceptual overview of differences between Canonical Pathway Analysis (CPA) and Upstream Regulatory Molecule Analysis (URMA).** Pairwise analyses on experimental gene expression data (A) identify significantly upregulated and downregulated genes (B). Significantly differentially expressed genes are then analyzed in two distinct IPA analyses (CPA and URMA) (C) Canonical Pathway Analysis predicts pathway activation based on overlap of gene expression data with molecules within the pathway. (D) Upstream Regulatory Molecule Analysis predicts activation of specific regulatory molecules based on downstream molecules in our gene expression dataset.

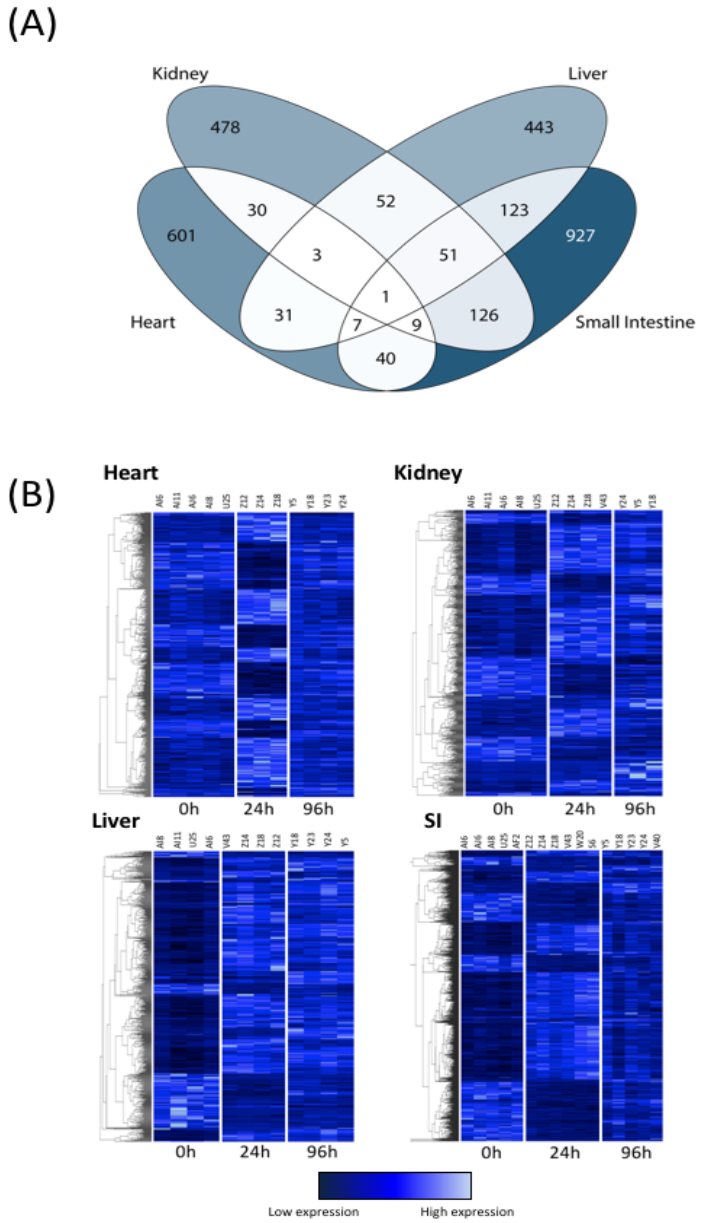


Figure 2.2. **Summary of significantly differentially expressed genes for all four organs identified via regression analysis.** (A) Venn diagram depicting the numbers of genes significantly differentially expressed across time points. Darker colors indicate a large number of genes and lighter colors indicate a smaller number of genes. (B) Heatmaps depicting all significantly differentially expressed genes across all time points in each organ. 722 genes were significantly differentially expressed in the heart. There were 750 genes significantly differentially expressed in the kidney. 711 genes were significantly differentially expressed in the liver and 1,284 genes showed significant differential expression in the small intestine.

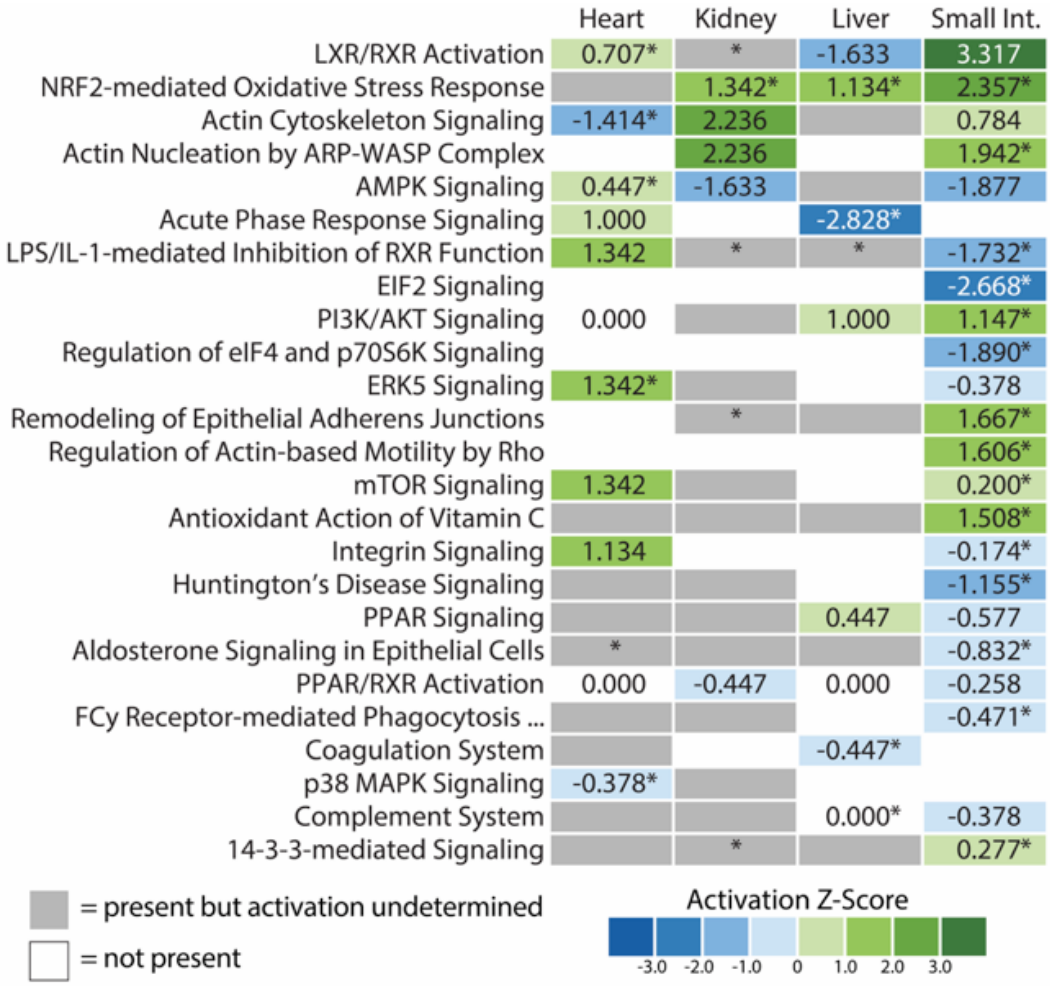


Figure 2.3. **Canonical pathways predicted to be activated or inhibited from gene expression data.** Each pathway shown is significantly enriched for our genes with a Fisher's Exact test p-value less than 0.01 (depicted with an asterisk). Pathways were shown only if they met our criteria for significance and had a predicted activation state in at least one organ. Z-scores of 0.000 indicate pathway predictions that lack a bias in the direction of gene regulation observed in our dataset. PPAR signaling ($P<0.05$) was also included.

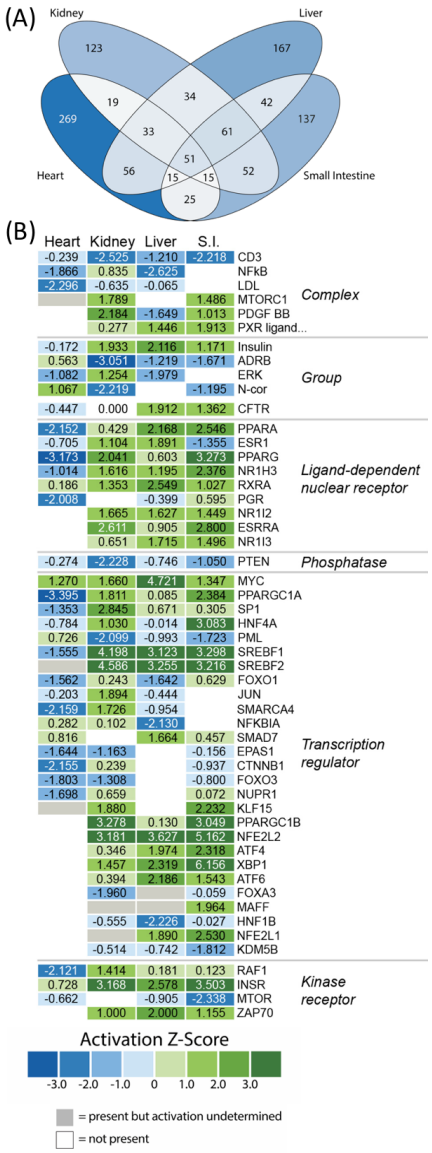


Figure 2.4. **Predicted upstream regulators from IPA analysis of gene expression changes from fasted to 1DPF.** (A) Venn diagram of all upstream regulatory molecules analyzed. (B) Heatmap of predicted activation z-scores for selected classes of upstream regulatory molecules. Green indicates predicted activation, blue indicates predicted inhibition, white indicates the regulator is not predicted to function in that organ, and grey indicates that the upstream regulator is predicted to have significant involvement but the activation state cannot be determined based on the gene expression data. Regulators shown in this heatmap were filtered by three conditions: 1) were present in at least three of the four organs, 2) are significantly predicted (p-value < 0.05), and 3) have activation z-scores greater than |1.5| in at least one organ. Biological drug, chemical, and microRNA categories were excluded from URM analyses.

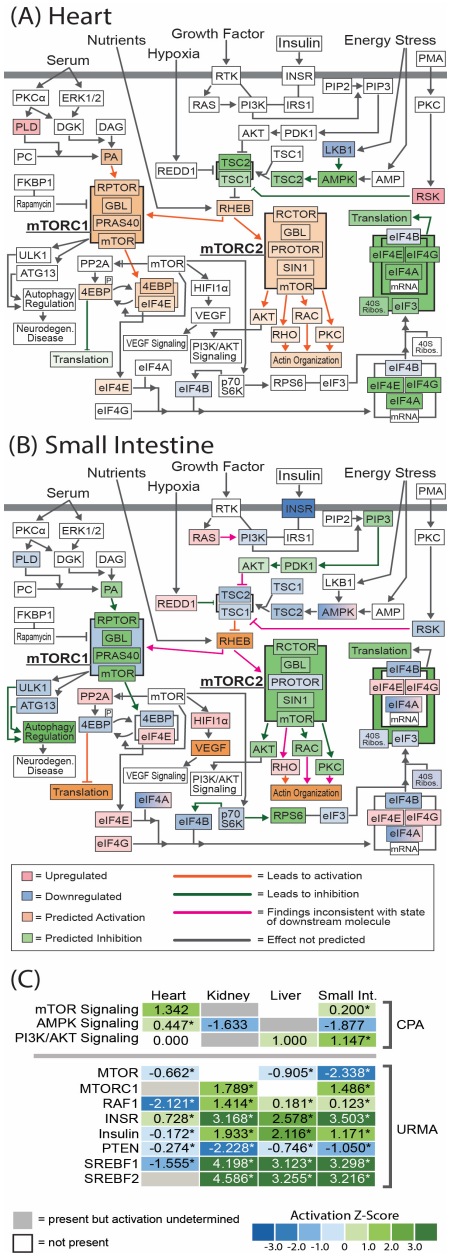


Figure 2.5. **Combined gene expression and predicted activation information for the mTOR pathway in the heart and small intestine.** (A) Gene expression and predicted activity for the mTOR pathway in the heart. (B) Gene expression and predicted activity for the mTOR pathway in the small intestine. Differentially expressed genes identified in our RNAseq data set are highlighted in red (upregulated) and blue (downregulated) while predicted activation states are highlighted in orange (activation) and green (inhibition). (C) CPA and URMA results for pathways and upstream regulatory molecules involved in mTOR signaling and other relevant growth pathways.

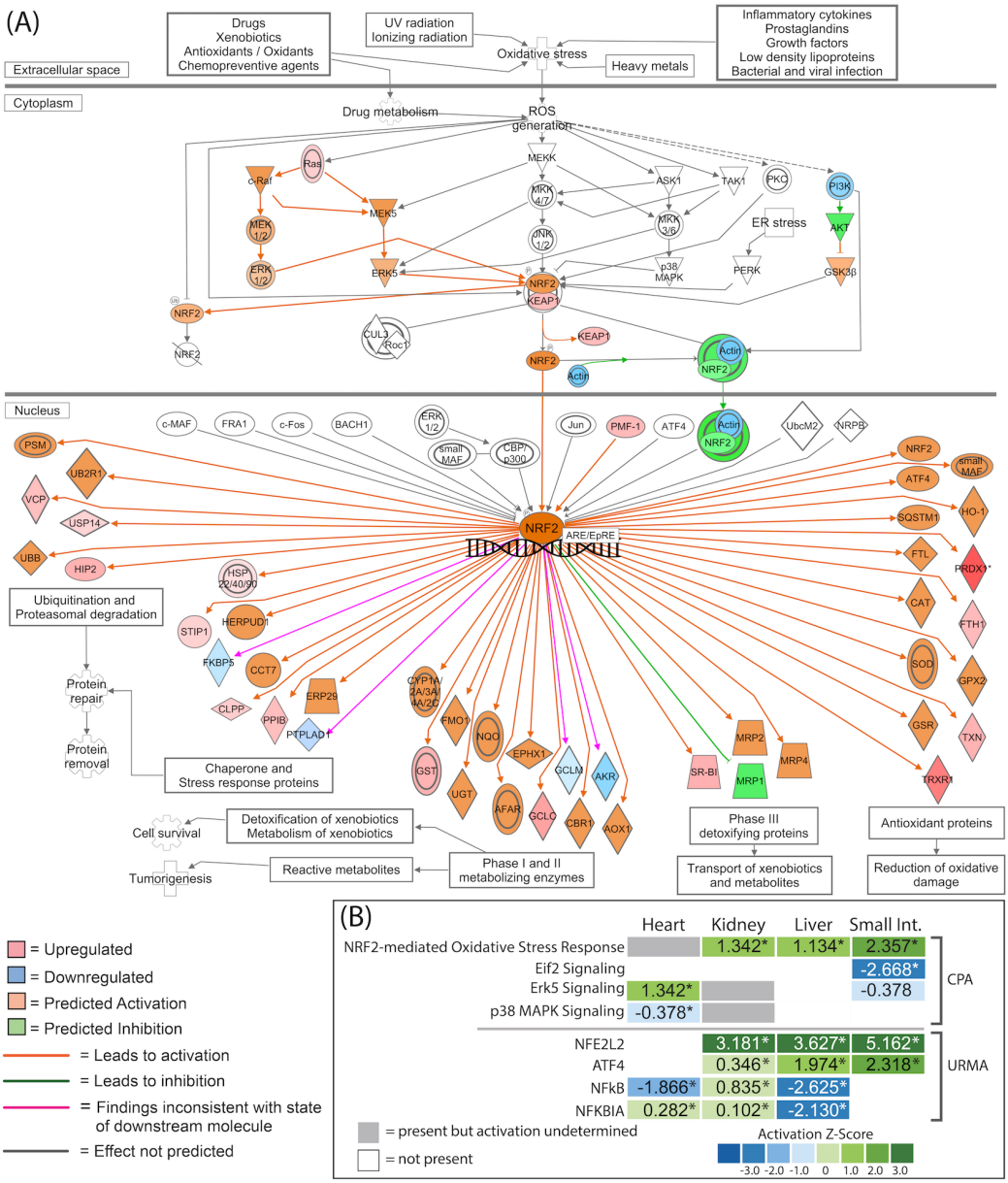


Figure 2.6. **IPA generated pathway prediction for the NRF2-mediated oxidative stress response in the small intestine.** Predicted activation state of the pathway was estimated using genes identified as significantly differentially expressed from our RNAseq data set.

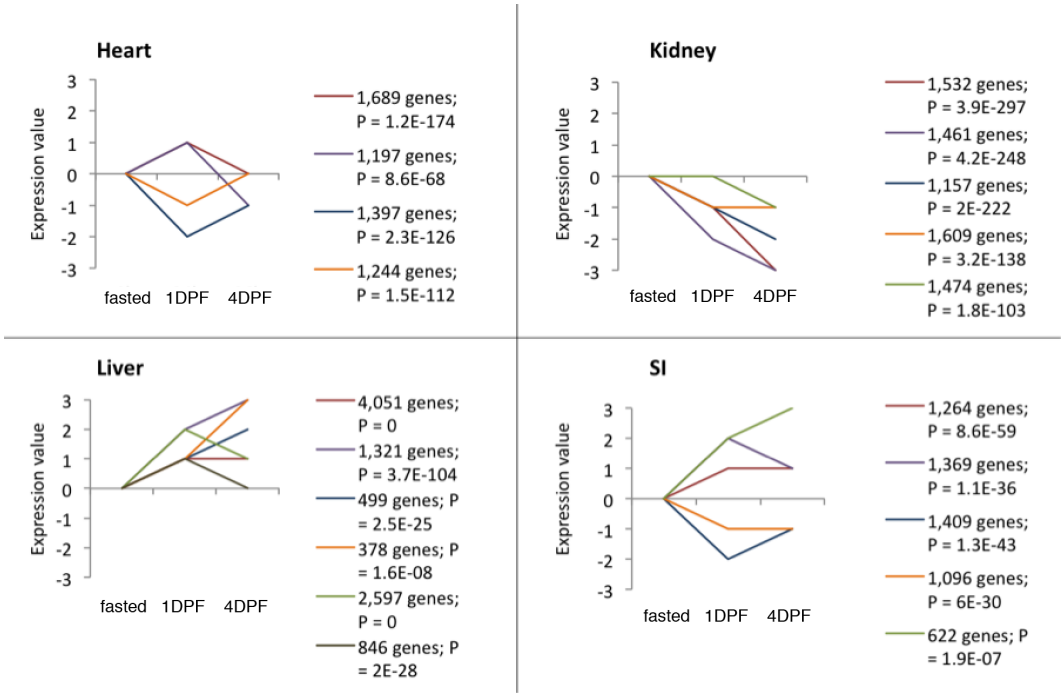


Figure 2.S1. **STEM analysis of all genes differentially expressed across all time points (fasted – 4DPF).** All significant expression profiles are shown with P-value and number of genes following that profile.

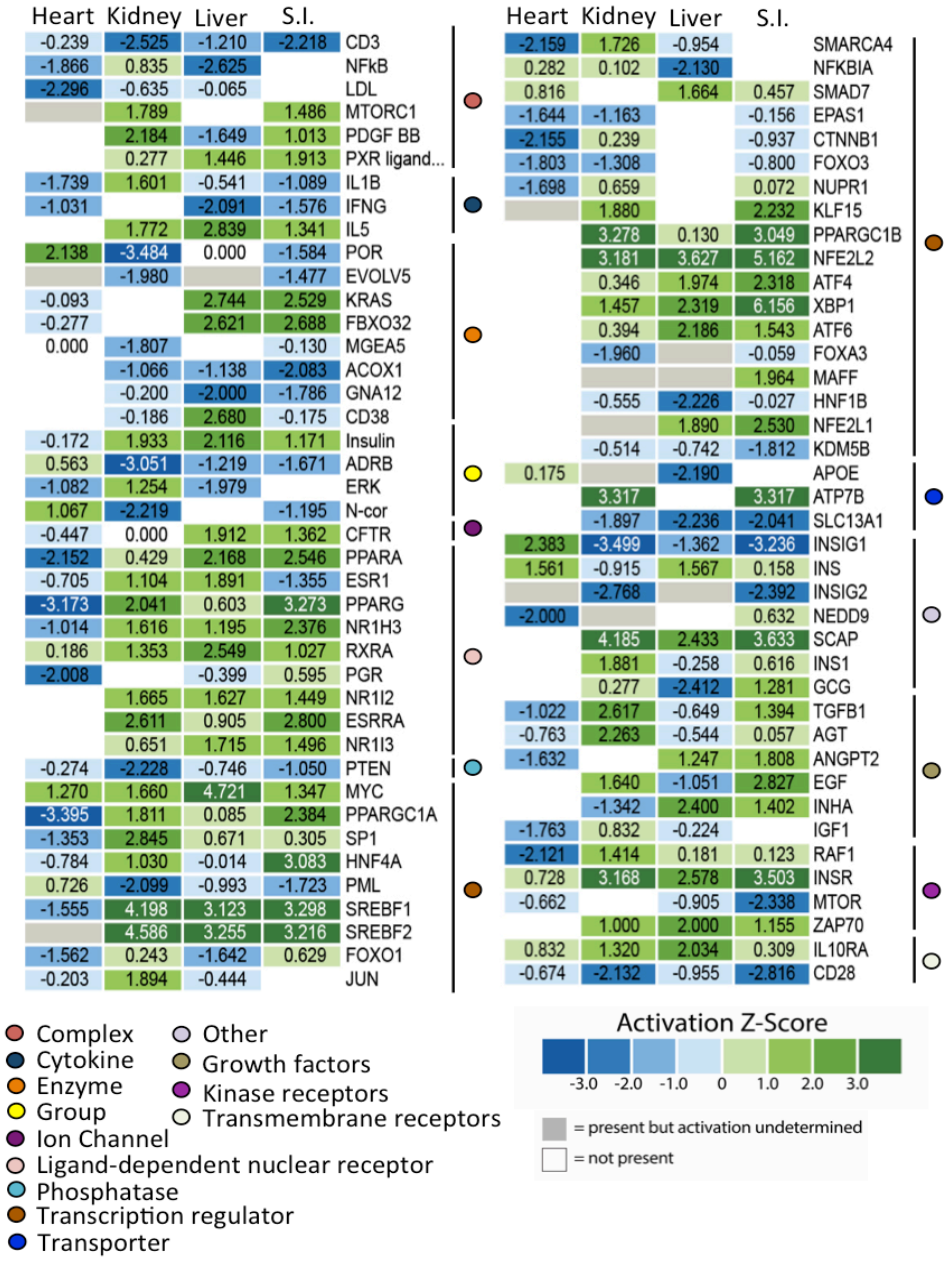


Figure 2.S2. **Heat maps depicting activation z-scores for classes of upstream regulator molecules significant between fasted and 1DPF.** Green indicates predicted activation, blue indicates predicted inhibition, white indicates that the regulator is not predicted to function in that organ, and grey indicates that the upstream regulator is predicted to have significant involvement but the activation state cannot be determined based on the gene expression data. Regulators shown on the heat maps were filtered by activation z-scores greater than |1.5| in at least one tissue.

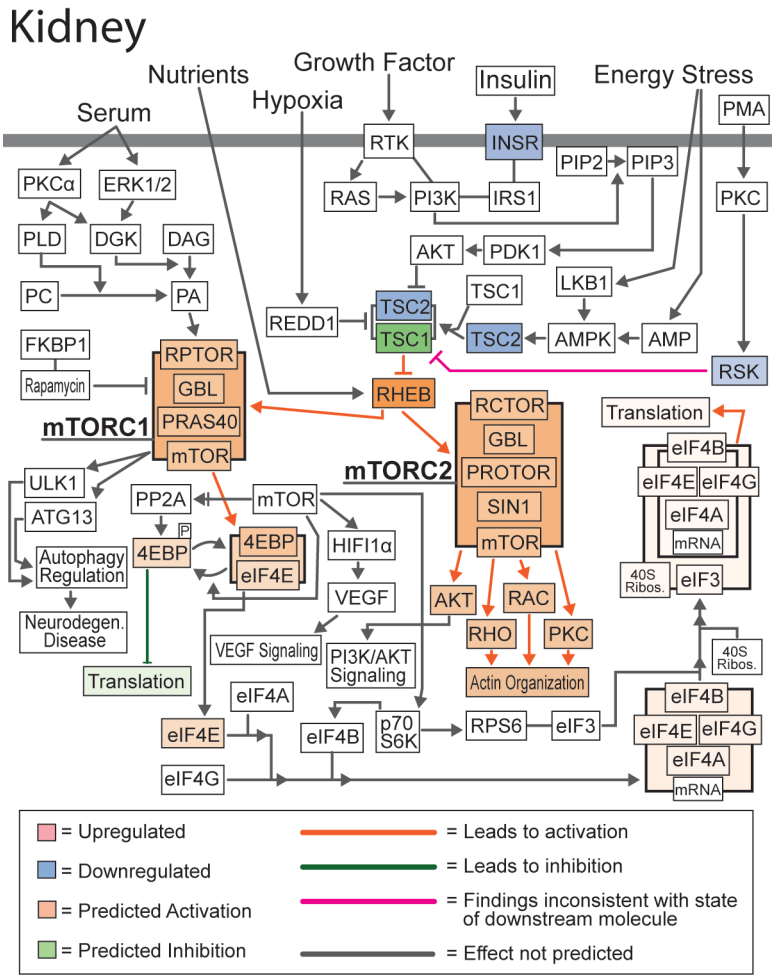


Figure 2.S3. **Combined gene expression and predicted activation information for the mTOR pathway in the kidney.** Differentially expressed genes identified in our RNA-seq data are highlighted in red (upregulated) and blue (downregulated) while predicted activation states are highlighted in orange (activation) and green (inhibition).

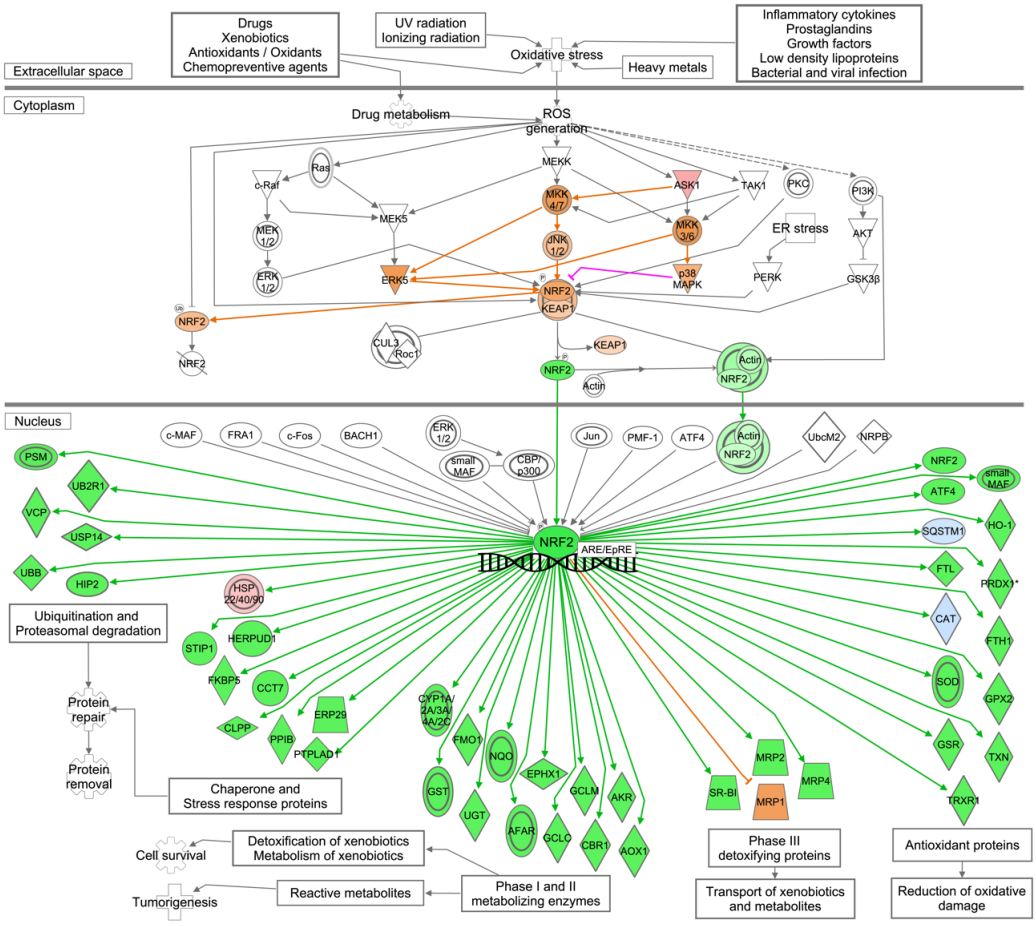


Figure 2.S4. **Pathway prediction for the NRF2-mediated oxidative stress response in the heart.** Predicted activation state of the pathway was estimated using genes identified as significantly differentially expressed form our RNA-seq data set.

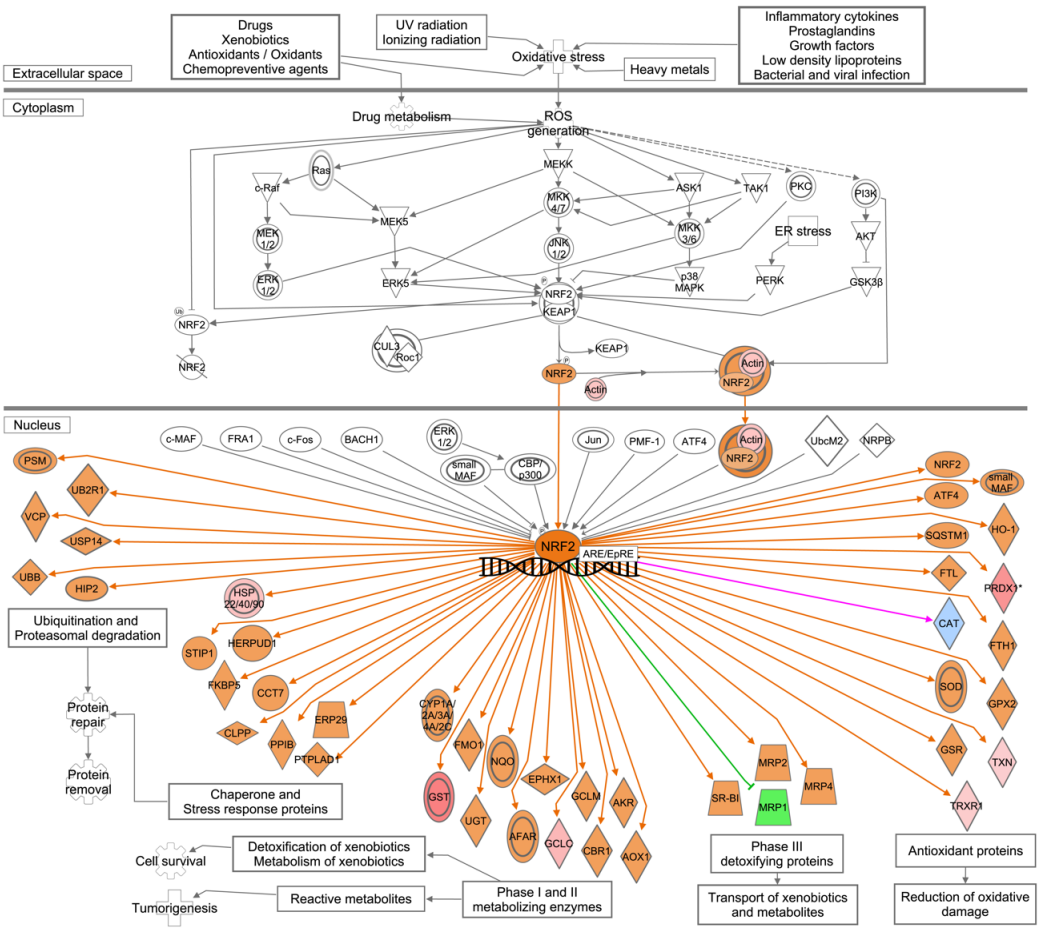


Figure 2.S5. **Pathway prediction for the NRF2-mediated oxidative stress response in the kidney.** Predicted activation state of the pathway was estimated using genes identified as significantly differentially expressed from our RNA-seq data set.

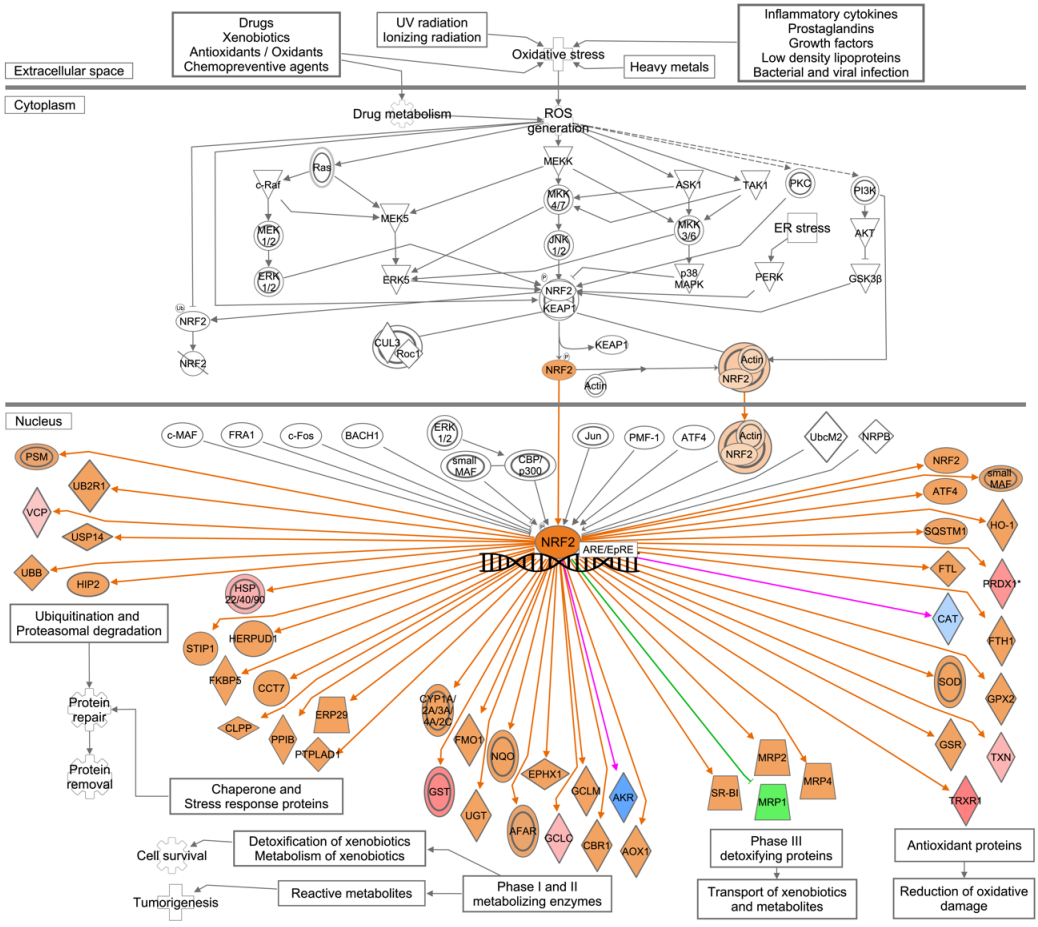


Figure 2.S6. **Pathway prediction for the NRF2-mediated oxidative stress response in the liver.** Predicted activation state of the pathway was estimated using genes identified as significantly differentially expressed from our RNA-seq data set.

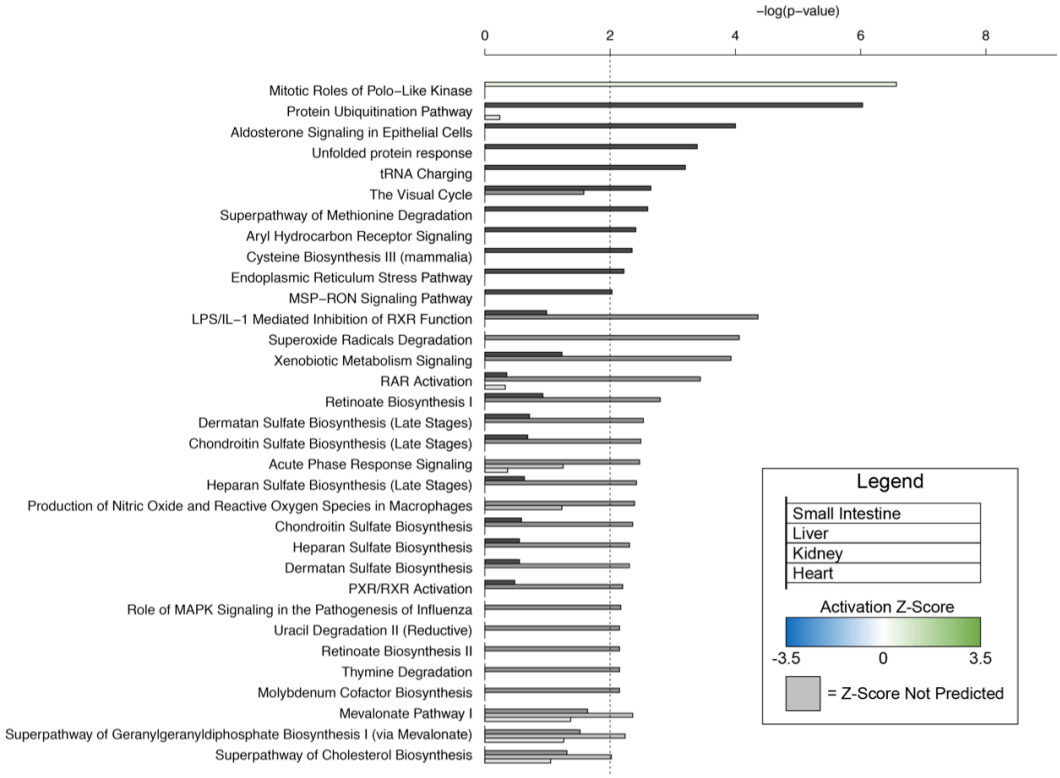


Figure 2.S7. **Pathway analysis of all genes significantly differentially expressed from 1DPF to 4DPF in the four organs.** Bar graph showing significant canonical pathways (Fisher's Exact test P<0.01) enriched for genes differentially expressed at these time points. Pathways were filtered to include those with at least one significant p-value in one of the four organs. Bars are colored based on the predicted activation Z-score for that pathway.

Chapter 3

# Identifying core signaling mechanisms underlying postprandial regenerative kidney growth in snakes using a multi-species comparative approach

## Introduction

Understanding the mechanisms underlying organ regenerative growth in vertebrates poses exciting potential for improving our understanding of the factors that regulate organ growth, as well as eventually for the treatment of human diseases. Traditional model systems, however, offer limited insight into natural organ regeneration due to the subtleties of this response in these organisms [1-4]. Among organ systems, kidney function, development, and diseases have been thoroughly studied in model vertebrate systems [2, 3, 5-12]. While some mechanisms of kidney regenerative growth are well understood, previous studies have been based mostly on regeneration following injury or disease [9, 10, 12-17], thereby lacking a perspective on kidney regenerative growth based on non-injurious natural conditions.

To provide new insight into mechanisms underlying natural tissue regeneration in vertebrates, new non-traditional model systems that possess extreme regenerative growth responses are valuable. Snakes represent one such non-traditional model system because multiple species of snakes demonstrate a number of extreme phenotypes, including extreme organ regenerative growth following feeding [18-32]. The quintessential model system for studying these extreme postprandial responses in snakes has been the Burmese python [18, 24-29, 31-34]. Burmese pythons have evolved the ability to conserve energy during long periods of fasting by downregulating the form and function of major organs [21, 25, 27, 29, 35, 36]. Upon feeding on a relatively large meal,

Burmese pythons can rapidly and reversibly upregulate major organ systems, as well as their physiology and metabolism, at scales that dwarf that observed in mammalian systems. For example, within 48 hours of feeding, the wet masses of the heart, kidney, liver, and small intestine increase by 40-150%, while the snakes may experience up to a 44-fold increase in metabolic rate and 160-fold increase in plasma triglycerides [18, 21, 25, 27, 35, 37].

Previous studies have addressed both the physiological and genomic mechanisms underlying this extreme organ regenerative growth across multiple organ systems in the Burmese python [21, 25-28, 31, 32, 35, 37]. Upon feeding, hundreds to thousands of genes are significantly differentially expressed per organ; these genes have been linked to pathways important in cell cycling, apoptosis, WNT signaling, and mTOR signaling, and include genes and pathways known to be important for human development and disease [25-27, 31, 32]. Previous analyses have also predicted the activation of the NRF2-oxidative stress response during these extreme growth responses, which is indicative of a cytoprotective response to oxidative stress likely linked to the protection of tissues during extreme growth conditions that may otherwise lead to cell death [26]. Despite substantial progress studying this response in the Burmese python, no previous molecular studies have focused exclusively on these regenerative growth responses in the kidney, nor have any studies conducted experiments on snake species outside of the python.

Multiple distantly related lineages of snakes, particularly those that feed on large meals and infrequently in nature, are known to experience postprandial regenerative organ growth [20, 38]. Despite this, no studies of the molecular mechanisms underlying postprandial organ regeneration have been conducted in species other than the Burmese python. This raises the question of whether mechanisms underlying regenerative organ

growth in the python are shared or distinct from those underlying organ regeneration in other lineages of snakes that possess this regenerating phenotype – this is particularly relevant considering some lineages of snakes that share similar regenerating phenotypes (e.g., rattlesnakes and pythons) may be as much as 100MY divergent from one another [39, 40]. Additionally, the large scale of the regenerative growth responses in pythons, involving differential expression of hundreds to thousands of genes per organ, makes it difficult to differentiate essential mechanisms underlying the response from the many responsive genes and pathways observed, which may include various species-specific nuances and/or genes upregulated during feeding but not essential for regenerative growth. Thus, a comparative framework involving multiple species of snake that do and do not experience regenerative growth after feeding is necessary to not only understand potential variation in regenerative growth mechanisms across divergent species with convergent regenerative phenotypes, but to also better dissect and understand the core genes, pathways, and regulatory interactions that drive this extreme regenerative response through comparison against non-regenerating species.

Here we use such a comparative approach for dissecting the molecular signaling mechanisms underlying postprandial kidney regenerative growth in snakes. We conduct analysis of kidney-specific gene expression in two snake species known to undergo organ regenerative growth, the Burmese python (*Python molurus bivittatus*) and the prairie rattlesnake (*Crotalus viridis*), to test the degree to which gene expression responses and signaling mechanisms underlying kidney regenerative growth are shared between these distantly related species, and to identify a reduced set of core shared mechanisms that underlie the regenerative response. We also compare these species to a third snake species, the diamondback water snake (*Nerodia rhombifer*), which does not regenerate its organs upon feeding, to differentiate between responses that may

accompany feeding in general from those that are specifically associated with regenerative growth. Our results broadly highlight the power of a comparative multi-species approach for understanding core signaling responses, and provide new evidence for a shared set of growth and stress-response mechanisms underlying regenerative kidney growth in snakes that likely is broadly relevant in vertebrates.

## Materials and methods

### *Feeding experiments and the generation of transcriptome libraries*

Burmese pythons used in this study were commercially bred, while both prairie rattlesnakes and diamondback water snakes were captured from the wild. All experimental protocols were approved by the University of Alabama Institutional Animal Care and Use Committee (14-06-0075). Snakes were humanely euthanized and sampled at three post-feeding time points, 30 days fasted, 1 day post-feeding (1DPF), and 4DPF. Meal size and methods for euthanization and tissue sampling were identical to those used in our previous studies of the Burmese python [25, 26].

Total RNA was extracted from ~50mg of snap frozen tissue, and all steps of RNA extraction and mRNAseq library generation follow previous studies [25, 26]. In brief, Illumina mRNA-seq libraries were constructed using either the Illumina TruSeq RNA-seq kit or the NEB Next RNA-seq kit, both of which include poly-A selection, RNA fragmentation, cDNA synthesis, and indexed Illumina adapter ligation. Libraries were quantified on a BioAnalyzer (Agilent), poled in equal molar ratios in various multiplex arrangements, and sequenced on either an Illumina GAIIx or HiSeq (see Supplementary Table S1).

*Gene expression analysis*

Raw Illumina RNA-seq reads were quality filtered using Trimmomatic v. 0.32 [41], and reads from each of the three snake species were mapped to the annotated Burmese python transcriptome[27] using BWA v. 0.6.1 [42] with default parameters except: mismatch penalty=2, gap open penalty=3, and alignment score minimum=20. We previously annotated all Burmese python transcripts with human Ensembl identifers [43, 44] to facilitate the use of pathway prediction programs [25, 26], and both rattlesnake and water snake genes (identified via mapping to the Burmese python transcriptome) were assigned human Ensembl identifiers based on this established orthology to python genes. Numbers of unique reads that mapped to annotated transcripts were counted using SAMtools v. 0.1.19 [45]. All newly generated RNAseq data were combined with data previously published from Burmese pythons [25, 26]. Newly-generated sequencing data were archived on the NCBI Short Read Archive (accession SRA###*PENDING*###).

Expression counts were TMM normalized in edgeR [46]. Pairwise exact tests for the binomial distribution were calculated in edgeR [46], and step-wise regression analysis of differential gene expression across time points was conducted in maSigPro [47]. The visualization and clustering of gene expression profiles in heatmaps was conducted using average linkage hierarchical clustering based on a Bray-Curtis dissimilarity matrix in the R package vegan [48]. All statistical methods followed approaches used in previous studies [25, 26]. In addition to the standard TMM normalization, we further scaled all expression counts using the harmonic mean of scale factors calculated for a set of 8 standard housekeeping genes: *ACTB*, *GAPDH*, *RPL13*, *SDHA*, *TBP*, *YWHAZ*, *USP30*, and *PPIA*. These methods were repeated for the additional two species. However, to provide more information going into functional analysis programs, we considered all genes with FDR < 0.2.

*Pathway and functional analysis of genes*

To infer the cellular mechanisms enriched for differentially expressed genes in our dataset, we performed gene enrichment analysis using g:Profiler [49] and focused specifically on Reactome pathways [50], which we found to provide more mechanistic insight than gene ontology (GO) terms. Only pathways enriched with a corrected p-value < 0.05 were considered significant. Cellular pathways and upstream regulatory molecules involved in this response were predicted using Ingenuity Pathway Analysis (IPA; Qiagen). Both Canonical Pathway Analysis (CPA) and Upstream Regulatory Molecule Analysis (URMA) with default parameters were used. As per IPA defaults, the fold-change value for each differentially expressed gene was used as input for IPA analyses to infer the activation direction or sign (activated versus inhibited) between particular time points. In rare cases in which gene duplicates existed, the maximum fold change was used. Upstream regulatory molecules with a p-value of less than 0.06 were considered significantly enriched for the gene expression data.

## Results

*Broad gene expression response during kidney regenerative growth*

Hundreds of genes are differentially expressed (FDR < 0.2) in all three species of snakes within the first 24 hours of consuming a meal (Fig. 1A). Consistent with the watersnake not undergoing post-feeding organ growth, this species shows differential regulation of only 197 genes, compared to 791 genes in the python and 2,108 genes in the rattlesnake. It is notable that, compared to the python, the rattlesnake shows consistently higher numbers of differentially regulated genes, and this is likely due to the rattlesnake having far greater numbers of mapped reads per sample. Additionally, the water snake samples also had a higher number of mapped reads than pythons, but a

lower number than rattlesnakes (see Fig. 1B & Supplementary Table S2). However, both the python and rattlesnake share a large number of genes (290) differentially expressed during kidney growth, while the water snake shares less than 70 genes with these two other species (Fig. 1A). Expression patterns of significantly differentially regulated genes also appear quite species specific, as well as variable between individuals within species (Fig. 1C). The python and rattlesnake show varying patterns of upregulation and downregulation of genes, along with differences in the rate of reset of these expression patterns. In contrast to the two regenerating species, the majority of genes in the water snake appear to be downregulated in response to feeding, and many of these genes appear to be nearly reset to fasted levels by 4DPF (Fig. 1C).

Regression analysis of genes from all three time points indicated similar patterns of unique and shared gene responses between species (Fig. S1A). The python showed significant differential expression (FDR < 0.05) of 888 genes, the rattlesnake had 3,046 genes, and the water snake showed differential regulation of 717 genes (Fig. S1B). The python and rattlesnake still shared the highest number of genes (~261), while the water snake shares less than 240 genes with either regenerating species (Fig. S1A). Interestingly, genes significantly differentially expressed across all three time points show faster levels of reset in the rattlesnake and water snake than in the python (Fig. S1B).

*Candidate gene responses during kidney regenerative growth*

Due to the known hyperplasic response of the kidney, we were interested in examining expression patterns for genes involved in cell cycling, along with those involved in apoptosis that may play a role in the atrophy of the organ once digestion is complete (Fig. 2). Both the python and the rattlesnake showed fairly clear expression

patterns for these candidate genes, regardless of significance, while few of these genes in the water snake showed clear expression patterns.

Intriguingly, many genes important to cell cycling and division are downregulated within 1DPF in both the python and rattlesnake. Chromosome open reading frame 166 (C14orf166), found to regulate gene expression and the G1/S phase transition during cell cycling, is downregulated upon feeding in the python. Cyclin I (CCNI), which is known to be expressed throughout cell cycle progression, and Cyclin dependent kinase like 1 (CDKL1) are also downregulated upon feeding in regenerating species. MOB Family member 4 (MOB4), important for the completion of mitosis and cytokinesis, as well as the dynein molecule DNAH10 also appear to be downregulated during digestion. RAD21 cohesin complex component (RAD21) has been associated with the cohesion of sister chromatids during mitosis as well as apoptotic processes and is also inhibited during organ regenerative growth along with Shugoshin 1 (SGOL1), which prevents the centromere cohesin complex from being prematurely cleaved during prophase, and Emerin (EMD), important to cytoskeletal organization (Fig. 2).

We also see significant upregulation of several cell cycle genes, including tubulin components TUBA4A and TUBB4B and several proteasome subunits. Heat shock protein HSP 90-alpha (HSP90AA1) is upregulated during this response and may play a role in the maintenance and regulation and proteins involved in cell cycling and growth control. In contrast to what we expected, we saw very few significantly upregulated genes shared between species involved in cyclin regulation and specific division processes, but instead saw significant differential regulation of genes involved in the periodicity of proteins (e.g., proteasome components) as well as those involved in cytoskeletal regulation during this response (Fig. 2).

We were also interested in examining the differential regulation of apoptosis, which likely contributes to the atrophy of the kidney following digestion. Cell death activator CIDE-3 (CIDEC), important to adipocyte apoptosis, is upregulated in both regenerating species within 1DPF along with Cytochrome C (CYCS). As expected, the majority of significantly downregulated apoptosis genes shared between species were downregulated during organ growth, including tumor suppressors Programmed cell death 4 (PDCD4) and Death associated protein kinase 1 (DAPK1), as well as several other genes identified in various apoptotic processes (Fig. 2).

Due to the massive gene expression changes during post-feeding regenerative growth of the kidney, we were also interested in epigenetic modifications that may contribute to this response. We observed the significant differential expression of three genes important to histone modifications across the three time points, KAT7, a histone acetyltransferase, HDAC5, a histone deacetylase, and PRMT1, a histone methyltransferase (Fig. 2.).

*Enrichment of pathway responses during tissue regeneration*

While gene expression levels yielded both shared and divergent responses across species, the stark contrast in gene expression and regulatory mechanisms between regenerating and non-regenerating species becomes increasingly clear with gene enrichment analyses of higher-level pathways (Fig. 3). Enrichment analyses of genes differentially expressed between fasted and 1DPF animals, predict 69 Reactome pathways shared between the python and rattlesnake, while the water snake showed significant enrichment of only 3 pathways (only one of which is shared with regenerating species). Those shared between the two regenerating species include multiple cell cycle and mitosis pathways, stress response pathways, apoptosis, lipid signaling, and

Hedgehog ligand biogenesis. The only pathways predicted to be enriched in the water snake were scavenging by class A receptors, glycogen storage disease type 0, and metabolism of amino acids and derivatives (Fig. 3).

*Predicted regulation of upstream regulatory molecules during kidney growth: fasted vs 1DPF*

Analysis of upstream regulatory molecules (URMs) also highlighted the consistent growth responses exhibited by different regenerating species. While many URMs predicted to be differentially regulated upon feeding are unique to individual species, we were able to identify 108 URMs shared between regenerating species. As expected, the water snake exhibited a very unique URM response with only 51 shared with the other two species (Fig. 4A).

Examining a subset of URMs shared between the python and rattlesnake, as well as those shared among all 3 species, a clear pattern of growth and stress response signaling emerges (Fig. 4B). Within 1DPF, pathway analysis predicts the significant involvement of several pathways related to growth, including insulin and mTOR signaling, as well as growth factor and lipid signaling pathways. Both the insulin receptor (INSR) and insulin 1 (INS1) are predicted to be activated during this feeding response (Fig. 4B). Insulin and insulin-like growth factors are responsible for the regulation of several downstream pathways we see activated here, including mTOR, growth responses, and lipid synthesis. URMA analysis also predicted the significant differential regulation of multiple regulatory molecules involved in mTOR signaling. V-Myc avian myelocytomatosis viral oncogene homolog (MYC) is predicted to be strongly activated (Z-score > 2) and is known to interact with mTOR and regulate cell proliferation. Transcription factor 7 like 2 (TCF7L2) is a modulator of MYC and is also activated during

kidney regenerative growth. Interestingly, RPTOR independent companion of MTOR complex 2 (RICTOR) is predicted to be strongly inhibited (Z-score < -3) (Fig. 4B). Phosphatase and tensin homolog (PTEN), a negative regulator of mTOR, is predicted to be inhibited in the python and slightly activated in the rattlesnake. Estrogen related receptor alpha (ESSRA) is activated in both regenerating species along with Epidermal growth factor (EGF) and its receptor (EGFR), indicating stimulation of cell growth and differentiation during kidney regenerative growth.

Lipid signaling was one of the most consistent shared pathways between the python and rattlesnake, with clear activation of sterol regulatory element-binding protein (SREBP) signaling. Both SREBF1 and SREBF2 were predicted to be strongly activated (Z > 3) in both the python and rattlesnake, with no involvement predicted in water snake. SREBF chaperone (SCAP) and Membrane bound transcription factor peptidase (MBTPS1), both important activators of SREBPs, also shows clear patterns of activation during this regenerative growth response. This is consistent with strong predicted inhibition of Insulin induced genes 1 & 2 (INSIG1 & INSIG2; Z < -2), which prevent the processing and activation of SREBPs. Diazepam-binding inhibitor (DBI), a fatty acyl binding protein, is also predicted to be activated (Z > 2) in both regenerating species along with the predicted inhibition of Acyl-CoA oxidase 1 (ACOX1) and Cytochrome P450 51A1 (CYP51A1), which is involved in cholesterol synthesis. We also see strong and consistent predicted activation of the PPAR signaling pathway, including Peroxisome proliferator activated receptor gamma (PPARG) and its coactivators (PPARGC1A & PPARGC1B) along with PPARA. Reinoid X receptor alpha (RXRA) along with transcription factors NR1I2 and NR1I3 are also activated and broadly regulated lipid signaling mechanisms (Fig. 4B).

As predicted, stress responses appear to be strongly activated during kidney regenerative growth during these extreme fluctuations in metabolism and physiology. Heat shock transcription factor 2 (HSF2) and CCAAT/Enhancer binding protein alpha (CEBPA), both regulated by stress responses, were predicted to be activated in both the python and rattlesnake within 1DPF. Predictions indicate that Nuclear factor, erythroid 2 like 2 (NFE2L2), Nuclear factor, erythroid 2 like 1 (NFE2L1), and Activating transcription factor 4 (ATF4) are activated upon feeding along with X-box binding protein 1 (XBP1), indicative of activation of the NRF2 oxidative stress response. Mitogen-activated protein 4K 4 (MAP4K4) and Tumor suppressor P53 (TP53) are predicted to be inhibited in both the python and rattlesnake. Endoplasmic Reticulum to nucleus signaling 1 (ERN1), which interacts with XBP1, is predicted to be inhibited in the python but strongly activated in the rattlesnake (Fig. 4B).

Three immune response regulators were also predicted to be involved in kidney regenerative growth. CD28 and CD3, regulators of T-cells, were predicted to be inhibited upon feeding, while Interleukin 5 (IL5), a B cell regulator, shows predicted activation in all three species. Additionally, we saw significant enrichment for upstream regulators involved in various kidney and miscellaneous functions. Kruppel like factor 15 (KLF15) showed significant activation in both the python and rattlesnake upon feeding and has been linked to podocyte differentiation. ATPase copper transporting beta (ATP7B) functions as a copper transporter and is also activated in response to feeding. LIM homeobox 1 (LHX1) is a transcription factor involved in renal development and shows contrasting patterns of regulation in both regenerating species, while Solute carrier family 13 member 1 (SLC13A1) was predicted to be inhibited during regenerative growth and is involved in renal absorption of sulfate (Fig. 4B).

*A role for mTOR signaling in kidney regenerative growth*

Using CPA to examine the mTOR pathway in detail reveals strong evidence for involvement of this response in regenerating species (Fig. 5). Observed and predicted expression responses of mTOR genes indicate activation of this pathway in both they python and rattlesnake. In contrast, mTOR signaling appears inhibited in the water snake, with very little responsiveness across regulators of this pathway in this non-regenerating species. Both regenerating species show strong predicted and observed inhibition of Tuberous sclerosis 1 (TSC1) and Tuberous sclerosis 2 (TSC2), potent negative regulators of mTOR signaling. In the python, both mTORC1 and mTORC2 are predicted to be activated, while in the rattlesnake mTORC1 appears inhibited while mTORC2 is activated. However, the predicted inhibition of mTORC1 in the rattlesnake is based only on the observed expression response of a single gene (PRAS40) (Fig. 5). Intriguingly, the fact that RICTOR was predicted as strongly inhibited in URMA analysis (Fig. 5B) would indicate that mTOR signaling is shunted through mTORC1 and not mTORC2. Several translation initiation factors linked downstream of mTOR show various patterns of up and downregulation in both regenerating species. Intriguingly, we see highly consistent regulation of mTOR signaling following feeding in the python and rattlesnake (Fig. 5).

*Response of upstream regulatory molecules during early phases of atrophy: 1DPF vs. 4DPF*

URMA analysis of genes significantly differentially expressed between 1DPF and 4DPF indicate a clear reversal of the response observed during kidney growth. As the peak of digestion ends and digestion begins to approach completion, we see significant

predicted inhibition of insulin and growth signaling (Fig. S2). While SREBF genes were strongly activated during growth (Fig. 4B), here we see strong and consistent signals of inhibition, along with less consistent responses of PPARs. MYC, also activated during growth (Fig. 4B), is also strongly inhibited during this later time point (Fig. S2).

## Discussion

While previous studies have identified key physiological and gene expression responses underlying post-feeding organ regenerative growth in the Burmese python [18, 20, 21, 25-27, 31, 35], this study provides the first analysis of such regenerative responses across multiple species of snakes (with both similar and divergent regenerative phenotypes), providing comparative insight into the core set of shared responses that underlie regenerative organ growth. Further, this study provides the first analysis of these responses specifically focused on the snake kidney. Previous comparative physiological and phenotypic studies have suggested that post-feeding regenerative organ growth in snakes has likely evolved multiple times and appears surprisingly plastic – coevolving with ecological shifts in feeding habits of species [38]. For example, this extreme feeding response has been observed in some species of boas, pythons, and also more distantly related vipers [21, 37, 38, 51], yet many species of snakes do not exhibit these extreme fluctuations in physiology during digestion [38, 52]. While such a complex trait (i.e., involving major shifts in expression of many genes) would be expected to show low evolutionary plasticity, the broad phylogenetic dispersion of post-feeding organ growth in divergent snake lineages begs the question of whether some core aspects of this response evolved early in ancestral snakes, and are thus shared among distantly related snake lineages possessing this phenotype. In the case of

the kidney, our results suggest hierarchically divergent support for this hypothesis – while only a subset of gene-specific responses were shared between regenerating species, regenerative responses at the level of pathway and upstream regulators appear highly conserved and indicative of a shared derived response.

In addition to providing a perspective on the evolutionary origins of the post-feeding regenerative phenotype in snakes, the phenotypic and evolutionary diversity of snake species that do and do not regenerate organs upon feeding provides a valuable comparative system. Specifically, comparisons across divergent lineages with shared or divergent phenotypes provides an ideal experimental design for determining pathways and mechanisms that are central to organ regenerative growth, while also allowing identification of species-specific nuances and responses that are differentially regulated simply due to feeding. Given the large number of responsive genes in regenerating species (e.g., 791 in the python kidney), such a comparative approach allows the narrowing of focus to a subset of these genes, and associated pathways, which can more tractably be studied using functional or experimental approaches. This rational was well demonstrated by our results, which highlight ~300 differentially expressed genes upon feeding that are shared between regenerating species, and a much smaller set of relevant shared pathways and upstream regulatory molecules.

*Differential gene expression following feeding: Divergent responses of regenerators and non-regenerators*

Divergent patterns of gene expression between regenerators and non-regenerators emerge immediately from pairwise analyses between fasted snakes and snakes at 1DPF. Both the python and rattlesnake have massive numbers of differentially regulated genes (~800 - ~2,000) upon feeding, while the water snake experiences

differential regulation of fewer than 200 genes. Additionally, 290 differentially regulated genes are shared between the python and rattlesnake, while fewer than 70 genes are shared between the water snake and both regenerating species (Fig. 1A). The water snake does not regenerate its kidney upon feeding [52], and thus, we would expect few commonalities in gene expression response with regenerating species, as we observed. Visualization of these differentially expressed genes is indicative of varying rates of reset following regenerative growth in both regenerating species, and importantly, it does not appear that genes activated in the kidney upon feeding are completely reset by 4DPF in either the python or the rattlesnake (Fig. 1B).

*The regulation of cell division and apoptosis during growth and subsequent atrophy of the kidney*

Previous analyses of the Burmese python small intestine have highlighted the role of cell cycle responses in hyperplasic regenerative organ growth [25], however candidate gene analysis of cell cycling in the kidney provides a mixed conclusion, possibly due to divergent responses of different cell types present in the kidney. For example, we found little differential regulation of cyclins and other genes specific to active cell cycling and division, and contrary to expectation, genes important to cell cycle and specific mitotic processes appear to be downregulated between fasting and 1DPF (Fig. 2). However, we do see clear and consistent upregulation of genes that form proteasome complexes and heat shock proteins that may play a role in regulating the periodicity of cell cycling proteins during this feeding response [53, 54]. Expression patterns of these same genes in the water snake are inconsistent across time points. These results suggest the possibility of post-translational modification modulating these cell cycle-specific proteins, rather than transcriptional activation/repression. In contrast to the

limited number of key candidate genes identified in this study, and consistent with cell division in kidney tissues upon feeding in regenerating species, enrichment analysis of genes differentially expressed during organ growth reveal a large number of significantly enriched pathways involved in cell cycling with no evidence of active cell division in the water snake (Fig. 3).

Upon completion of digestion, atrophy of organ systems is likely regulated, at least to some extent, by apoptosis [25], and regulation of apoptotic processes was also evident in the kidney of regenerating species. Studies of cell death activator *CIDEC*, identified as upregulated in both the python and rattlesnake upon feeding, have shown the overexpression of this gene in cases of clear cell renal cell carcinoma [55]. Other pro-apoptotic genes are downregulated upon feeding and remain inactivated through 4DPF (Fig. 2). Additionally, tumor suppressor TP53 is predicted to be slightly inhibited in both python and rattlesnake but activated in the water snake (Fig. 4), indicative of active cell cycling and inhibition of apoptosis during kidney regeneration. This pattern of inactivation of pro-apoptotic genes indicates that apoptosis is not occurring at 4DPF and that cell death may occur at later time points. This is consistent with the previous findings that the execution of apoptosis in the Burmese python small intestine likely does not occur until around 10DPF [25].

*Shared responsive pathways in snake kidney regeneration: mTOR signaling*

Previous studies in the python have inferred a central role for tightly regulated growth responses (largely integrated through insulin and mTOR signaling) coupled with the activation of stress responses pathways mediated by NRF2 during organ regenerative growth in the kidney and other organs (small intestine and liver) [26]. mTOR signaling has been implicated in a wide variety of renal growth and disease pathways

[56-59], and expression analysis of this pathway in the Burmese python has indicated that is likely a major driver of post-feeding regenerative growth across major tissues [26]. Strikingly, activation of mTOR upon feeding appears specific to species that regenerate organs upon feeding, with little to no response of this pathway seen in the water snake (Fig. 5). This is indicative of conserved regulation of mTOR signaling during regenerative growth across highly divergent lineages of infrequently feeding species of snakes. Additionally, MYC, a potent activator of both cell cycle and apoptosis [60-65], appears to be consistently activated upon feeding in both the python and rattlesnake with no detected activity in the water snake, and studies have shown that mTOR and MYC interactions contribute to cancer cell proliferation and survival [66, 67], indicating this response is likely to elicit cell proliferative growth activity in regenerating snake kidneys. Epidermal growth factor (EGF), important to regulating DNA synthesis during the cell cycle, is also activated during regenerative growth and has been shown to interact with mTOR during mitogenesis in intestinal epithelial cells [68].

A key characteristic of mTOR signaling in regenerating species was the strong and consistent predicted inhibition of RICTOR, a key component of the mTORC2 complex, during post-feeding kidney regenerative growth. This leads us to believe that mTORC2 may not be involved in regulating kidney regeneration, but that all mTOR activity is shunted instead through the mTORC1 complex. This is relevant, and particularly interesting, as the mTORC2 complex is known to inhibit insulin signaling [69], and recent evidence points to a role of mTORC2 in lipid regulation [70, 71]. Additionally, deletion of RICTOR in *Myf5* precursor cells has been shown to promote the oxidative metabolism of brown adipose tissue and prevent obesity [72], while insulin is unable to suppress lipolysis in RICTOR-null fat cells [73]. Studies of the Burmese python heart have shown that fats do not accumulate in cardiac tissue despite extremely high levels of

circulating plasma triglycerides [21, 31]. In the kidney, fat accumulation may be prevented through the inhibition of RICTOR, and thus inhibition of mTORC2, leading to increased breakdown of fats despite the activation of insulin signaling.

*Lipid signaling during post-prandial kidney regenerative growth*

The role of fatty acid signaling via PPAR-driven pathways in renal disease has been well-established [74-77], and fatty acid signaling has been identified as a clear and consistent systemic mechanistic response during organ regenerative growth in the Burmese python [26]. mTORC1 is known to activate PPARG [70], and both the python and rattlesnake exhibit highly significant (Z-score > 2) activation of PPARG and its coactivators (Fig. 4). PPARG is a known regulator of adipogenesis, cell cycling, and insulin sensitivity [74, 78-82], and studies have shown that PPARG can protect against age-related kidney diseases [83]. Additionally, activation of PPARG stimulates expression of renin, modulating blood pressure [84, 85]. Thus, activation of PPARG in post-feeding kidney regenerative growth in snakes likely modulates a variety of processes, including regulation of insulin sensitivity during the observed 44-fold increases in circulating insulin levels during this response and blood pressure (as demonstrated in the python [21]). Surprisingly, PPARA activation was not only predicted in regenerating species, but also showed slight activation (Z-score < 1) in the water snake (Fig. 4), and has been shown to regulate genes controlling lipid catabolism in the liver [86]. SREBPs, considered master regulators of lipid regulation, are also consistently activated during organ regenerative growth in the Burmese python [26], and the kidney is no exception (Fig. 4). SREBP signaling contributes to increased lipid accumulation in the kidney caused by diabetes and aging [87, 88]. Patterns in the python and rattlesnake indicate positive regulation of lipid synthesis coupled with increased catabolism of fats potentially

mediated through the inhibition of RICTOR discussed above, which may prevent excessive accumulation of fats in the tissues. Additionally, while the majority of this study focused on growth responses, a brief examination of upstream regulatory molecules indicates that growth and stress response processes are beginning to reverse by 4DPF (Fig. S2).

*Stress response signals in the kidney*

Organ regenerative growth in snakes is associated with massive fluctuations in metabolism and organ physiology that will undoubtedly lead to the elevated generation of reactive oxygen species along with other stress-induced cellular reactions that would normally lead to cell death. However, the python has been shown to employ a mechanism – activation of the NRF2 Stress Response Pathway – to combat these extreme cellular pressures and convey cytoprotection during these extreme bouts of organ regenerative growth [26]. This same protective stress response is evident in the python and rattlesnake kidney upon feeding, indicating a surprisingly conserved mechanism for maintaining cellular integrity during such extreme changes in physiology (Fig. 4). Among the multiple URMs associated with NRF2 activation, only ATF4 showed increased activity in all three species, yet the response of the NRF2 pathway in the water snake was minimal (Z-score < 1) compared to the strong activation of the NRF2 pathway inferred for the python and rattlesnake (Z-score > 2; Fig. 4). This is notable because previous studies have demonstrated that NRF2 conveys a similar protective response during acute kidney injury and disease [89, 90].

*Conclusion*

Overall, shared mechanisms of kidney growth in both the python and rattlesnake correlated with pathways and upstream regulatory molecules identified as broad predicted regulators of post-feeding regenerative growth across multiple organs in previous studies of the Burmese python [26]. The majority of this study focused on growth responses, but a brief examination of upstream regulatory molecules indicates that these processes are beginning to reverse by 4DPF (Fig. S2). While large subsets of genes were species-specific (Fig. 1), examination of upper-level regulatory responses reveals a large set of conserved growth and stress response mechanisms in regenerating species (Figs. 3, 4, & 5), and this likely indicates that evolution may have led to the divergence of specific gene expression responses among species, while maintaining the core shared mechanistic pathways regulating organ regenerative growth. Additionally, this suggests that many snake species, as well as vertebrates in general, may have retained the ability to respond to these growth signals. This has already been generally demonstrated in mammalian cells that grow and divide upon exposure to snake signaling molecules that are present in post-fed python blood plasma [19, 31]. Thus, the presence or absence of this phenotype may not be dependent on the differential regulation of thousands of genes, or on a particular species-specific genetic background, but instead may be more tightly linked to the ability to produce particular high-level regulatory signals that induce the response. If this were indeed the case, it would also explain well the high degree of evolutionary plasticity observed in the presence/absence of organ regenerative phenotypes in snake species.

The ability to dissect how vertebrate systems can elicit and direct the regeneration of kidney tissue would be an exciting and important step towards the

development of therapeutics for treating various renal diseases and injuries. Specifically, both mTOR and fatty acid signaling have been extensively studied in renal systems [75, 76, 91-93], and we further predicted activation of KLF15, which has been implicated in podocyte differentiation [94]. These parallels between post-feeding organ regeneration in snakes and known signaling mechanisms underlying renal function, growth and disease suggest that organ regeneration in snake kidneys may provide surprising and highly relevant yet novel perspectives into signaling mechanisms underlying vertebrate kidney regeneration and disease. However, it is also important to note that many genes, including those involved in mTOR signaling, have apparently experienced extensive positive selection in reptiles, presumably to alter protein function [95], and thus, it is an open question of to what extent do mechanisms and pathways in snakes function similarly to homologous pathways in other vertebrates, including humans.

## References


1. Michalopoulos GK, DeFrances MC: **Liver regeneration**. *Science* 1997, **276**(5309):60-66.

2. Diep CQ, Ma D, Deo RC, Holm TM, Naylor RW, Arora N, Wingert RA, Bollig F, Djordjevic G, Lichman B *et al*: **Identification of adult nephron progenitors capable of kidney regeneration in zebrafish**. *Nature* 2011, **470**(7332):95-100.

3. Lin F: **Stem cells in kidney regeneration following acute renal injury**. *Pediatr Res* 2006, **59**(4 Pt 2):74R-78R.

4. Poss KD: **Getting to the heart of regeneration in zebrafish**. *Semin Cell Dev Biol* 2007, **18**(1):36-45.

5. Jin DK, Fish AJ, Wayner EA, Mauer M, Setty S, Tsilibary E, Kim Y: **Distribution of integrin subunits in human diabetic kidneys**. *J Am Soc Nephrol* 1996, **7**(12):2636-2645.

6. Pinto M, Vieira J, Ribeiro FR, Soares MJ, Henrique R, Oliveira J, Jeronimo C, Teixeira MR: **Overexpression of the mitotic checkpoint genes BUB1 and**

**BUBR1 is associated with genomic complexity in clear cell kidney carcinomas**. *Cell Oncol* 2008, **30**(5):389-395.

7. Takasato M, Er PX, Chiu HS, Maier B, Baillie GJ, Ferguson C, Parton RG, Wolvetang EJ, Roost MS, Chuva de Sousa Lopes SM *et al*: **Kidney organoids from human iPS cells contain multiple lineages and model human nephrogenesis**. *Nature* 2015, **526**(7574):564-568.

8. Freedman BS: **Modeling Kidney Disease with iPS Cells**. *Biomark Insights* 2015, **10**(Suppl 1):153-169.

9. LeBleu VS, Taduri G, O'Connell J, Teng Y, Cooke VG, Woda C, Sugimoto H, Kalluri R: **Origin and function of myofibroblasts in kidney fibrosis**. *Nat Med* 2013, **19**(8):1047-1053.

10. Kulkarni OP, Hartter I, Mulay SR, Hagemann J, Darisipudi MN, Kumar Vr S, Romoli S, Thomasova D, Ryu M, Kobold S *et al*: **Toll-like receptor 4-induced IL-22 accelerates kidney regeneration**. *J Am Soc Nephrol* 2014, **25**(5):978-989.

11. Ramos KS, Nanez A: **Genetic regulatory networks of nephrogenesis: deregulation of WT1 splicing by benzo(a)pyrene**. *Birth Defects Res C Embryo Today* 2009, **87**(2):192-197.

12. Kim TM, Ramirez V, Barrera-Chimal J, Bobadilla NA, Park PJ, Vaidya VS: **Gene expression analysis reveals the cell cycle and kinetochore genes participating in ischemia reperfusion injury and early development in kidney**. *PLoS One* 2011, **6**(9):e25679.

13. Mari C, Winyard P: **Concise Review: Understanding the Renal Progenitor Cell Niche In Vivo to Recapitulate Nephrogenesis In Vitro**. *Stem Cells Transl Med* 2015, **4**(12):1463-1471.

14. Davidson AJ: **Uncharted waters: nephrogenesis and renal regeneration in fish and mammals**. *Pediatr Nephrol* 2011, **26**(9):1435-1443.

15. Sander V, Davidson AJ: **Kidney injury and regeneration in zebrafish**. *Semin Nephrol* 2014, **34**(4):437-444.

16. Dong L, Stevens JL, Fabbro D, Jaken S: **Regulation of protein kinase C isozymes in kidney regeneration**. *Cancer Res* 1993, **53**(19):4542-4549.

17. Wise AF, Williams TM, Kiewiet MB, Payne NL, Siatskas C, Samuel CS, Ricardo SD: **Human mesenchymal stem cells alter macrophage phenotype and promote regeneration via homing to the kidney following ischemia-reperfusion injury**. *Am J Physiol Renal Physiol* 2014, **306**(10):F1222-1235.

18. Secor SM: **Digestive physiology of the Burmese python: broad regulation of integrated performance**. *The Journal of experimental biology* 2008, **211**(Pt 24):3767-3774.

19. Secor S, Choudhary A, Lundh M, Wagner B: **Is extreme physiology of Burmese pythons relevant to diabetes?(1108.8)**. *The FASEB Journal* 2014, **28**(1 Supplement):1108.1108.

20. Secor SM: **Evolutionary and cellular mechanisms regulating intestinal performance of amphibians and reptiles**. *Integr Comp Biol* 2005, **45**(2):282-294.

21. Secor SM, Diamond J: **A vertebrate model of extreme physiological regulation**. *Nature* 1998, **395**(6703):659-662.

22. Secor SM, Stein ED, Diamond J: **Rapid upregulation of snake intestine in response to feeding: a new model of intestinal adaptation**. *The American journal of physiology* 1994, **266**(4 Pt 1):G695-705.

23. Secor SM, White SE: **Prioritizing blood flow: cardiovascular performance in response to the competing demands of locomotion and digestion for the Burmese python, Python molurus**. *Journal of Experimental Biology* 2010, **213**(1):78-88.

24. Ott BD, Secor SM: **Adaptive regulation of digestive performance in the genus Python**. *The Journal of experimental biology* 2007, **210**(Pt 2):340-356.

25. Andrew AL, Card DC, Ruggiero RP, Schield DR, Adams RH, Pollock DD, Secor SM, Castoe TA: **Rapid changes in gene expression direct rapid shifts in intestinal form and function in the Burmese python after feeding**. *Physiol Genomics* 2015, **47**(5):147-157.

26. Andrew AL, Perry BW, Card DC, Schield DR, Ruggiero RP, McGaugh SE, Choudhary A, Secor SM, Castoe TA: **Growth and stress response mechanisms underlying post-feeding regenerative organ growth in the Burmese python**. *BMC Genomics* 2017, **18**(1):338.

27. Castoe TA, de Koning AP, Hall KT, Card DC, Schield DR, Fujita MK, Ruggiero RP, Degner JF, Daza JM, Gu W *et al*: **The Burmese python genome reveals the molecular basis for extreme adaptation in snakes**. *Proc Natl Acad Sci U S A* 2013, **110**(51):20645-20650.

28. Helmstetter C, Reix N, T'Flachebba M, Pope RK, Secor SM, Le Maho Y, Lignot JH: **Functional changes with feeding in the gastro-intestinal epithelia of the Burmese python (Python molurus)**. *Zoolog Sci* 2009, **26**(9):632-638.

29. Cox CL, Secor SM: **Matched regulation of gastrointestinal performance in the Burmese python, Python molurus**. *The Journal of experimental biology* 2008, **211**(Pt 7):1131-1140.

30. Cohn MJ, Tickle C: **Developmental basis of limblessness and axial patterning in snakes**. *Nature* 1999, **399**(6735):474-479.

31. Riquelme CA, Magida JA, Harrison BC, Wall CE, Marr TG, Secor SM, Leinwand LA: **Fatty acids identified in the Burmese python promote beneficial cardiac growth**. *Science* 2011, **334**(6055):528-531.

32. Wall CE, Cozza S, Riquelme CA, McCombie WR, Heimiller JK, Marr TG, Leinwand LA: **Whole transcriptome analysis of the fasting and fed Burmese python heart: insights into extreme physiological cardiac adaptation**. *Physiol Genomics* 2011, **43**(2):69-76.

33. Astarita G, Rourke BC, Andersen JB, Fu J, Kim JH, Bennett AF, Hicks JW, Piomelli D: **Postprandial increase of oleoylethanolamide mobilization in small intestine of the Burmese python (Python molurus)**. *Am J Physiol Regul Integr Comp Physiol* 2006, **290**(5):R1407-1412.

34. Esbaugh AJ, Secor SM, Grosell M: **Renal plasticity in response to feeding in the Burmese python, Python molurus bivittatus**. *Comp Biochem Physiol A Mol Integr Physiol* 2015, **188**:120-126.

35. Secor SM, Diamond J: **Adaptive responses to feeding in Burmese pythons: pay before pumping**. *The Journal of experimental biology* 1995, **198**(Pt 6):1313-1325.

36. Starck JM, Beese K: **Structural flexibility of the intestine of Burmese python in response to feeding**. *The Journal of experimental biology* 2001, **204**(Pt 2):325-335.

37. Secor SM: **Regulation of digestive performance: a proposed adaptive response**. *Comp Biochem Physiol A Mol Integr Physiol* 2001, **128**(3):565-577.

38. Secor SM, Diamond JM: **Evolution of regulatory responses to feeding in snakes**. *Physiol Biochem Zool* 2000, **73**(2):123-141.

39. Yin W, Wang ZJ, Li QY, Lian JM, Zhou Y, Lu BZ, Jin LJ, Qiu PX, Zhang P, Zhu WB *et al*: **Evolutionary trajectories of snake genes and genomes revealed by comparative analyses of five-pacer viper**. *Nature communications* 2016, **7**:13107.

40. Hsiang AY, Field DJ, Webster TH, Behlke ADB, Davis MB, Racicot RA, Gauthier JA: **The origin of snakes: revealing the ecology, behavior, and evolutionary history of early snakes using genomics, phenomics, and the fossil record**. *BMC evolutionary biology* 2015, **15**.

41. Bolger AM, Lohse M, Usadel B: **Trimmomatic: a flexible trimmer for Illumina sequence data**. *Bioinformatics* 2014, **30**(15):2114-2120.

42. Li H, Durbin R: **Fast and accurate short read alignment with Burrows-Wheeler transform**. *Bioinformatics* 2009, **25**(14):1754-1760.

43. Aken BL, Ayling S, Barrell D, Clarke L, Curwen V, Fairley S, Banet JF, Billis K, Girón CG, Hourlier T: **The Ensembl gene annotation system**. *Database* 2016, **2016**:baw093.

44. Cunningham F, Amode MR, Barrell D, Beal K, Billis K, Brent S, Carvalho-Silva D, Clapham P, Coates G, Fitzgerald S *et al*: **Ensembl 2015**. *Nucleic Acids Res* 2015, **43**(Database issue):D662-669.

45. Li H, Handsaker B, Wysoker A, Fennell T, Ruan J, Homer N, Marth G, Abecasis G, Durbin R, Genome Project Data Processing S: **The Sequence Alignment/Map format and SAMtools**. *Bioinformatics* 2009, **25**(16):2078-2079.

46. Robinson MD, McCarthy DJ, Smyth GK: **edgeR: a Bioconductor package for differential expression analysis of digital gene expression data**. *Bioinformatics* 2010, **26**(1):139-140.

47. Conesa A, Nueda MJ, Ferrer A, Talon M: **maSigPro: a method to identify significantly differential expression profiles in time-course microarray experiments**. *Bioinformatics* 2006, **22**(9):1096-1102.

48. Dixon P: **VEGAN, a package of R functions for community ecology**. *J Veg Sci* 2003, **14**(6):927-930.

49. Reimand J, Arak T, Adler P, Kolberg L, Reisberg S, Peterson H, Vilo J: **g:Profiler-a web server for functional interpretation of gene lists (2016 update)**. *Nucleic Acids Res* 2016, **44**(W1):W83-89.

50. Croft D, Mundo AF, Haw R, Milacic M, Weiser J, Wu G, Caudy M, Garapati P, Gillespie M, Kamdar MR *et al*: **The Reactome pathway knowledgebase**. *Nucleic Acids Res* 2014, **42**(Database issue):D472-477.

51. Andrade DV, Cruz-Neto AP, Abe AS: **Meal size and specific dynamic action in the rattlesnake Crotalus durissus (Serpentes : Viperidae)**. *Herpetologica* 1997, **53**(4):485-493.

52. Cox CL, Secor SM: **Integrated postprandial responses of the diamondback water snake, Nerodia rhombifer**. *Physiol Biochem Zool* 2010, **83**(4):618-631.

53. King RW, Deshaies RJ, Peters JM, Kirschner MW: **How proteolysis drives the cell cycle**. *Science* 1996, **274**(5293):1652-1659.

54. Burrows F, Zhang H, Kamal A: **Hsp90 activation and cell cycle regulation**. *Cell Cycle* 2004, **3**(12):1530-1536.

55. Yu M, Wang H, Zhao J, Yuan Y, Wang C, Li J, Zhang L, Zhang L, Li Q, Ye J: **Expression of CIDE proteins in clear cell renal cell carcinoma and their prognostic significance**. *Mol Cell Biochem* 2013, **378**(1-2):145-151.

56. Godel M, Hartleben B, Herbach N, Liu S, Zschiedrich S, Lu S, Debreczeni-Mor A, Lindenmeyer MT, Rastaldi MP, Hartleben G *et al*: **Role of mTOR in podocyte function and diabetic nephropathy in humans and mice**. *J Clin Invest* 2011, **121**(6):2197-2209.

57. Chen G, Chen H, Wang C, Peng Y, Sun L, Liu H, Liu F: **Rapamycin ameliorates kidney fibrosis by inhibiting the activation of mTOR signaling in interstitial macrophages and myofibroblasts**. *PLoS One* 2012, **7**(3):e33626.

58. Pantuck AJ, Seligson DB, Klatte T, Yu H, Leppert JT, Moore L, O'Toole T, Gibbons J, Belldegrun AS, Figlin RA: **Prognostic relevance of the mTOR pathway in renal cell carcinoma: implications for molecular patient selection for targeted therapy**. *Cancer* 2007, **109**(11):2257-2267.

59. Rak-Raszewska A, Hauser PV, Vainio S: **Organ In Vitro Culture: What Have We Learned about Early Kidney Development?** *Stem Cells Int* 2015, **2015**:959807.

60. Prendergast GC: **Mechanisms of apoptosis by c-Myc**. *Oncogene* 1999, **18**(19):2967-2987.

61. Dang CV: **c-Myc target genes involved in cell growth, apoptosis, and metabolism**. *Mol Cell Biol* 1999, **19**(1):1-11.

62. Phesse TJ, Myant KB, Cole AM, Ridgway RA, Pearson H, Muncan V, van den Brink GR, Vousden KH, Sears R, Vassilev LT *et al*: **Endogenous c-Myc is essential for p53-induced apoptosis in response to DNA damage in vivo**. *Cell death and differentiation* 2014, **21**(6):956-966.

63. Bretones G, Delgado MD, Leon J: **Myc and cell cycle control**. *Biochim Biophys Acta* 2015, **1849**(5):506-516.

64. Zornig M, Evan GI: **Cell cycle: on target with Myc**. *Curr Biol* 1996, **6**(12):1553-1556.

65. Pajic A, Spitkovsky D, Christoph B, Kempkes B, Schuhmacher M, Staege MS, Brielmeier M, Ellwart J, Kohlhuber F, Bornkamm GW *et al*: **Cell cycle activation by c-myc in a burkitt lymphoma model cell line**. *Int J Cancer* 2000, **87**(6):787-793.

66. Pourdehnad M, Truitt ML, Siddiqi IN, Ducker GS, Shokat KM, Ruggero D: **Myc and mTOR converge on a common node in protein synthesis control that confers synthetic lethality in Myc-driven cancers**. *Proc Natl Acad Sci U S A* 2013, **110**(29):11988-11993.

67. Csibi A, Lee G, Yoon SO, Tong H, Ilter D, Elia I, Fendt SM, Roberts TM, Blenis J: **The mTORC1/S6K1 pathway regulates glutamine metabolism through the eIF4B-dependent control of c-Myc translation**. *Curr Biol* 2014, **24**(19):2274-2280.

68. Chiu T, Santiskulvong C, Rozengurt E: **EGF receptor transactivation mediates ANG II-stimulated mitogenesis in intestinal epithelial cells through the PI3-kinase/Akt/mTOR/p70S6K1 signaling pathway**. *American journal of physiology Gastrointestinal and liver physiology* 2005, **288**(2):G182-194.

69. Brosius FC, Coward RJ: **Podocytes, signaling pathways, and vascular factors in diabetic kidney disease**. *Adv Chronic Kidney Dis* 2014, **21**(3):304-310.

70. Laplante M, Sabatini DM: **An emerging role of mTOR in lipid biosynthesis**. *Curr Biol* 2009, **19**(22):R1046-1052.

71. Yuan M, Pino E, Wu L, Kacergis M, Soukas AA: **Identification of Akt-independent regulation of hepatic lipogenesis by mammalian target of rapamycin (mTOR) complex 2**. *The Journal of biological chemistry* 2012, **287**(35):29579-29588.

72. Hung CM, Calejman CM, Sanchez-Gurmaches J, Li H, Clish CB, Hettmer S, Wagers AJ, Guertin DA: **Rictor/mTORC2 loss in the Myf5 lineage reprograms brown fat metabolism and protects mice against obesity and metabolic disease**. *Cell Rep* 2014, **8**(1):256-271.

73. Kumar A, Lawrence JC, Jr., Jung DY, Ko HJ, Keller SR, Kim JK, Magnuson MA, Harris TE: **Fat cell-specific ablation of rictor in mice impairs insulin-regulated fat cell and whole-body glucose and lipid metabolism**. *Diabetes* 2010, **59**(6):1397-1406.

74. Guan Y, Breyer MD: **Peroxisome proliferator-activated receptors (PPARs): novel therapeutic targets in renal disease**. *Kidney Int* 2001, **60**(1):14-30.

75. Guan Y: **Targeting peroxisome proliferator-activated receptors (PPARs) in kidney and urologic disease**. *Minerva Urol Nefrol* 2002, **54**(2):65-79.

76. Yoshihara D, Kurahashi H, Morita M, Kugita M, Hiki Y, Aukema HM, Yamaguchi T, Calvet JP, Wallace DP, Nagao S: **PPAR-gamma agonist ameliorates kidney and liver disease in an orthologous rat model of human autosomal recessive polycystic kidney disease**. *Am J Physiol Renal Physiol* 2011, **300**(2):F465-474.

77. Kanjanabuch T, Ma LJ, Chen J, Pozzi A, Guan Y, Mundel P, Fogo AB: **PPAR-gamma agonist protects podocytes from injury**. *Kidney Int* 2007, **71**(12):1232-1239.

78. Hu E, Kim JB, Sarraf P, Spiegelman BM: **Inhibition of adipogenesis through MAP kinase-mediated phosphorylation of PPARgamma**. *Science* 1996, **274**(5295):2100-2103.

79. Hevener AL, Olefsky JM, Reichart D, Nguyen MT, Bandyopadyhay G, Leung HY, Watt MJ, Benner C, Febbraio MA, Nguyen AK *et al*: **Macrophage PPAR gamma is required for normal skeletal muscle and hepatic insulin sensitivity and full antidiabetic effects of thiazolidinediones**. *J Clin Invest* 2007, **117**(6):1658-1669.

80. Moller DE, Berger JP: **Role of PPARs in the regulation of obesity-related insulin sensitivity and inflammation**. *Int J Obes Relat Metab Disord* 2003, **27 Suppl 3**:S17-21.

81. Yang FG, Zhang ZW, Xin DQ, Shi CJ, Wu JP, Guo YL, Guan YF: **Peroxisome proliferator-activated receptor gamma ligands induce cell cycle arrest and apoptosis in human renal carcinoma cell lines**. *Acta Pharmacol Sin* 2005, **26**(6):753-761.

82. Theocharis S, Margeli A, Vielh P, Kouraklis G: **Peroxisome proliferator-activated receptor-gamma ligands as cell-cycle modulators**. *Cancer treatment reviews* 2004, **30**(6):545-554.

83. Yang HC, Deleuze S, Zuo Y, Potthoff SA, Ma LJ, Fogo AB: **The PPARgamma agonist pioglitazone ameliorates aging-related progressive renal injury**. *J Am Soc Nephrol* 2009, **20**(11):2380-2388.

84. Todorov VT, Desch M, Schmitt-Nilson N, Todorova A, Kurtz A: **Peroxisome proliferator-activated receptor-gamma is involved in the control of renin gene expression**. *Hypertension* 2007, **50**(5):939-944.

85. Todorov VT: **PPARgamma-Dependent Control of Renin Expression: Molecular Mechanisms and Pathophysiological Relevance**. *PPAR Res* 2013, **2013**:451016.

86. Kersten S, Desvergne B, Wahli W: **Roles of PPARs in health and disease**. *Nature* 2000, **405**(6785):421-424.

87. Sun L, Halaihel N, Zhang W, Rogers T, Levi M: **Role of sterol regulatory element-binding protein 1 in regulation of renal lipid metabolism and glomerulosclerosis in diabetes mellitus**. *The Journal of biological chemistry* 2002, **277**(21):18919-18927.

88. Jiang T, Liebman SE, Lucia MS, Li J, Levi M: **Role of altered renal lipid metabolism and the sterol regulatory element binding proteins in the pathogenesis of age-related renal disease**. *Kidney Int* 2005, **68**(6):2608-2620.

89. Ruiz S, Pergola PE, Zager RA, Vaziri ND: **Targeting the transcription factor Nrf2 to ameliorate oxidative stress and inflammation in chronic kidney disease**. *Kidney Int* 2013, **83**(6):1029-1041.

90. Shelton LM, Park BK, Copple IM: **Role of Nrf2 in protection against acute kidney injury**. *Kidney Int* 2013, **84**(6):1090-1095.

91. Mostov KE: **mTOR is out of control in polycystic kidney disease**. *P Natl Acad Sci USA* 2006, **103**(14):5247-5248.

92. Kim HJ, Moradi H, Yuan J, Norris K, Vaziri ND: **Renal mass reduction results in accumulation of lipids and dysregulation of lipid regulatory proteins in the remnant kidney**. *Am J Physiol Renal Physiol* 2009, **296**(6):F1297-1306.

93. Huber TB, Walz G, Kuehn EW: **mTOR and rapamycin in the kidney: signaling and therapeutic implications beyond immunosuppression**. *Kidney Int* 2011, **79**(5):502-511.

94. Mallipattu SK, Liu R, Zheng F, Narla G, Ma'ayan A, Dikman S, Jain MK, Saleem M, D'Agati V, Klotman P *et al*: **Kruppel-like factor 15 (KLF15) is a key regulator of podocyte differentiation**. *The Journal of biological chemistry* 2012, **287**(23):19122-19135.

95. McGaugh SE, Bronikowski AM, Kuo CH, Reding DM, Addis EA, Flagel LE, Janzen FJ, Schwartz TS: **Rapid molecular evolution across amniotes of the IIS/TOR network**. *Proc Natl Acad Sci U S A* 2015, **112**(22):7055-7060.

Tables

Table 3.S1. **Sequencing details for all snake samples included in this study.** SE50 or PE120 indicate the read type and length (e.g., Paired-end 120bp), and the year represents the year in which that sample was sequenced.

| Species | Time point | Animal ID | Insrument | cDNA prep kit | Year | Sequence type |
|---|---|---|---|---|---|---|
| Python | fasted | AI8 | HiSeq | NEB Next | 2013 | SE50 |
| Python | fasted | U25 | HiSeq | NEB Next | 2013 | SE50 |
| Python | fasted | AI6_1 | HiSeq | Illlumina Truseq | 2011 | SE50 |
| Python | fasted | AI6_2 | GAIIx | Illlumina Truseq | 2011 | PE120 |
| Python | fasted | AI11_1 | HiSeq | Illlumina Truseq | 2011 | SE50 |
| Python | fasted | AI11_2 | GAIIx | Illlumina Truseq | 2011 | PE120 |
| Python | fasted | AJ6_1 | HiSeq | Illlumina Truseq | 2011 | SE50 |
| Python | fasted | AJ6_2 | GAIIx | Illlumina Truseq | 2011 | PE120 |
| Python | fasted | AJ6_3 | GAIIx | Illlumina Truseq | 2011 | PE120 |
| Python | 1DPF | Z12_1 | HiSeq | Illlumina Truseq | 2011 | SE50 |
| Python | 1DPF | Z12_2 | GAIIx | Illlumina Truseq | 2011 | PE120 |
| Python | 1DPF | Z14_1 | HiSeq | Illlumina Truseq | 2011 | SE50 |
| Python | 1DPF | Z14_2 | GAIIx | Illlumina Truseq | 2011 | PE120 |
| Python | 1DPF | Z18_1 | HiSeq | Illlumina Truseq | 2011 | SE50 |
| Python | 1DPF | Z18_2 | GAIIx | Illlumina Truseq | 2011 | PE120 |
| Python | 1DPF | Z18_3 | GAIIx | Illlumina Truseq | 2011 | PE120 |
| Python | 1DPF | V43 | HiSeq | NEB Next | 2013 | SE50 |
| Python | 1DPF | Z14_3 | HiSeq | NEB Next | 2013 | SE50 |
| Python | 4DPF | Y18_1 | HiSeq | NEB Next | 2013 | SE50 |
| Python | 4DPF | Y24 | HiSeq | NEB Next | 2013 | SE50 |
| Python | 4DPF | Y5_1 | HiSeq | Illlumina Truseq | 2011 | SE50 |
| Python | 4DPF | Y5_2 | GAIIx | Illlumina Truseq | 2011 | PE120 |
| Python | 4DPF | Y5_3 | GAIIx | Illlumina Truseq | 2011 | PE120 |
| Python | 4DPF | Y18_2 | HiSeq | Illlumina Truseq | 2011 | SE50 |
| Python | 4DPF | Y18_3 | GAIIx | Illlumina Truseq | 2011 | PE120 |
| Python | 4DPF | Y23_1 | HiSeq | Illlumina Truseq | 2011 | SE50 |
| Python | 4DPF | Y23_2 | GAIIx | Illlumina Truseq | 2011 | PE120 |
| Rattlesnake | fasted | CV7 | HiSeq | Illlumina Truseq | 2014 | PE100 |
| Rattlesnake | fasted | CV4 | HiSeq | Illlumina Truseq | 2014 | PE100 |
| Rattlesnake | fasted | CV1 | HiSeq | Illlumina Truseq | 2014 | PE100 |
| Rattlesnake | fasted | CV2 | HiSeq | Illlumina Truseq | 2014 | PE100 |
| Rattlesnake | 1DPF | CV8 | HiSeq | Illlumina Truseq | 2014 | PE100 |

| | | | | | | |
|---|---|---|---|---|---|---|
| Rattlesnake | 1DPF | CV5 | HiSeq | Illlumina Truseq | 2014 | PE100 |
| Rattlesnake | 1DPF | CV3 | HiSeq | Illlumina Truseq | 2014 | PE100 |
| Rattlesnake | 1DPF | CV6 | HiSeq | Illlumina Truseq | 2014 | PE100 |
| Rattlesnake | 4DPF | CV11 | HiSeq | Illlumina Truseq | 2014 | PE100 |
| Rattlesnake | 4DPF | CV12 | HiSeq | Illlumina Truseq | 2014 | PE100 |
| Rattlesnake | 4DPF | CV9 | HiSeq | Illlumina Truseq | 2014 | PE100 |
| Rattlesnake | 4DPF | CV10 | HiSeq | Illlumina Truseq | 2014 | PE100 |
| Water snake | fasted | NR1317 | HiSeq | Illlumina Truseq | 2016 | PE150 |
| Water snake | fasted | NR1315 | HiSeq | Illlumina Truseq | 2016 | PE150 |
| Water snake | fasted | NR1464 | HiSeq | Illlumina Truseq | 2016 | PE150 |
| Water snake | fasted | NR1416 | HiSeq | Illlumina Truseq | 2016 | PE150 |
| Water snake | 1DPF | NR1357 | HiSeq | Illlumina Truseq | 2016 | PE150 |
| Water snake | 1DPF | NR1436 | HiSeq | Illlumina Truseq | 2016 | PE150 |
| Water snake | 1DPF | NR1331 | HiSeq | Illlumina Truseq | 2016 | PE150 |
| Water snake | 1DPF | NR1388 | HiSeq | Illlumina Truseq | 2016 | PE150 |
| Water snake | 4DPF | NR1324 | HiSeq | Illlumina Truseq | 2016 | PE150 |
| Water snake | 4DPF | NR1327 | HiSeq | Illlumina Truseq | 2016 | PE150 |
| Water snake | 4DPF | NR1354 | HiSeq | Illlumina Truseq | 2016 | PE150 |
| Water snake | 4DPF | NR1442 | HiSeq | Illlumina Truseq | 2016 | PE150 |

Table 3.S2. **Total number of post-filtered mapped reads per individual.** Mapped reads were count following quality filtering and trimming.

| Species | Time point | Animal ID | Post-filtered total mapped reads |
|---|---|---|---|
| Python | fasted | AI8 | 177,238 |
| Python | fasted | U25 | 608,720 |
| Python | fasted | AI6 | 541,534 |
| Python | fasted | AI11 | 5,038,183 |
| Python | fasted | AJ6 | 3,745,154 |
| Python | 1DPF | Z12 | 2,796,229 |
| Python | 1DPF | Z14 | 338,002 |
| Python | 1DPF | Z18 | 2,273,794 |
| Python | 1DPF | V43 | 921,418 |
| Python | 4DPF | Y18 | 624,561 |
| Python | 4DPF | Y24 | 601,437 |
| Python | 4DPF | Y5 | 2,491,020 |
| Rattlesnake | fasted | CV7 | 4,840,677 |
| Rattlesnake | fasted | CV4 | 4,774,838 |
| Rattlesnake | fasted | CV1 | 2,749,330 |
| Rattlesnake | fasted | CV2 | 3,907,801 |
| Rattlesnake | 1DPF | CV8 | 6,428,650 |
| Rattlesnake | 1DPF | CV5 | 4,280,014 |
| Rattlesnake | 1DPF | CV3 | 4,377,150 |
| Rattlesnake | 1DPF | CV6 | 5,207,605 |
| Rattlesnake | 4DPF | CV11 | 4,292,286 |
| Rattlesnake | 4DPF | CV12 | 6,855,628 |
| Rattlesnake | 4DPF | CV9 | 973,895 |
| Rattlesnake | 4DPF | CV10 | 3,764,908 |
| Water snake | fasted | NR1317 | 1,976,825 |
| Water snake | fasted | NR1315 | 3,423,288 |
| Water snake | fasted | NR1464 | 2,981,186 |
| Water snake | fasted | NR1416 | 1,512,414 |
| Water snake | 1DPF | NR1357 | 1,595,480 |
| Water snake | 1DPF | NR1436 | 3,225,394 |
| Water snake | 1DPF | NR1331 | 1,847,455 |
| Water snake | 1DPF | NR1388 | 3,275,460 |
| Water snake | 4DPF | NR1324 | 1,075,312 |
| Water snake | 4DPF | NR1327 | 1,643,121 |
| Water snake | 4DPF | NR1354 | 1,060,715 |

| | | | |
|---|---|---|---|
| Water snake | 4DPF | NR1442 | 925,846 |

Figures

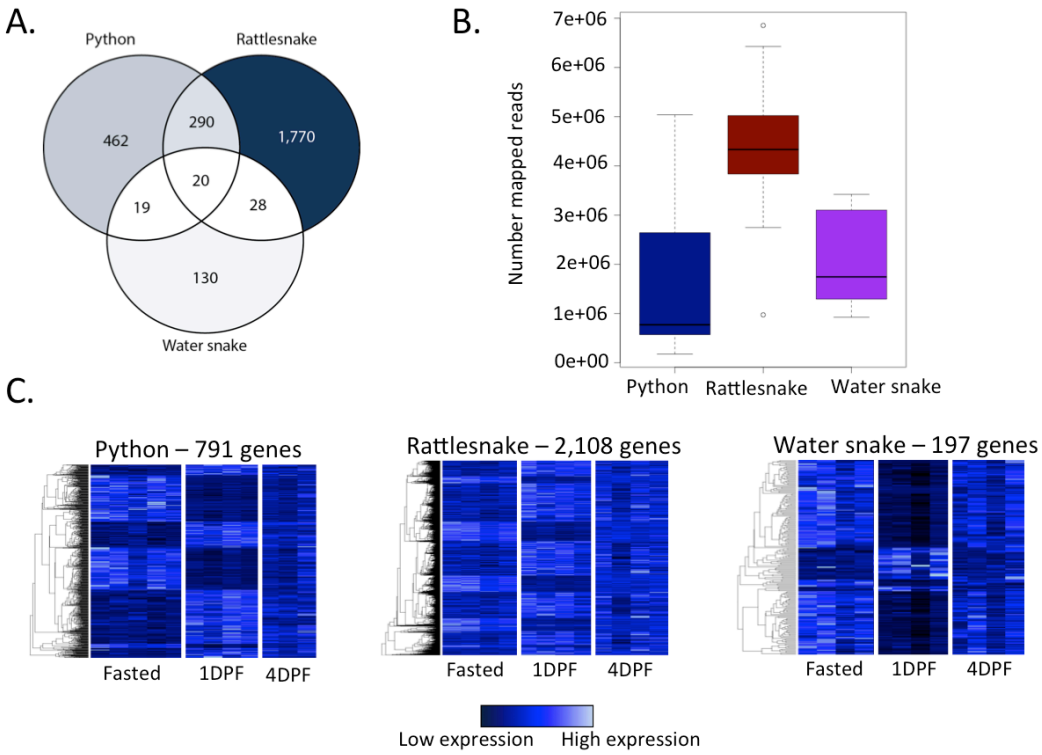


Figure 3.1. **Comparison of expression response of genes differentially expressed between fasted and 1DPF animals.** (A) Venn diagram of all genes differentially expressed (FDR <0.2) between fasted and 1DPF animals. (B) Box plot showing the numbers of mapped reads for all time points combined per species. (C) Clustered heatmaps of all genes displayed in the venn. Pythons exhibited the significant differential expression of 791 genes, Rattlesnakes showed significant differential expression of 2,108 genes, and the water snake only exhibited differential expression of 197 genes.

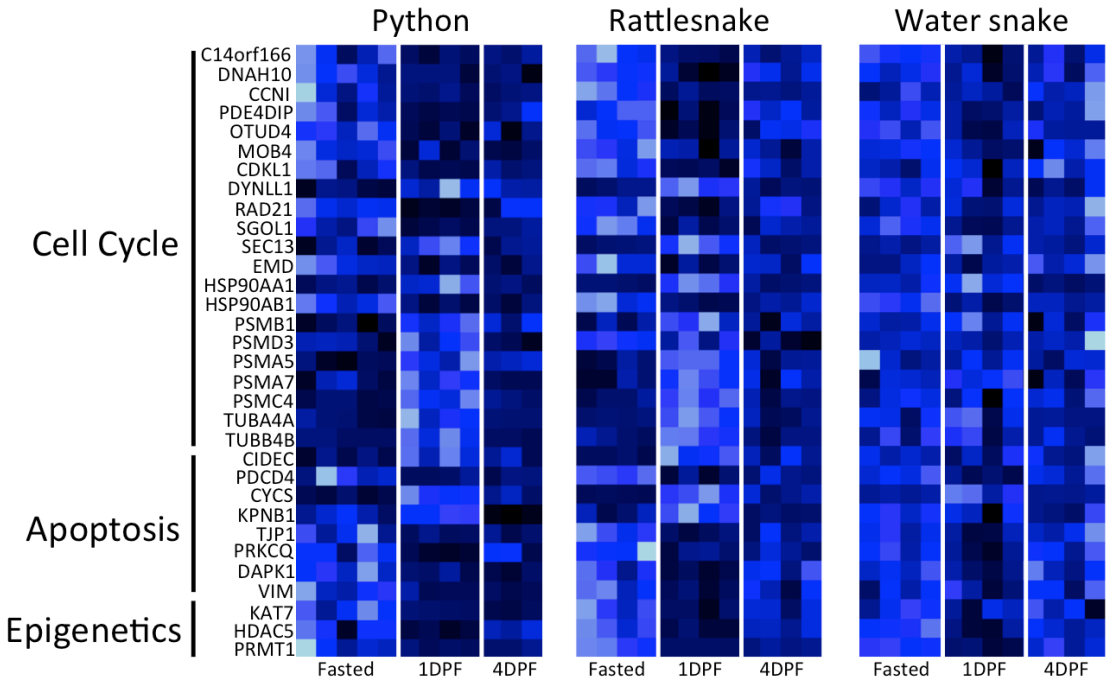


Figure 3.2. **Gene expression patterns of genes involved in cell cycling, apoptosis, and epigenetic modifications.** Each gene shown was identified as significantly differentially regulated (FDR < 0.05) via regression analyses, and candidate genes were selected from those significant in both the python and rattlesnake or all three species.

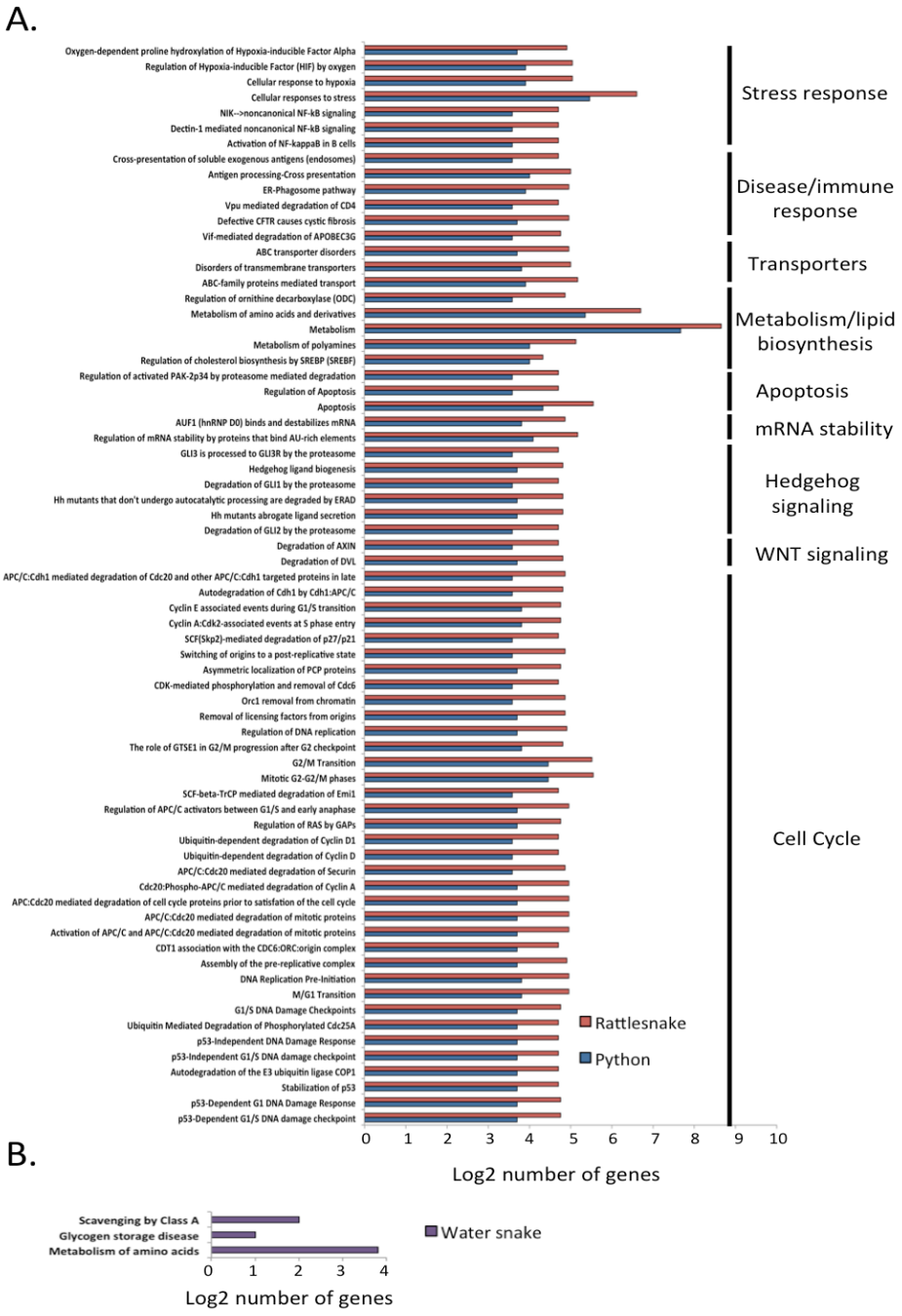


Figure 3.3. **Enrichment of genes for Reactome pathways identifed via g:Profiler.** (A) All pathways significantly enriched in both the python and rattlesnake. (B) All pathways significantly enriched in the water snake. Pathways were enriched (corrected p-value < 0.05) for genes significantly differentially expressed (FDR < 0.2) between fasted and 1DPF animals.

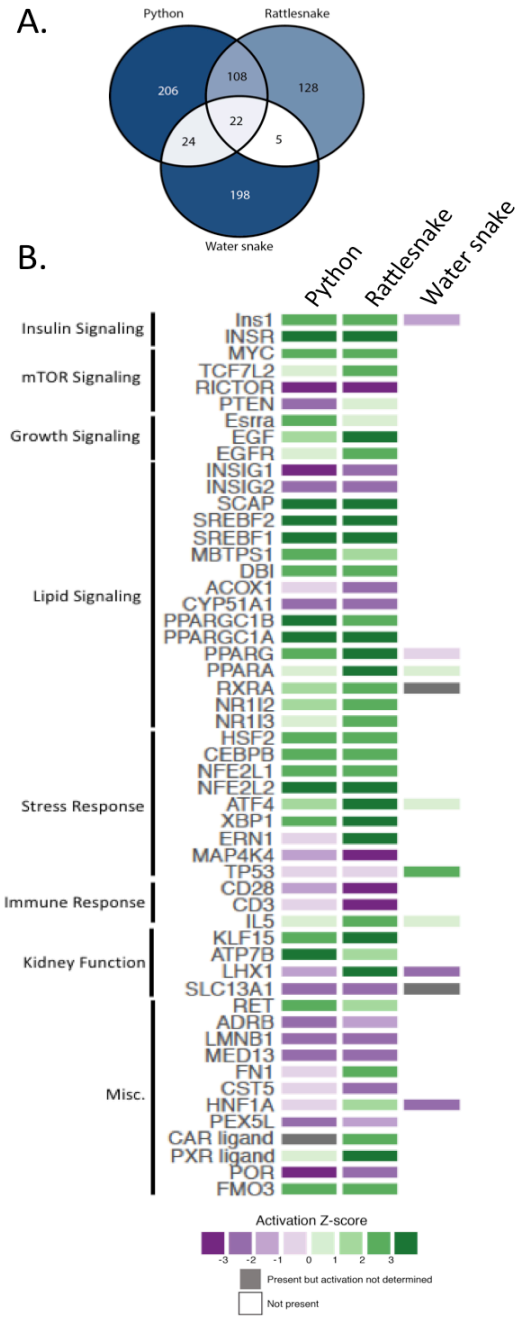


Figure 3.4. **Comparative analysis of URMs in the three species.** (A) Venn diagram depicts URMs deemed significant (P<0.06) between fasted and 1DPF animals. (B) The selection of URMs depicted in heatmap were either significant (P<0.06) in all three species or between the python and the rattlesnake with a Z-score greater than 2 or less than -2 in at least one species.

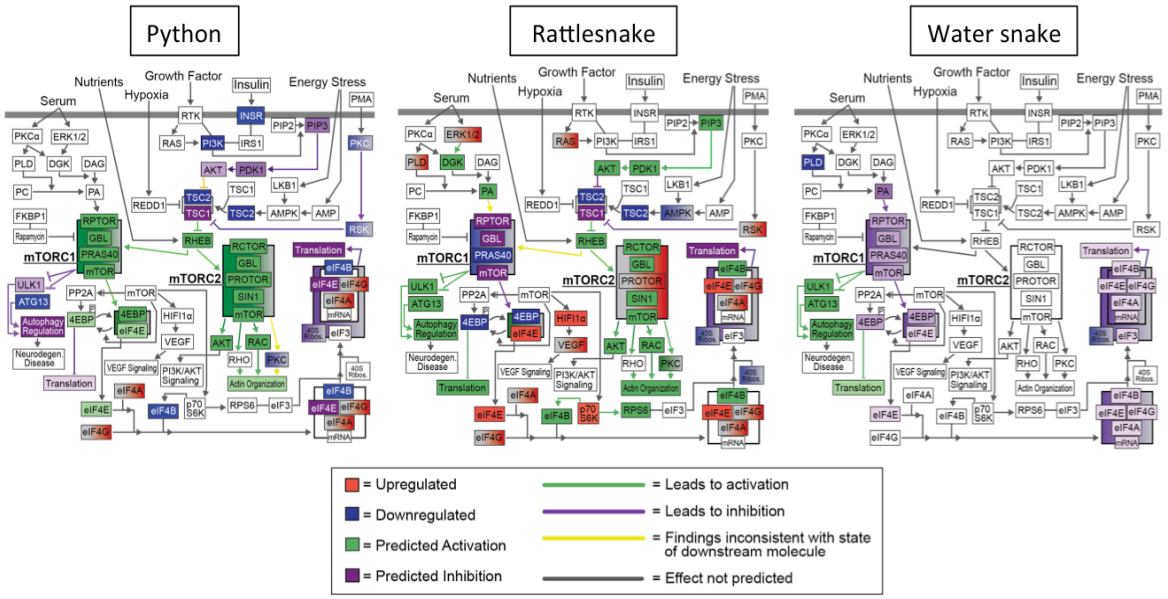


Figure 3.5. **Comparative IPA canonical pathway analysis of the predicted activation state of the mTOR pathway.** Both observed gene expression patterns from our RNAseq dataset (red for observed upregulation and blue for observed downregulation) and predicted pathway responses (orange for predicted activation and purple for predicted inhibition) are shown. Both python and rattlesnake show similar (though not identical) patterns of activation. The water snake shows very little involvement of mTOR signaling following feeding.

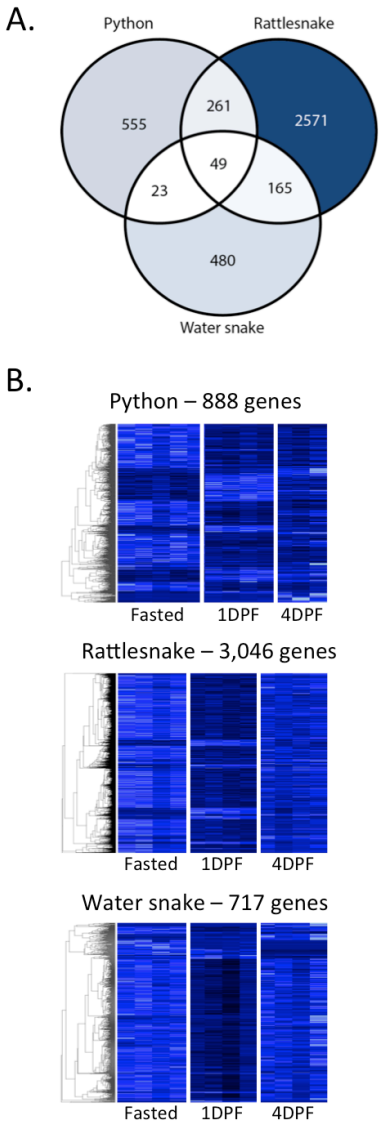


Figure 3.S1. **Comparison of expression response of genes significantly differentially expressed across all three timepoints identified via regression analysis.** (A) Venn diagram of all genes differentially expressed (FDR < 0.05) across time points. (B) Clustered heatmaps of all genes displayed in the venn. Pythons exhibited the significant differential expression of 888 genes, Rattlesnakes showed significant differential expression of 3,046 genes, and the water snake only exhibited differential expression of 717 genes.

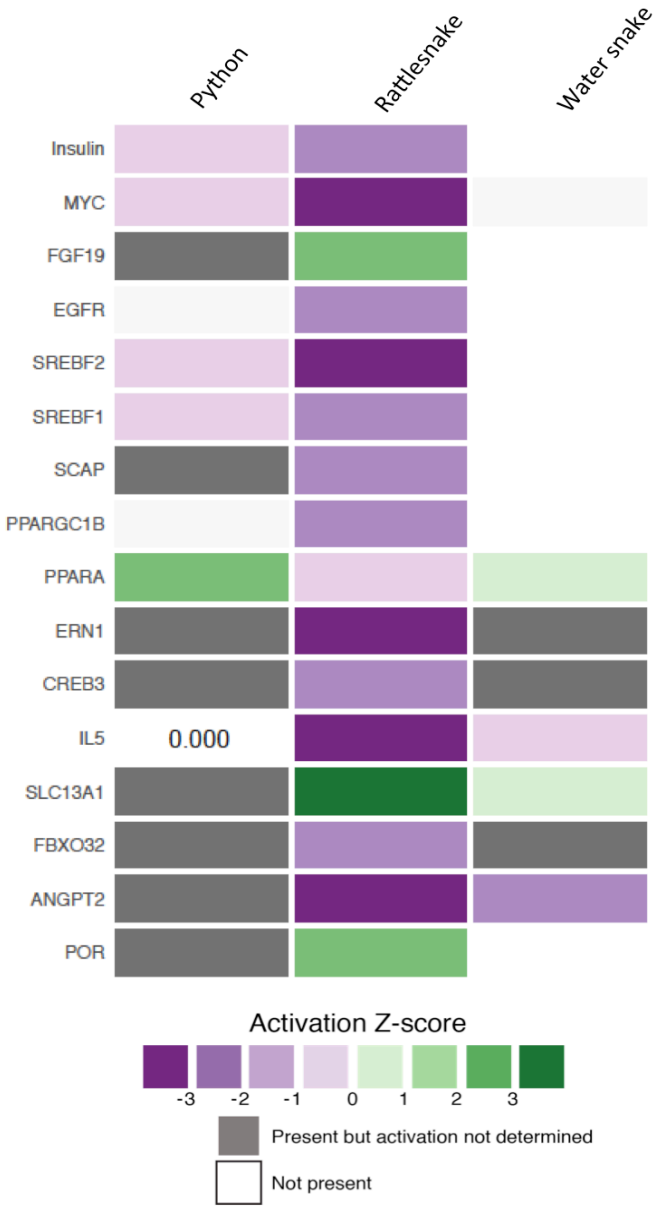


Figure 3.S2. **Expression response of URMs predicted to be significantly involved (P<0.06) in the regulation of gene expression patterns between 1DPF and 4DPF animals.** Those shown in the heatmap were either significant in both the python and rattlesnake or in all three species and had a Z score greater than 2 or less than -2 in at least one species.

Appendix A – Supplemental methods from Chapter 2

*Feeding Experiments*

The following information pertains to snakes that were sampled and sequenced for this study (see also Additional file 1, Table S1; and [5, 13] for details regarding previously sequenced data incorporated in this study). Burmese pythons (*Python molurus bivittatus*) were purchased within 1-2 months of hatching from commercial vendors. All snakes included in this study originated from captive colonies, were phenotypically normal in coloration (i.e., no albino animals), and ranged in age from 9 months to 6 years (mean = 1.9 years) and in mass from 406 to 5,776 grams (mean = 1,036 g). Snakes were housed individually in 12L plastic bins that slide into customized racks in the Central Animal Care Facility at the University of Alabama. Each bin featured a floor substrate of newspaper and contained a water bowl. All pythons were maintained on a light/dark cycle of 14 hours of light followed by 10 hours of dark. Room temperature was maintained at 26-28°C and was constantly monitored by the Central Animal Care Facility. Prior to experimentation, pythons were fed weekly a meal of 1-2 rodents (adult mice or small rats) and water was provided *ad libitum*. Pythons were monitored daily by the Animal Care staff and personnel of the laboratory of Dr. Stephen Secor prior to and during experimentation. There were no interventions in snake care prior to or during experimentation. All experimentation and dissection was performed by Secor lab personnel. No special attention was given to selecting animals randomly from a research colony, however there was an attempt for matching in sexes (7 males: 6 females), so that there would be no bias due to sex in any treatment or the experiment overall. At the time of sampling, all animals were in good health and had not been subjected to any previous procedures or drug administration. Fasted snakes had been fasted for a minimum of 30

days prior to sampling. Snakes of the 1 and 4 days post-feeding treatments had been fasted for 30 days and then fed a rodent meal equal in mass to 25% of the snake body mass, and sampled 1 and 4 days after feeding, respectively. The mean mass of snakes in each treatment were: fasted (1,504 g), 1DPF (892 g), and 4DPF (593 g). At the time of sampling, snakes were sacrificed by humanely severing the spinal cord immediately behind the head; this provided the most efficient and rapid means to obtain organ samples for storage and study without compromising physiological responses of interest. Organ tissues were immediately extracted, snap frozen in liquid nitrogen, and stored at -80°C. Feeding experiments and subsequent sampling of snakes were completed over a span of several years, with fasted snakes sampled in 2005 and 2009, and 1 and 4DPF snakes sampled in 2005 and 2006. There was no particular order to the sampling of tissues from animals. No adverse events occurred during animal care or experimentation, and thus no modifications to the experimental protocol were undertaken as a result.

The Burmese python has become an outstanding animal model (compared to traditional mammal model systems) to explore the cellular and molecular mechanisms underlying regenerative organ growth and physiology, and therefore serves as an excellent replacement for exploring such systems in typical mammalian models. We made efforts to minimize the number of animals used overall in this study, as evident in the relatively small sample sizes for each treatment (3-6 individuals). Additionally, dissection of snakes included the removal and storage of all organs and other tissues (muscle, blood, etc.) so that subsequent studies can utilize these tissues to study this regenerative phenotype in other organ systems without the need for the sacrifice of additional animals.